Reconstruction of UV-radiation and its potential implications on development of skin cancer

Master Thesis in Meteorology

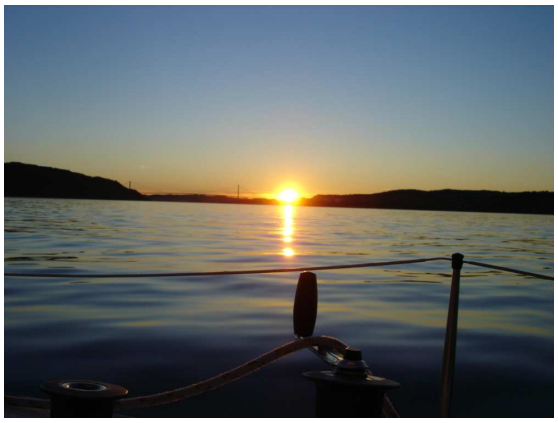

Iselin Medhaug

UNIVERSITY OF BERGEN
GEOPHYSICAL INSTITUTE

June 1, 2007

Figure on the front cover shows the sunset on Byfjorden,
Tuesday evening, 11. October 2006.
Picture is taken by yours truly.

Acknowledgments

It is with sadness, but also with great joy that I now say thanks and goodbye.

Thanks to Bjørn Johnsen at NRPA for giving me the UV data and the secrets behind them, Georg Hansen at NILU for contributing with the Tromsø ozone data, Asgeir Sorteberg for giving me the opportunity (through his ozone interpolation program) to tamper with the data received from Georg Hansen, Anders Lindfors for giving me the data reconstructed with his own model, and last but not least Trude Eid Robsahm at the Cancer Registry of Norway for both contributing with cancer data and literature on the matter.

Thanks to my great supervisors Jan Asle and Jochen! At first you were a bit skeptical of my choice of a somewhat unusual subject (at least in meteorological point of view). You've done a great job. And, Jan Asle, thanks for not always sticking to the asked question. When least expected, a story in the form of a digression just slips out. Jochen, thanks for letting me use your model.

It has been a great pleasure studying here at Geofysen. Thanks to all my fellow students, especially you guys at ODD! Thank you very much for joining me in a barbecue whether there is sun, rain or hail, an umbrella will do the trick.

A special thanks to Anders and Tarjei for proof reading my thesis.

Contents

1 Introduction **2**

2 Theory **6**
2.1 Solar radiation 6
2.2 Solar ultraviolet radiation 8
2.3 CIE-weighting function 8
2.4 Parameters affecting UV radiation 11
2.4.1 Solar elevation 11
2.4.2 Ozone 11
2.4.3 Turbidity 13
2.4.4 Surface albedo 14
2.4.5 Clouds 15
2.5 Skin cancer 17

3 Methods and Data **20**
3.1 STAR model 20
3.2 Input data to STAR 22
3.2.1 Solar elevation 22
3.2.2 Ozone 22
3.2.3 Turbidity 30
3.2.4 Surface Albedo 31
3.2.5 Clouds 32
3.3 Lindfors model 37
3.4 GUV 38
3.5 Cancer 40

4 Comparison and Trends **42**
4.1 Observed and modeled UV 42
4.1.1 STAR vs GUV 42
4.1.2 STAR vs Lindfors 54
4.2 Temporal and spatial variations 57

4.2.1 Variations in UV radiation 57
4.2.2 Variations in cancer incidences 62
4.3 Correlation between UV and cancer 65

5 Summary and Conclusion **76**

Appendices **79**

A Station Information **79**
A.1 Ozone 79
A.2 Synoptic stations 81
A.3 UV-stations 85

B Cloud information **86**

C Decadal trends in UVA, UVB and ERY **88**

D Statistics **92**

E Cancer incidences **93**

Appendices **79**

Bibliography **101**

Chapter 1

Introduction

Since the early 1980s there has been an increased focus on the decay of the stratospheric ozone. The scientific community and the mass media showed great interest for the "ozone-hole" found over Antarctica in the spring. A similar "hole" was also found over the Arctic, but to a much lesser extent because of the more efficient exchange of stratospheric air between lower and higher latitudes in the northern hemisphere. In the following years the ozone depletion increased mainly because of human-made gases, like CFC's.

As a consequence of the decrease of stratospheric ozone (WMO, 2003, 2006) the ultraviolet (UV) radiation at the ground has increased (Komhyr et al., 1994).

For plants and animals, a change in UV can cause change in primary production and altered species composition (Caldwell and Flint, 1994). For humans, UV can cause damage to the eyes and immune system, and it can cause skin cancer (Longstreth et al., 1998). When it comes to UV radiation and skin cancer there are two contradictory points of view. First, UV is a known risk factor for development of skin cancer (Armstrong and Kricker, 1993; Autier and Dore, 1998). On the other hand, there is observed a higher survival rate of the skin cancer type cutaneous malignant melanoma (CMM) in sunny areas relative to areas with less sun (Hughes et al., 2004; Berwick et al., 2005). Besides, UVB is the most important source of vitamin-D, which potentially can have restraining effect on skin cancer (Egan et al., 2005).

CMM is the second most common cancer form for both sexes in the age group 30-55 years in Norway. Norway is in third place in the world regarding incidences per inhabitant, following Australia and New Zealand (Robsahm and Tretli, 2004). There has been a dramatic increase in incidences since the

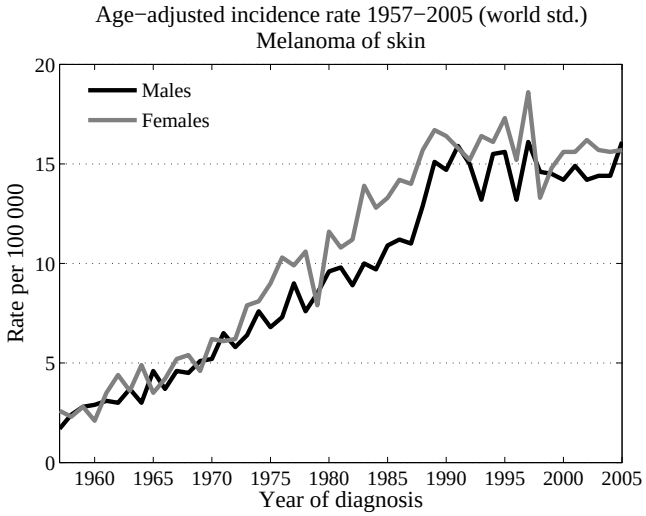

Figure 1.1: *Age-adjusted incidence rates of cutaneous malignant melanoma (CMM) for the Norwegian population 1957-2005.*

registration of cancer in Norway started in the 1950s (Figure 1.1).

Some sites have measurements of UV so far back in time that long term trends can be studied (WMO, 2003; Herman et al., 1996). However, most places do not have that long time series, and then models have to be used for reconstruction of UV data.

At the Meteorological Institute in Munich (Germany) the radiation transfer model STAR (Schwander et al., 2001; Ruggaber et al., 1994) has been developed. The model calculates the amount of UV radiation for a given location at a given time (Reuder and Koepke, 2005). This model will be used to reconstruct data for 17 of the Norwegian counties for a study of the climatology of the UV radiation during the past 50 years. The seasonal variation and the year to year variation will be investigated in addition to time trends and gradients in both east-west and north-south directions. Finally the reconstructed UV will be used to study the relationship between UV level and the number of cancer incidences in the different Norwegian counties. No such large scale reconstruction to be compared to cancer incidences has ever been done before. In most cases the focus was either only on reconstruction of UV or only on cancer. Cancer studies on an entire population have been done before (Robsahm and Tretli, 2001), but not with such long datasets of UV.

The cloud algorithm of the STAR model was developed on the basis of data from Garmisch-Partenkirchen. Recent publications (Sætre, 2006; Koepke et al., 2007) indicate a slight but systematic overestimation of STAR compared to measurements for different locations. However, this study will focus on trends and variations instead of absolute values. Therefore the STAR model is a suitable tool for this investigation.

The EU project, "Long term changes and climatology of UV radiation over Europe", has a main objective to advance the understanding of UV radiation distribution under various meteorological conditions in Europe in order to determine UV radiation climatology and assess UV changes over Europe (COST 726, 2007). The project is divided into four parts; data collection, UV modeling, biological effectiveness and quality control. This thesis will give contribution to the first three of the four parts.

In Chapter 2, theory about solar radiation in general, UV radiation, the CIE-weighting function, parameters affecting UV radiation and skin cancer will be outlined. In Chapter 3, the STAR model is described together with the methods used to convert cloud, snow and ozone observations into data that can be used as input by the model. Finally Chapter 4 presents the results where the reconstructed UV values are first compared to measurements. Next, the time trends and north-south and east-west gradients will be investigated both for reconstructed UV data and for cancer incidences. The last part will then focus on the implications UV radiation might have on the development of malignant melanoma.

Chapter 2

Theory

2.1 Solar radiation

The sun emits radiation which can be approximated by a black body of 6000 K. The spectral distribution of the emission can be described by Planck's law. Therefore the sun emits more than 99 % of its energy in the wavelength interval between 0.2 and 4.0 μm (micrometers). The main part is in the visible and Near Infrared (NIR) region, 0.39-0.77 μm and $\lambda > 0.77$ μm, respectively (Figure 2.1). The remaining part of the solar radiation is then the ultraviolet radiation (UV), which is to be explained below.

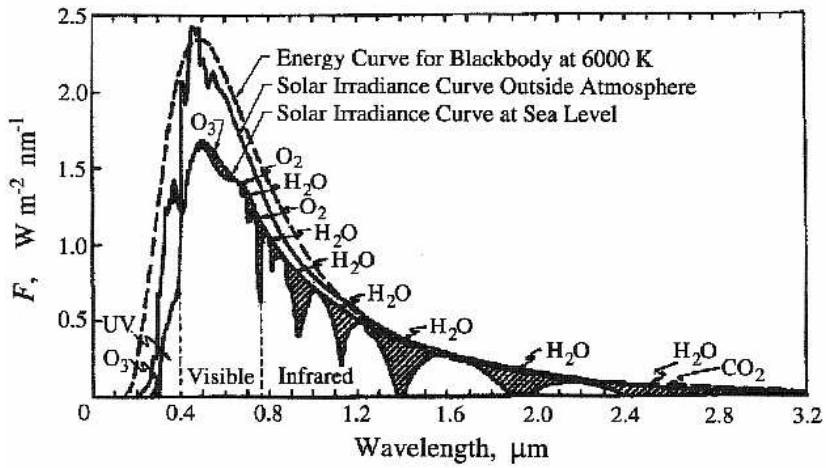

Figure 2.1: *Spectral solar irradiance at the top of the atmosphere and at sea level for a cloud free day with the sun in zenith. The dashed line shows the idealized curve for a black body of 6000 K (from Seinfeld and Pandis (1998)).*

Figure 2.1 shows the spectral irradiance from the sun (solar energy arriving at a surface per unit area and wavelength). The irradiance arriving at the top of the atmosphere is shown as solid curve. The upper dashed line gives the corresponding irradiance of an average blackbody of 6000 K at the average sun-earth distance. The lowest line represents the irradiance reaching sea level. The dark areas represent gaseous absorption bands, where the different constituents in the atmosphere absorb energy. The main absorbers are O_3 in the visible and UV regions, and H_2O in the near infrared region, however O_2 and CO_2 have small contributions, too.

The global radiation (E), i.e. the solar radiation incident on a horizontal surface, can be divided into a direct (E_{dir}) and a diffuse (E_{dif}) component.

$$E = E_{dir} + E_{dif} \tag{2.1}$$

The direct radiation is dependent on the solar zenith angle (θ_0) and on the optical depth of the atmosphere (τ).

$$E_{dir}(\tau, \theta_0) = \mu_0 * E_\infty e^{-\tau/\mu_0} \tag{2.2}$$

where $\mu_0 = \cos\theta_0$ and E_∞ is the irradiance at the top of the atmosphere (Hartmann, 1994). E and τ are both functions of the wavelength (λ).

The diffuse radiation is defined as the solar radiation scattered by atmospheric constituents before it reaches the ground. The equation can be written as:

$$\begin{aligned} -\mu \frac{dE_{dif}(\tau, \mu, \phi)}{d\tau} &= E_{dif}(\tau, \mu, \phi) \\ &+ \frac{\tilde{\omega}}{4\pi} \int_0^{2\pi} \int_{-1}^{1} E_{dif}(\tau, \mu', \phi') P(\mu, \phi, \mu', \phi') d\mu' d\phi' \\ &+ \frac{\tilde{\omega}}{4\pi} E_\infty P(\mu, \phi, -\mu_0, \phi_0) e^{-\tau/\mu_0} \end{aligned} \tag{2.3}$$

where ϕ is the azimuth angle, μ represents the elevation, $\tilde{\omega}$ the single-scattering albedo, and P the scattering phase function. The single scattering albedo is the probability for one scattering event to occur. The phase function describes the angular distribution of the scattered radiation. The primed parameters define the direction of the incoming radiation before scattering. μ and -μ denotes the upward and downward directions of radiation, respectively. The parameters with subscript zero refer to the position of the sun. The single-scattering albedo and the phase function depend on wavelength,

and size and shape of the scattering particles.

The left hand side of Equation 2.3 describes the change of diffuse radiation while passing through an atmospheric layer of optical depth $d\tau$. The three terms on the right hand side describe the incoming diffuse radiation in direction θ, μ, the multiple and the single scattered radiation, respectively (Liou, 1992).

2.2 Solar ultraviolet radiation

The UV wavelength range is divided into three parts, UVA, UVB and UVC.

UVA: wavelengths between 315-400 nm.

UVB: wavelengths between 280-315 nm.

UVC: wavelengths between 200-280 nm.

In literature, the boundary between UVA and UVB can be found as 315 nm (nanometers) or as 320 nm. In accordance to most publications related to biological UV effects, the value of 315 nm has been used in the following (Diffey, 2004).

Only about 8 % of the extraterrestrial solar radiation is within the UV spectral region (Iqbal, 1983), even a smaller portion reaches the surface. However, due to the inverse proportionality between wavelength and photon energy, the energy of a single photon is high enough to break up chemical bonds of various molecules. This also induces potential for biological hazards. Since UVC usually does not reach the surface, UVB is the part of the UV radiation which is regarded as most harmful for life on the surface.

2.3 CIE-weighting function

The effect of UV radiation on biological systems is usually described by weighting functions. These weighting functions define how strong the different wavelengths contribute to the overall biological effect of interest. For the UV effect on human skin (E_{ery}), a standard weighting function has been defined by CIE (Commission Internationale de l'Eclairage) (Long, 2003). The weighting function for human skin is presented in Equation 2.4, taken from McKinlay and Diffey (1987) and also illustrated in Figure 2.2.

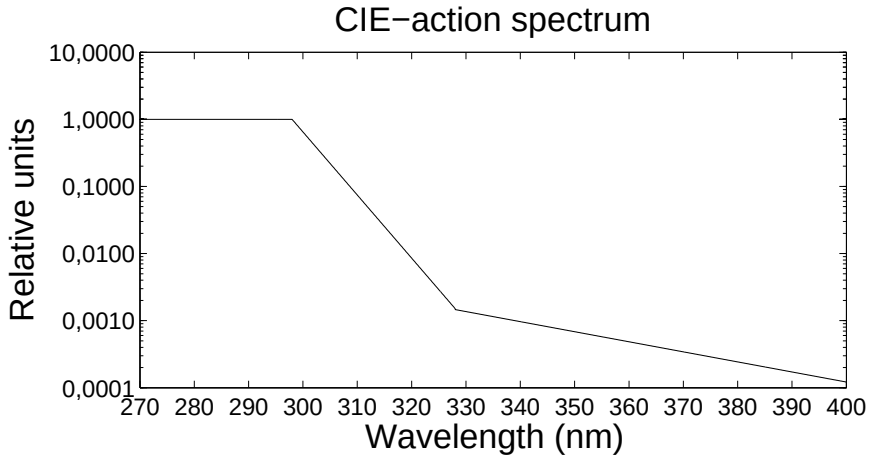

Figure 2.2: *Action spectrum for UV induced erythema (sunburn) in human skin (Equation 2.4).*

$$E_{ery}(\lambda) = E(\lambda) * \begin{cases} 1 & \text{for } 250 \text{ nm} < \lambda \leqslant 298 \text{ nm}, \\ 10^{0.094(298-\lambda)} & \text{for } 298 \text{ nm} < \lambda \leqslant 328 \text{ nm}, \\ 10^{0.015(139-\lambda)} & \text{for } 328 \text{ nm} < \lambda \leqslant 400 \text{ nm}, \end{cases} \tag{2.4}$$

The action spectra has its highest efficiency of 1 below 298 nm, and then decreases rapidly until 328 nm. For longer wavelengths in the UVA the relative efficiency is negligible. This means that UVB induces most of the sunburn (erythema) on the skin.

The biological effect depends not only on the weighting function, but also on the available radiation, as shown in Figure 2.3. The figure presents both the spectral unweighted irradiance modeled with STARsci (see Chapter 3.1) and the corresponding CIE-weighted irradiance for a cloud free day in Bergen (60.38^{o}N, 5.33^{o}E). The calculation is made for summertime conditions with solar elevation of 51^o, total ozone content of 340 DU (Dobson Units), surface pressure of 1013 hPa, and aerosol optical depth of 0.1 in a maritime clean atmosphere.

It can be seen that the wavelength range around 310 nm is most important, although the spectral irradiance in this region is quite low. The UVA region ($\lambda > 315nm$) also contributes to the biological effect. Here, the low values of the weighting function are compensated for by high irradiance levels.

On the basis of the CIE-weighting function, the UV-index has been defined by WMO (World Meteorological Organization) and WHO (World Health Orga-

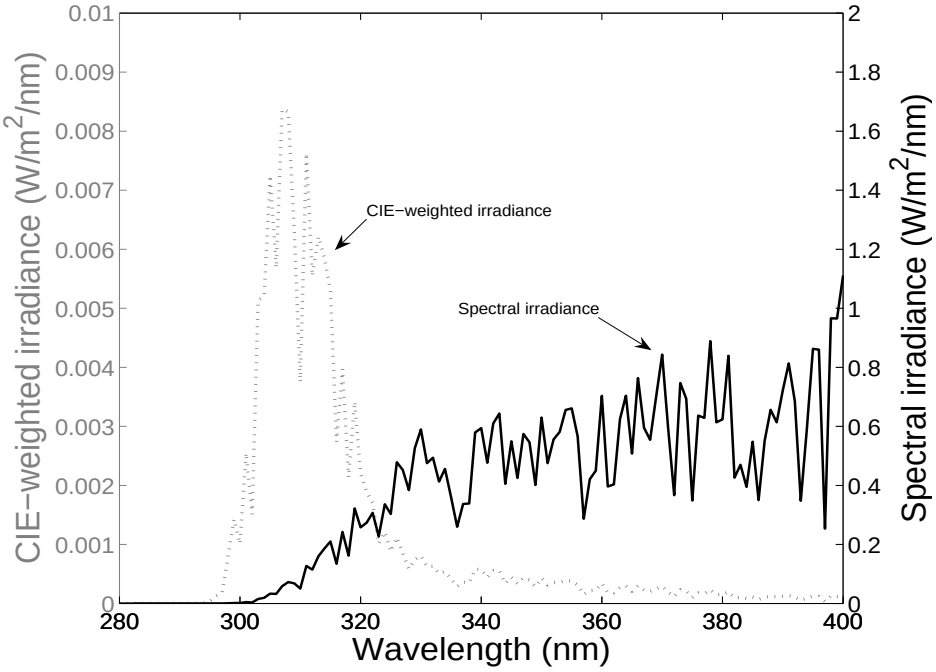

Figure 2.3: *Modeled spectral global irradiance (using STARsci; see Chapter 3.1) for Bergen (60.38°N, 5.33°E) for a cloud free day with solar elevation of 51° (solid curve) and the corresponding erythemally weighted irradiance using the CIE-action spectrum (dotted curve).*

nization) (Long, 2003). It is the erythemally weighted irradiance, multiplied by 40 m^2/W to give a dimensionless number.

$$UVI = \int E_{ery}(\lambda)d\lambda * 40 \tag{2.5}$$

In this thesis the UV-index will not be used. All irradiances are presented in W/m^2. Time integrated values, i.e. exposures are given as J/m^2.

2.4 Parameters affecting UV radiation

2.4.1 Solar elevation

The solar elevation determines the path length of photons through the atmosphere. For low solar elevation the radiation has a longer path length to travel to reach the ground. This results in a higher probability for the radiation to become scattered or absorbed. High solar elevation gives a short path length through the atmosphere and low extinction probability, which gives higher radiation at the ground.

The solar elevation is the main reason for both the daily and seasonal variations in UV at the ground. The clear sky values are largest at solar noon at summer solstice in the northern hemisphere for latitudes northwards of 23.45^oN, this because of the declination of the earth.

2.4.2 Ozone

More than 90 % of the total ozone column is found in the stratosphere, between 10-50 km altitude. However, the maximum concentration is between 20-35 km. The total amount of ozone at standard atmospheric pressure and temperature will amount to a layer of only 3-4 mm, corresponding to 300-400 Dobson Units (DU).

Ozone has several absorption bands both in the UV, visible and in the infrared regions. The strength of the absorption in these bands are dependent on the amount of total ozone. For UV radiation the shortest wavelengths are absorbed in repeated absorption processes. When a UV photon collides with oxygen atoms, the energy of the photon is absorbed. For wavelengths up to approximately 290 nm the ozone layer is almost opaque, for longer wavelengths the attenuation diminishes rapidly, and for wavelengths longer than 350 nm the ozone becomes transparent (Iqbal, 1983). If the ozone content decrease, less collisions will occur and a smaller part of the UV radiation is absorbed. Then a larger amount of the UV radiation reaches the ground.

The highest concentration of ozone is found in the mid-to-high latitudes of the northern and southern hemispheres in spring. Lowest concentration is found in autumn, as shown in Figure 2.4. March is the month with the largest climatological values (Iqbal, 1983). This is because of the stratospheric wind patterns known as the Brewer-Dobson circulation, shown in Figure 2.5. The main part of the ozone is produced in the tropics, and then

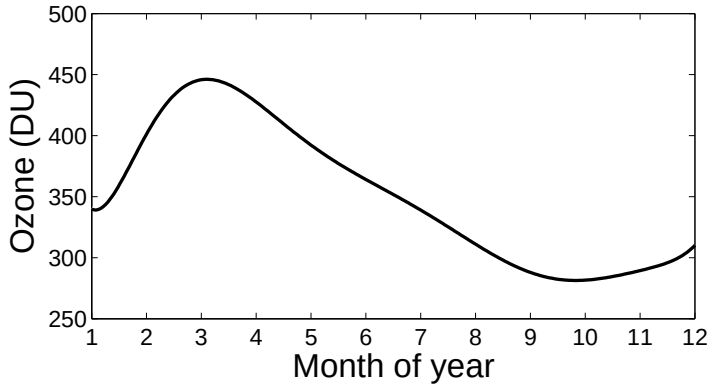

Figure 2.4: *Yearly ozone variation from climatological data, taken from Iqbal (1983) for 70° N.*

transported to higher latitudes by the stratospheric circulation. The ozone is then transported downward into the lower stratosphere where it accumulates. The ozone layer is found at a higher altitude in the tropics than in the polar regions because of this mechanism. There is a time delay of several months from when the ozone is produced to it reaches the high latitudes.

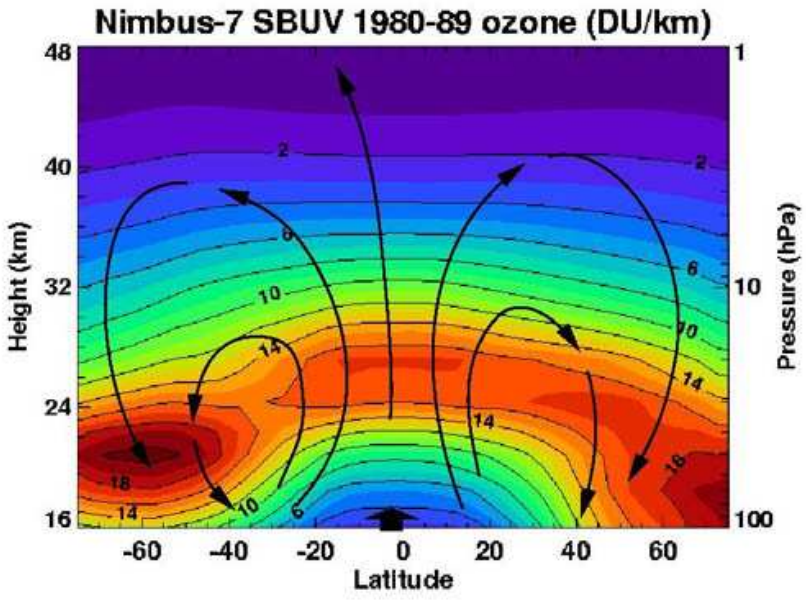

Figure 2.5: *Dobson-Brewer circulation in the stratosphere (NASA, 2005).*

The radiation amplification factor (RAF) describes how much the radiation

changes when the total ozone amount is changed by 1 %. The RAF for erythemally weighted UV is 0.7-1.2 (Madronich and De Gruijl, 1994), depending on solar elevation. Thus when the ozone amount decreases by 1 % the erythemally weighted UV is increased by 0.7-1.2 % for a cloud free atmosphere. The integral UVA radiation has a RAF of 0.02 (United Nations Enviromental Programme, 1998), and is therefore nearly unaffected by ozone. The integral UVB radiation has a RAF of 1.5-2.3 % (Lim and Cooper, 1999).

2.4.3 Turbidity

The turbidity of the air affects UV radiation with respect to scattering and absorption. The turbidity due to aerosols is highly variable in time and space, from clean air to heavily polluted. Anthropogenic pollution, desert dust, biomass burning and volcanic eruptions contribute to this. Most of the aerosols are located in the troposphere, but for the volcanic eruptions there is also a major contribution to the stratospheric aerosol content. The stratospheric aerosols might enhance UV radiation at the ground significantly because they can lead to a decrease in ozone. Aerosol particles contribute to the absorption and scattering of UV, where the attenuation of UV radiation due to aerosols is largest for small particles (Iqbal, 1983). Low visibility, which means high turbidity (large number of particles), will also contribute to an attenuated radiation because of an increased optical depth.

Aerosol types:
Polluted air contain large amounts of soot and mineral particles which are strong absorbers. This results in a warming of the layer. Other types of air have more particles that scatter the radiation. The polluted air has a large amount of aerosols with diameter below 1 μm.

Continental air has the main aerosol sizes in the range 0.01-1.0 μm, consisting of aerosols from windblown dust and emissions from industries. The amount of aerosols, however, is less than for polluted air.

Maritime air has the least amount of aerosols, and the aerosols mainly consist of salt particles. These particles are fairly big, and does not contribute to as much attenuation of UV as the smaller particles (Wallace and Hobbs, 1977).

Figure 2.6 illustrates the aerosol effect on erythemal UV as a function of the aerosol optical depth. As the aerosol optical depth increases the differences between the aerosol types get more pronounced. For aerosol optical depth of 0.3, a change in aerosol type from maritime clean to urban, reduces

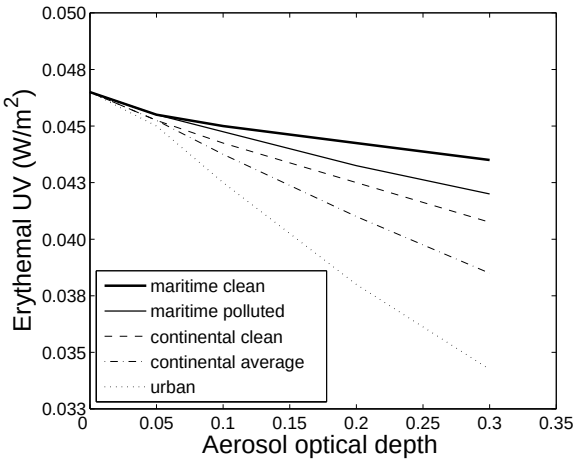

Figure 2.6: *Erythemal UV vs aerosol optical depth for different aerosol types (in the STAR-model) for solar zenith angle of* 60^o *and total ozone amount 350 DU (adapted from Sætre (2006))*

erythemal radiation by 20 %.

2.4.4 Surface albedo

Increasing ground albedo, means increased reflection, which results in an enhancement of the diffuse part of UV irradiance due to multiple scattering. The reflective properties of the ground strongly depend on the structure and material of the surface. The wavelength dependence of the local spectral albedo in the UV region is low, though the albedo shows a slight increase towards longer wavelengths. Natural surfaces, except snow, have quite low spectral albedo, less than 0.05. The albedo for snow can vary considerably, from 0.4 to close to 1, where the age, moisture content, snow depth and surface structure are the decisive factors.

In a cloudless case, an increase of surface albedo from 3 % (snow free ground) to 80 % (snow covered ground) would result in an wavelength dependent UV irradiance enhancement of 30-40 %. The maximum albedo effect is around 320 nm. Towards longer wavelengths in the UVA region, the albedo effects decreases due to decreased Rayleigh backscattering. In the UVB region, the albedo effect decreases due to ozone absorption of backscattered photones (Koepke et al., 2002).

2.4.5 Clouds

In the presence of clouds, UV radiation is influenced in a more complex way. This depends on whether there is a homogeneous cloud layer or scattered clouds.

For overcast conditions, the irradiance below the cloud depends largely on the optical depth of the cloud and not so much on the height of the cloud base. Low clouds usually have a higher optical thickness than medium-high or high clouds. Low cumulonimbus (Cb) clouds can have optical thickness of 100 times that of a high cirrus cloud. A cloud modification factor (CMF) defines the influence the clouds have on the UV irradiance compared to the clear sky UV irradiance. CMF is shown in Figure 2.7 for high, medium-high and low clouds at a wavelength of 380 nm and solar zenith angle varying between 80-30^o. For cirrus clouds, the cloud effect on the UV radiation is marginal (CMF $\approx$ 0.9). However, for the Cb clouds, the cloud effect is significant, CMF lower than 0.2, i.e. more than 80 % reduction of the UV radiation. Normal medium-high and low clouds have CMF closer to 0.55, i.e. 45 % reduction (Koepke et al., 2002). As shown in Figure 2.7, the UV radiation decreases with increasing cloud amount for all cloud levels. For high clouds, there is also an overall increase in radiation with decreasing solar elevation. For medium-high and low clouds, the solar elevation dependency is more complex as it depends on the cloud amount. Besides, in the UV region, there is also an increasing cloud effect with decreasing wavelength.

For scattered clouds the UV-irradiance depends on the position of the cloud in the sky relative to the sun and the observer. Scattered clouds gives a clear solar elevation dependency for high cloud amount for medium-high clouds, where the attenuation is strongest for high solar elevation. If the solar disk is visible during scattered cloudiness the UV radiation can sometimes exceed the cloud free amount, because the diffuse radiation can be enhanced by reflection from the edge of nearby clouds.

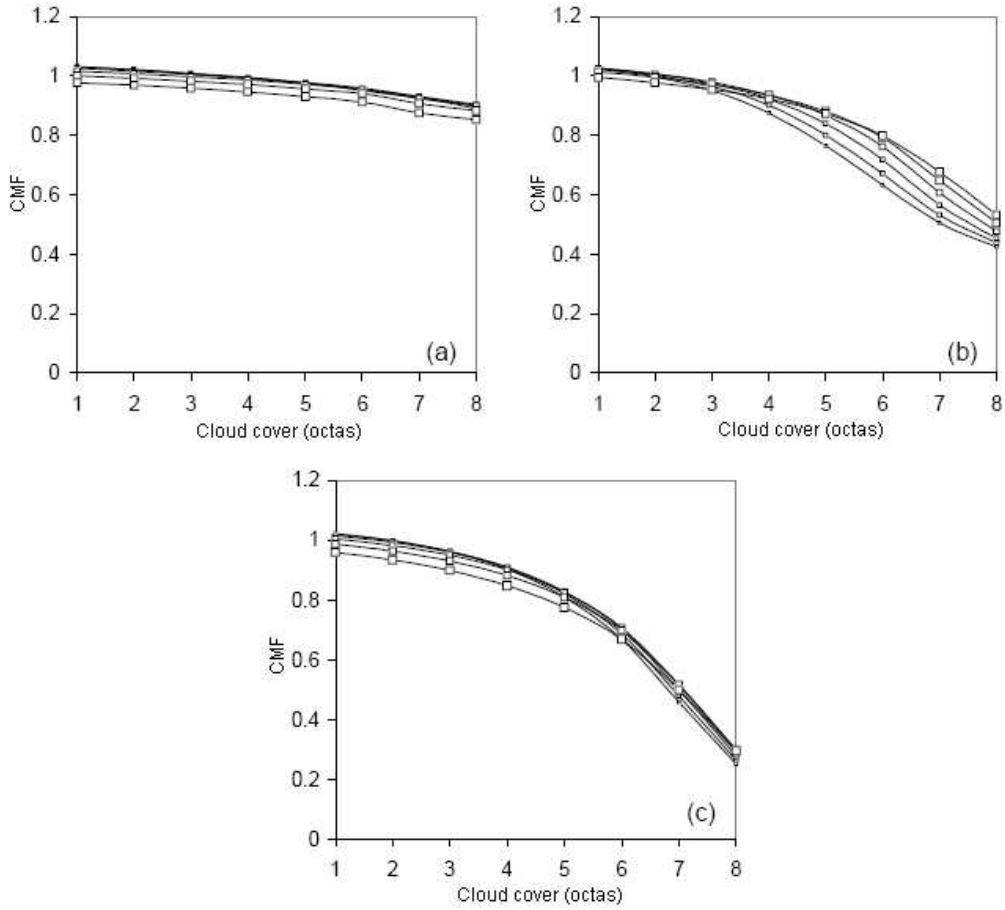

Figure 2.7: *Cloud modification factors for high (a), medium-high (b), and low (c) clouds for varying cloud amount at 380 nm for solar zenith angles (sza) 80-30º. Largest squares denote sza of* 80^o *and smallest squares denote sza of* 30^o *(adapted from Schwander (1999))*

2.5 Skin cancer

Skin cancer is divided into three groups; basal cell carcinoma (BCC), squamous cell carcinoma (SCC) and cutaneous malignant melanoma (CMM). Although there are differences between these cancer forms, UV radiation is assumed to be a common main risk factor (Armstrong and Kricker, 1993; Autier and Dore, 1998; Smedby et al., 2005).

The cancer type focused on here is CMM, also known as mole or nevi cancer, shown in Figure 2.8. This is not the most common type of skin cancer, however, it is the most lethal one.

Figure 2.8: *Malignant melanoma (Kreftforeningen, 2007)*

CMM develops from the pigment producing cells called melanocytes, which are located in the dermis layer of the skin. The cancer cells then grow and invade healthy tissue and disrupt their functions. The cancer cells are detectable on the skin surface, but the melanoma can grow deeper and thus, spread to other locations or organs by the blood.

Although CMM occurs predominantly in white population, the geographical differences are large. The variation in incidence rates and studies of migrant groups has revealed valuable information about its aetiology (Khlat et al., 1992; Iscovich and Howe, 1998; Parkin and Klath, 1996). The high incidence in Australia illustrates the vital importance of UV exposure. In Europe, the incidence rates in the Nordic countries are higher than the rates at lower latitudes in the southern Europe. This could be due to intermittent exposure as well as susceptibility in the populations (Autier et al., 1994; Moan et al., 1999). Additionally, the thickness of the ozone layer may play a significant role (Moan and Dalback, 1992). Local traditions of time spent outdoors, patterns of vacations, sunbathing and clothing fashions are revealed to influence

the melanoma risk (Chen et al., 1996). Excessive sun exposure, especially severe blistering sunburns early in life, seem to promote melanoma development. The risk of CMM is increasing by increasing age. Freckles, nevi and number of sunburns are factors that are associated with CMM (Longstreth et al., 1998).

Melanoma can occur any place on the body surface, even in places not directly exposed to the sun, like the eyes, mouth, genitals, or internal organs. However, the most common locations are head and upper body in men and legs and arms in women (Kreftregisteret, 2007). Melanoma is usually brown or black in color. It can arise from a pre-existing mole, or appear on previously normal skin. Melanomas grow slowly and therefore, growth, changes, or irregular lesions should arouse suspicion.

For information to the public an ABCD rule has been developed and published about how to discover and identify melanomas (Kreftforeningen, 2007).

- **A**symmetry - One half is different from the other. Melanomas are usually asymmetric.
- **B**order Irregularity - The edge, or border, of melanomas are usually ragged or blurred.
- **C**olor - Single mole will be only one color, but there are often a variety of colors within the same melanoma.
- **D**iameter - While moles remain small, melanomas continue to grow to more than 1/2 cm in diameter.

All of these features can be found in Figure 2.8.

Chapter 3

Methods and Data

The first part of this chapter describes the reconstruction of UV radiation by use of the radiation transfer model STAR and the compilation of the required input data. In the next part, UV measurements and model calculations used for comparison with STAR results in Chapter 4, will be presented. Finally the cancer data provided by the Cancer Registry of Norway will be described. These data will be used for the correlation with the reconstructed UV radiation in Chapter 4.3.

3.1 STAR model

STAR (System for Transfer of Atmospheric Radiation) is a radiation transfer model developed at the Meteorological Institute, University of Munich, Germany. It is based on a one-dimensional radiation transfer algorithm from Nakajima and Tanaka (1988) that solves the equations for radiation transport by using the method for discrete ordinate and addition. The model was developed for use in research on photo biological and photochemical effects of UV radiation.

STAR is available in two versions, STARsci (Ruggaber et al., 1994) and STARneuro (Schwander et al., 2002). STARsci calculates UV irradiance for cloud free atmosphere or in the presence of a homogeneous cloud layer. The model is developed for reconstructing the part of the UV radiation that can penetrate down to the ground (UVA and UVB) but it also extends into the visible region.

The model calculates spectral irradiance which can be integrated using arbitrary biological weighting functions. The weighting functions of erythema

of human skin, for DNA damage and plant damage are already included. User-defined weighting functions can be added.

To reduce the computational time, STARneuro uses neural network techniques, one for reduction of wavelengths and one for cloud effects. For the wavelength reduction network the model is run for 7 different wavelengths in the UV and visible wavelengths (290-610 nm) and then the neural network algorithm replenishes the rest of the wavelengths (280-700 nm) to give a high spectral resolution to a full spectrum without significant loss of accuracy (Schwander et al., 2001).

STARneuro can calculate irradiances for any cloud amount and/or cloud type in the atmosphere. The cloud effect is described by a CMF that represent the ratio between the radiation in the presence of clouds and the radiation under a clear sky with otherwise identical atmospheric conditions. The wavelength dependent CMF is determined on the basis of a second neural network algorithm. The model then provide a spectrally resolved and weighted irradiance under the condition of the cloud description. The underlying neural network has been trained by spectral UV radiation measurements and parallel cloud observations at Garmisch-Partenkirchen, Germany (Schwander, 1999).

STARneuro offers different combinations of cloud related input parameters:

i) Only total cloud amount.
ii) Cloud amount and type of low, medium-high and high clouds.
iii) As ii) but with additional flag if the solar disk is visible.
iv) Total cloud amount and global radiation measurements.
v) Total cloud amount and luxmeter measurement.

The input type ii) has been used for most of the UV reconstruction in this work. The input type i) has also been applied for reconstruction of a period (1981-1997) for Oslo, as only total cloud cover was available (discussed in Chapter 4.1.1). These methods, with only cloud information as input, are more applicable than other reconstruction models since there are more stations observing clouds than for instance stations measuring global radiation.

3.2 Input data to STAR

In the following sub-chapter details about the required input parameters, like solar elevation, ozone, turbidity, ground albedo, and cloud information, will be described.

3.2.1 Solar elevation

The solar elevation is defined by the coordinates of each station and date and time of the day. However, as the topography around the stations is not included, there is no exact information on whether the sun is below the horizon or not.

3.2.2 Ozone

Both the spatial and temporal distribution of total ozone measurement stations are limited. For Norway there have only been 6 measurement sites in the period 1957-2005, and 4 of them are situated on Svalbard. For a long and narrow country such as Norway, these stations are not representative for the whole country. Since ozone is an important parameter when reconstructing UV, a way of overcoming this problem was to use data from other available stations and then interpolate between the different stations.

20 stations from the database WOUDC (World Ozone and Ultraviolet Radiation Data Center) were inside the area limited by Denmark (55^oN) in the south, Svalbard (80^oN) in the north, England (10^oW) in the west and Russia (40^oE) in the east. The available stations can be found in Table A.1 and Figure A.1. Further, the Cressmann interpolation (IRI, 2006) is used to interpolate between all the stations to get the most representable values for each county.

The Cressmann interpolation is a sophisticated interpolation method where the ozone value is weighted as a function of the distance between the ozone stations and the target point. If there are several sites with observed total ozone amount, the station nearest the target point carry most weight and the weighting of the other stations decrease as the distance increase.

The weight of each station is controlled by two variables, the maximum distance, R, (where the weight equals 0) and the distance between the station and the target point, r. The weight W is given by:

$$W = \exp((-r^2)/(0.1 * R^2)) \tag{3.1}$$

It was then made sure that the sum of the weights equal 1 to get a correct weighting of the data. An example of an interpolation is shown in Figure 3.1. When the R in the denominator in Equation 3.1 is multiplied with 0.1, it means that the most weight is put on the nearest site.

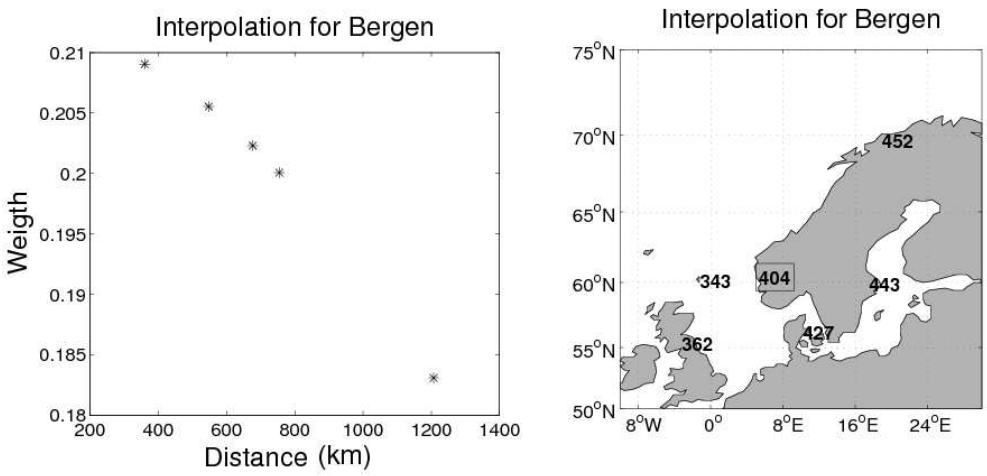

Figure 3.1: *Interpolation for Bergen for 2/3-1958 using the Cressmann interpolation. Weighting function (W) vs distance to ozone measuring station (left). Placement and O_3-amount (right).*

Tromsø file

The most complete of all available ozone data series in the study, were for Tromsø. This is the second longest total ozone series of the world, dating back to 1935. The dataset was received from Georg Hansen at NILU and documented by Svenøe (2000). Up until end of 1972 a Dobson Spectrophotometer was used for recording. The Dobson series have missing data for the period 1973-1984, but the latter part of this period can be replaced with TOMS (Total Ozone Mapping Spectrometer) satellite data starting from 1979. The Dobson measurements started up again in 1985 and lasted until end of 2001. From June 1994 a Brewer instrument was also running parallel to the Dobson spectrophotometer. In March 2000 the Brewer instrument was moved to the ALOMAR observatory at Andøya Rocket Range, 150 km southwest of Tromsø.

To get a complete ozone dataset for Tromsø for the period 1957-2005 both

Dobson, Brewer and TOMS data were used. The ground measurements had the highest priority and the satellite measurements were used to fill in gaps from 1979.

The TOMS data are taken from the NIMBUS-7 satellite. TOMS does not measure the ozone amount directly in the atmosphere, but uses a radiation model to calculate a theoretical reflected irradiance from the ground as a function of ozone amount, latitude, visibility-field and ground albedo. By comparing the theoretical and measured radiance, the algorithm can estimate the ozone amount needed to give the same radiance as the one measured by the instrument (McPeters et al., 1996). From Carlson (2005) there has been implied that TOMS has a mean bias of +2.2 % compared to the Brewer measurements, and a mean bias of +0.45 % compared to the Dobson measurements.

The Dobson data were of highest priority since Dobson instruments were the first instruments used, and besides, to keep the dataset as homogeneous as possible. Both Dobson and Brewer are ground based measurements while TOMS is satellite based. TOMS data had then the lowest priority of these measurements and are only used in the period 1979-1984. For periods with no measurements, a monthly average for the actual "decade" was used ("decades" were divided into 1957-1965, 1966-1975, 1976-1985, 1986-1995 and 1996-2005).

From 2002 ground based Brewer data from Andøya were used. For missing days in December and January, 300 DU (Dobson Units) were used since the sun is below the horizon (no observations missing in November). For the rest of the year the monthly "decadal" average mentioned above were used.

Tromsø data

When studying the yearly mean of ozone for the whole period, 1957-2005, a clear decreasing trend can be seen (Figure 3.2a). By analyzing 5-year running averages, the trends are shown more clearly (Figure 3.2b). Before 1980 there was an increase in the total ozone amount. Then, in the years to come the depletion was significant until the mid 1990's. 1993 was the year of minimum ozone content over Tromsø. For the years afterwards, the ozone amount increased again. For the whole globe (Figure 3.3, taken from the Scientific Assessment of Ozone Depletion of 2002, WMO (2003)), the same trends can be found. The minimum of total ozone is found in the years 1993-1994. The largest negative trend is found in the years 1980-1993. The

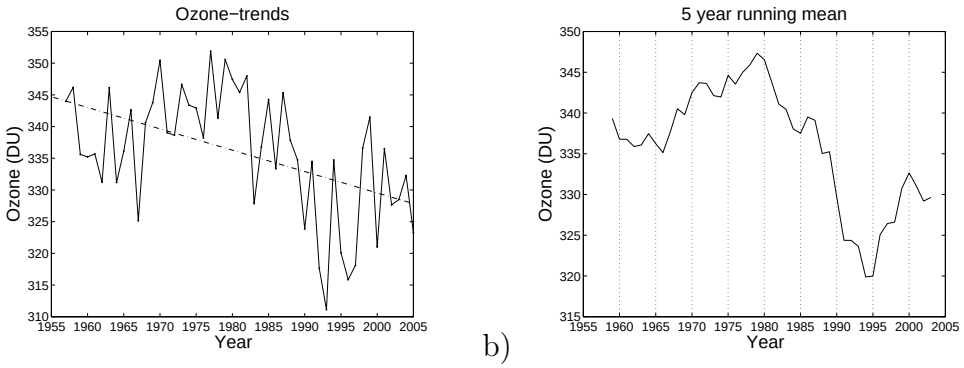

a) b)

Figure 3.2: *a) Yearly mean ozone values with trends (._.) for the periods 1957-2005. b) 5 year running mean for the same data*

positive trend afterwards is maybe the first sign of "recovery" of the ozone-layer. The positive trend can be seen until the end of the period (1993-2005). Since, the previously mentioned modifications have been made to the Tromsø

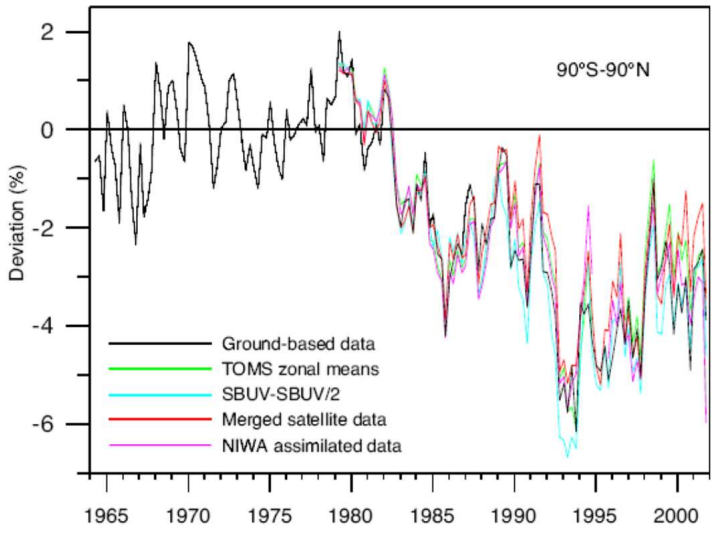

Figure 3.3: *Deseasonalized, area-weighted seasonal (3-month average) total ozone deviations (Figure 4-2 from WMO (2003))*

dataset, a comparison with the changes found in the assessments of ozone depletion in WMO (2003, 2006) has been made. The assessments can not be directly compared to the Tromsø dataset, because a deviation from the pre-1980 average and not the absolute values are given in Figure 3.2. The two figures, however, show a close resemblance. Thus, the modifications done to the Tromsø dataset agree reasonably to the average for the rest of the world.

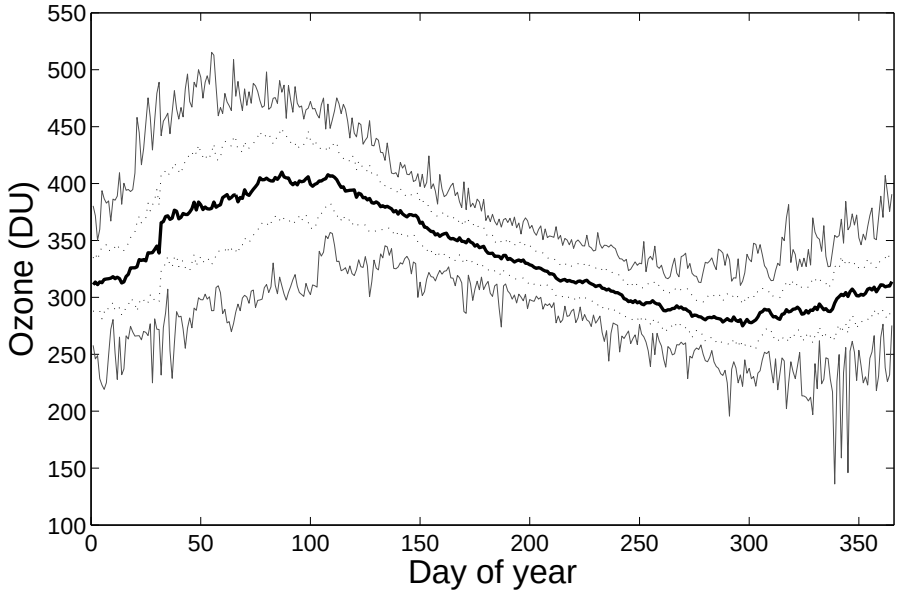

Figure 3.4: *Variations in the daily ozone measurements for Tromsø in the period 1957-2005. Mean value for each day (bold black line), ± 1 standard deviation (dotted lines) and maximum and minimum values (thin grey lines).*

Figure 3.4 shows how the total ozone amount varies throughout the year in Tromsø for the period 1957-2005. As described in Chapter 2.4.2, the maximum total ozone content is found in spring and the minimum in autumn. In addition to having the maximum ozone content, the largest year-to-year variations are also found in spring. This can be seen from the curves of maximum, minimum and the standard deviation in Figure 3.4.

From January 31. to February 1. there is a discontinuity in Figure 3.4. The reason for this is that large amounts of missing data in January, by technical reasons, are replaced with 300 DU, which result in a lower mean value. For most of the month the sun is below the horizon in Tromsø, so this discontinuity will only increase the radiation negligibly compared to the February values. For southern stations, the lower ozone amount will give a somewhat larger increase in the UV, but for interpolated ozone values, the Tromsø data will be the least weighted value because of the large distance to the southern stations.

The three extreme minimum values are found in December of 1959 (136

DU for 5/12) and 1960 (159 DU for 8/12 and 146 DU for 11/12). There are no explanations for this in literature.

The monthly variation in ozone per decade for the 17 selected stations covering most of Norway can be seen in Table 3.1. For the entire period, 1957-2005, there are only slight variations between the different stations. This is as expected since the ozone amount for the other stations are interpolations between stations that show similar trends. The largest reduction can be found in February and March, with predominantly a decrease of about 2.5 % per decade. On the other hand, when looking at the trends for Oslo, which only has data for the period 1957-1980 (Figure 3.5), it is clear that the ozone depletion occurs after 1980 (as can also be seen in Figure 3.2a)). If the same figure had been shown for Tromsø for the same period, the linear trend would be similar to that of Oslo. For Oslo, Table 3.1 shows a decrease in February, and almost no change for January and March, which can be found when looking at the whole period (1957-2005). For the rest of the year there is an increase. The shorter periods for Oslo, Færder Fyr and Rena are because of limitation when it comes to cloud information (explained in Chapter 3.2.5).

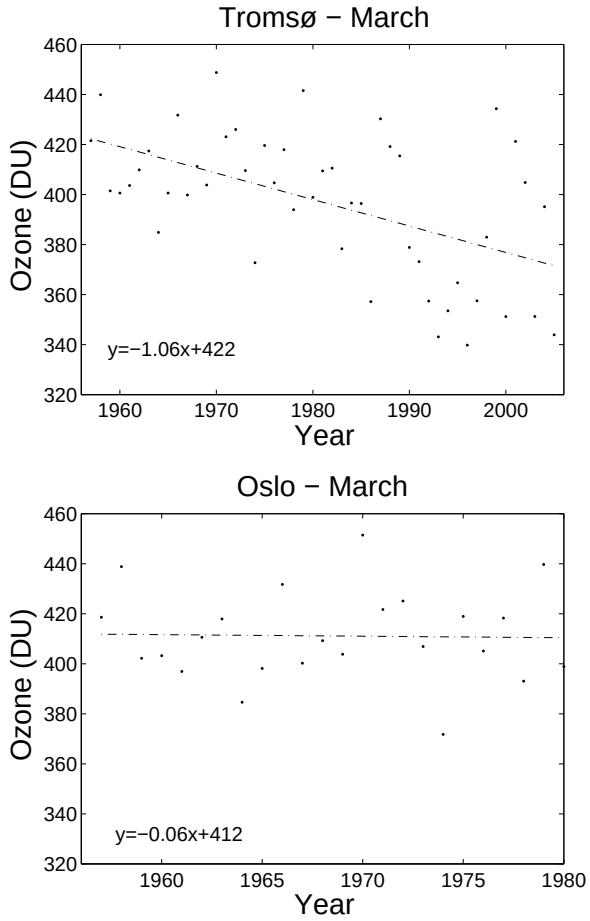

Figure 3.5: *Monthly averages of total ozone for March for Tromsø (upper) and Oslo (lower). In addition linear regression lines are given.*

Table 3.1: *Trends in totalozone in % per decade for the period 1957-2005 for the 17 stations, listed from north to south.*

Station	**Jan**	**Feb**	**March**	**April**	**May**	**June**	**July**	**Aug**	**Sept**	**Oct**	**Nov**	**Dec**
(16) Tromsø	-1.3	-2.5	-2.5	-1.7	-1.0	-0.4	-0.6	-0.1	-0.2	0.3	-0.3	-0.1
(17) Sihccajavri	-1.3	-2.5	-2.5	-1.7	-1.0	-0.4	-0.6	-0.1	-0.2	0.3	-0.3	-0.1
(15) Bodø	-1.4	-2.5	-2.5	-1.7	-1.0	-0.5	-0.6	-0.2	-0.3	0.2	-0.3	-0.2
(13) Ørland	-1.4	-2.5	-2.5	-1.7	-1.0	-0.5	-0.6	-0.2	-0.3	0.2	-0.3	-0.2
(14) Værnes	-1.4	-2.5	-2.5	-1.7	-1.0	-0.5	-0.6	-0.2	-0.3	0.2	-0.3	-0.2
(12) Tafjord	-1.6	-2.7	-2.5	-1.6	-0.9	-0.5	-0.4	-0.3	-0.3	0.1	-0.5	-0.5
(11) Rena - Haugedal*	-1.6	-2.2	-2.5	-1.8	-0.9	-0.4	-0.7	-0.2	-0.2	0.2	-0.4	-0.4
(10) Takle	-1.6	-2.7	-2.5	-1.6	-1.0	-0.5	-0.4	-0.3	-0.3	0.1	-0.5	-0.5
(9) Bergen - Florida	-1.5	-2.5	-2.5	-1.6	-1.0	-0.5	-0.6	-0.3	-0.3	0.2	-0.3	-0.3
(8) Gardermoen	-1.5	-2.5	-2.5	-1.6	-1.0	-0.5	-0.6	-0.3	-0.3	0.2	-0.3	-0.3
(7) Oslo*	-0.0	-2.2	-0.2	2.1	0.1	0.1	0.5	0.6	2.5	3.2	3.8	4.0
(6) Lyngdal - Nummedalen	-1.5	-2.5	-2.5	-1.6	-1.0	-0.5	-0.6	-0.3	-0.3	0.2	-0.3	-0.3
(5) Rygge	-1.5	-2.5	-2.5	-1.6	-1.0	-0.5	-0.6	-0.3	-0.3	0.2	-0.3	-0.3
(4) Tveitsund	-1.5	-2.5	-2.5	-1.6	-1.0	-0.5	-0.6	-0.3	-0.3	0.1	-0.3	-0.3
(3) Færder Fyr*	-1.6	-2.6	-2.4	-1.6	-1.1	-0.5	-0.6	-0.2	-0.3	0.4	-0.4	-0.4
(2) Sola	-1.5	-2.5	-2.5	-1.6	-1.0	-0.5	-0.6	-0.3	-0.4	0.1	-0.3	-0.3
(1) Kjevik	-1.5	-2.5	-2.5	-1.6	-1.0	-0.5	-0.6	-0.3	-0.3	0.1	-0.3	-0.3

*Shorter periods: Rena; 1958-2005, Oslo;1957-1980, Færder Fyr;1957-2003

3.2.3 Turbidity

Aerosol type:
Norway has a long coast line, and thus 14 of the 19 counties have a climate strongly influenced by the sea. To keep the model setup as simple and similar for all stations as possible, the maritime clean (mc) aerosol type was used for all stations. Besides, Norway does not have the typical large cities, so the large pollution will not occur. In addition, how the UV-level varies in time is of more interest than the absolute radiation values. The choice of one similar aerosol type is justified.

Aerosol optical depth:
The southern stations (numbers 1-14 from Table 3.1), were given fixed time dependent quantities, but with seasonal variation shown in Table 3.2. The aerosol optical depths at 550 nm were decided from the article of Olseth and Skartveit (1989). For all stations, winter is defined as December-February,

Table 3.2: *Aerosol optical depth for different seasons.*

	Winter	**Spring**	**Summer**	**Autumn**
Southern Stations	0.10	0.15	0.20	0.15
Northern Stations	0.05	0.05	0.10	0.05

Spring as March-May, Summer as June-August, and Autumn as September-November.

The humidity will also affect the aerosols by swelling for increasing humidity. Here a standard humidity profile for mid-latitudes with seasonal differences has been used.

Pressure:
The model does not have a parameter for the altitude of the stations. However, the pressure at station level (P) has been used. P then represent the amount of atmosphere that is overhead the station, and as a consequence, it affects the Rayleigh scattering and absorption. For lower pressure (higher altitude) there is less attenuation of the UV radiation because of less scat-

tering and absorption.

Some stations had missing pressure observations for a shorter period, while others had missing data all together. For single observations missing, the mean of the observations before and after were inserted. If several consecutive observations were missing, standard sea-level pressure was used because the day-to-day variations would be larger than the deviation from the standard pressure. For all stations above 40 m above sea-level, P was corrected for the station elevation, and the he equation used for the correction is:

$$P = P_0 - (H * h) \tag{3.2}$$

where (P_0) is standard sea-level pressure (1013.25 hPa), H is the elevation of the station above sea-level and h=1 hPa/8 m, which is the rate of change of pressure with height (Wallace and Hobbs, 1977).

3.2.4 Surface Albedo

Snow observations are taken once each day (at 06 UTC). This observation was used as albedo information for the whole day. For snow free conditions snow-depth and snow-cover were set to 0. The snow cover is observed in 0/4 - 4/4, and the snow depth is given in cm. Snow depth less than 0.5 cm is considered snow free when observations are taken.

STAR can not interpret the snow observations, these have to be converted into numbers in the form of albedo (α).

The default spectral ground albedo was set to 0.03 for snow free conditions. This is a typical value for vegetative covered surface (Koepke et al., 2002). The albedo of snow covered surface is strongly dependent on snow depth, snow age, and surface structure. Information on the snow age was not available. From literature the albedo values range from 0.4 to close to 1.
Depending on snow cover (SA) and snow depth (SD) observations the following albedo values have been selected for the UV reconstruction.

$$\text{SA} = 1 \Rightarrow \alpha = 0.1$$
$$\text{SA} = 2 \Rightarrow \alpha = 0.2$$
$$\text{SA} = 3 \Rightarrow \alpha = 0.3$$

For complete snow cover of the surface (SA=4) an additional snow depth dependence has been applied:

$$\begin{aligned} \text{SD} < 5 \text{ cm} &\Rightarrow \alpha = 0.5 \\ 5 \text{ cm} < \text{SD} < 20 \text{ cm} &\Rightarrow \alpha = 0.6 \\ \text{SD} > 20 \text{ cm} &\Rightarrow \alpha = 0.8 \end{aligned}$$

The choice of the albedo value given above was guided by previously published data (Iqbal, 1983; Schwander et al., 1999; Feister and Grewe, 1995).

3.2.5 Clouds

For the cloud input ii) to the STAR model, used in this study, the information on cloud amount and type in all cloud layers are needed. The information on cloud amount in the different layers is not available, so a method for this had to be developed.

Routine cloud observations for low, medium-high, and high clouds are made by the Norwegian Meteorological Institute. The cloud observations are downloaded from the eKlima database (met.no, 2006).

The goal was to find one station for each county, representative for the most populated areas and with sufficient long and continuous time-series (1957-2005) of cloud data. For several counties there was only one station possible to use, and for the counties Oppland and Aust-Agder there were no suitable stations at all. Figure 3.6 shows the selected stations for the UV reconstruction.

The cloud information from the data base included:

- Total cloud amount (NN)
- Amount of low/medium-high clouds (NH)
- Type of low clouds (CL)
- Type of medium-high clouds (CM)
- Type of high clouds (CH)

For some stations, however, there were some missing or erroneous data, which had to be edited manually. As examples, in some occasions NH exceeded NN, and sometimes one of the cloud types were missing. The data were then compared to the prior and following observations, and replaced by reasonable values.

Figure 3.6: *Overview of the synoptic stations. For more information about every station see Chapter A (Norge.no, 2007)*

The cloud amounts are observed in octas, e.g. 8 octa equals 8/8 of the sky covered by clouds. For cloud cover 1 and 7 octas the reported value is not necessary the real value. 1 octa means that there are clouds in the sky up to 1 octa even if there is only one small cloud. For 7 octas it means that the sky is not completely covered by clouds, only a small spot of blue has to show for 7 octas to be reported.

The parameter NH can represent the amount of low or medium-high clouds. If low clouds are observed, NH defines the cloud amount of low clouds cloud, otherwise it defines the amount of middle-high clouds.

Every cloud layer (low, medium-high and high) can be split into 9 classification codes. This results in a total of 27 different cloud categories divided on the three cloud layers (WMO (1987), see Appendix B).

Table 3.3 shows the conversion of the cloud types from observations into the corresponding STAR cloud code. In addition, the WMO main cloud classification is given. The STAR-code exclude one of these cloud types, Cirrocumulus (Cc). For the reconstruction, Cc is treated as Cirrostratus (Cs). This was done because the Cirrostratus has an optical thickness that is more comparable to the Cirrocumulus than a Cirrus cloud would have. In contrast to the observations, Nimbostatus (Ns) is treated as low cloud in STAR. The observations have been adapted correspondingly.

In some cases NN is reported larger than NH although only one cloud layer is observed. In such incidences another cloud layer was added for the UV reconstruction (Alto stratus (As) as middle-high, and Cirrus (Ci) as high cloud type).

As mentioned above there is no direct information on the cloud amount of the different layers (NCL, NCM, NCH; cloud amount for low, medium-high and high clouds, respectively). Therefore, a method was developed for the derivation of the required information.

If only one cloud layer has been observed, the amount of clouds in the corresponding layer is set to equal NN.

In case of two cloud layers, the cloud amount of the lower layer is set to

NH. The cloud amount for the upper layer (N_{up}) is derived by Equation 3.3.

$$N_{up} = \left(\frac{N_{upmin} + N_{upmax}}{2}\right)\downarrow = \left(\frac{(NN - NH) + NN}{2}\right)\downarrow \tag{3.3}$$

where $\downarrow$ means that the amount is rounded downwards. N_{upmin} is the lowest possible value for the cloud amount, and N_{upmax} is the largest possible value.

If three cloud layers have been observed the following equations are used:

$$NCL = NH \tag{3.4}$$

For the medium-high layer, the amount is decides by Equation 3.5.

$$NCM = \left(\frac{NCM_{min} + NCM_{max}}{2}\right)\downarrow = \left(\frac{(NN - 1 - NH) + NN}{2}\right)\downarrow \tag{3.5}$$

For the highest layer Equation 3.6 is used.

$$NCH = \left(\frac{NCH_{min} + NCH_{max}}{2}\right)\uparrow = \left(\frac{1 + NN}{2}\right)\uparrow \tag{3.6}$$

Table 3.3: *Classification of all cloud types with corresponding code for ordinary, WMO and STAR classifications*

Low clouds:	**Cu**	**Cu**	**Cb**	**Sc**	**Sc**	**St**	**St**	**Cu**	**Cb**	**Ns**
Classification code	1	2	3	4	5	6	7	8	9	X
WMO	8	8	9	6	6	7	7	8	9	X
STAR	4	4	5	2	2	1	1	4	5	3
Medium-high:	**As**	**Ns**	**Ac**	**Ac**	**Ac**	**Ac**	**Ac**	**Ac**	**Ac**	
Classification code	1	2	3	4	5	6	7	8	9	
WMO	4	5	3	3	3	3	3	3	3	
STAR	2	X	1	1	1	1	1	1	1	
High:	**Ci**	**Ci**	**Ci**	**Ci**	**Cs**	**Cs**	**Cs**	**Cs**	**Cc**	
Classification code	1	2	3	4	5	6	7	8	9	
WMO	0	0	0	0	1	1	1	1	2	
STAR	1	1	1	1	2	2	2	2	(2)	

where ↑ means that the amount is rounded upwards.

These equations make sure that the sum of NCL, NCM and NCH either equals or exceeds NN. So the method also represents overlapping of clouds in the different layers.

STAR can not handle overcast conditions (NN=8) of Cumulus, Altocumulus or Cirrus clouds. In these cases the cloud amount was just set to 7 octas.

For no reported clouds (CL=X), it means that the sky could not be observed. This is most often because of either fog or heavy precipitation (often heavy snowfall) that reduces the visibility. There is no way of deciding one or the other without more information, so a general method was used. For southerly stations (south of Nordland county) the observations from March-October and for northern stations in the period April-September where the cloud type could not be observed was set low stratus (CL6) with NN=NH=8. For the rest of the year with this incidence the cloud type was set to Cb because then it was expected to be an optically thick precipitable cloud, NN=NH=8.

Early in the reconstruction period, most stations only have observations every 6 hours during the day and no observations taken during the night. Later in the period observations are taken more often. As UV reconstruction is done as often as on an hourly basis, the first cloud observations were copied forward to the next observation. However, if the following observation was the next day, the first observation was then copied forward to midnight, while the following was copied backwards to midnight.

3.3 Lindfors model

The Lindfors model (Lindfors et al., 2007) is another method for reconstruction of UV radiation in the past. Measured global radiation, total ozone column, total water vapor column taken from the ERA-40 data set, surface albedo estimated from the snow depth, typical annual cycle of aerosol loading and the altitude of the location are used as input parameters. The Lindfors-model needs measured global irradiance as input. This model is theoretical and is only based on physical relationships determined through radiative transfer calculations. These calculations are based on the libRadtran radiation transfer package described by Mayer and Kylling (2005).

For each zenith angle, look-up-tables are calculated by the libRadtran model with varying cloud optical depth. Cloud modification factors for both the global radiation (CMF_G) and for the UV radiation (CMF_{UV}) were thus produced for numerous solar zenith angles and cloud optical thicknesses.

The model is run in three steps: (i) Simulate clear-sky irradiance, both global (G_{clear}) and UV (UV_{clear}), using libRadtran; (ii) Use the measured global radiation (G) and the simulated clear-sky irradiance to find a CMF_G according to

$$CMF_G = \frac{G}{G_{clear}}$$

and then find the corresponding CMF_{UV} in the look-up-table. (iii) Use this information to reconstruct the UV irradiance (UV_{rec}) according to

$$UV_{rec} = UV_{clear} * CMF_{UV}$$

Erythemally weighted UV according to the CIE action spectrum is used as output in this model, but the same approach can be used for reconstructing UV radiation weighted with other action spectra.

Reconstructed daily CIE-weighted values for Bergen for the period 1982-2005, made by the Lindfors-model, were provided by Anders Lindfors.

3.4 GUV

The Norwegian UV monitoring network is operated by The Norwegian Radiation Protection Authority (NRPA) and the Norwegian Pollution Control Authority (SFT) via the Norwegian Institute for Air Research (NILU). It consists of 9 measuring sites, and covers the whole country from Ny-Ålesund in the north to Landvik in the south, and from Bergen in the west to Kise in the east (shown in Figure 3.7 and Table A.2). The first station, Blindern, started recording in February 1994. In 2000 the station in Tromsø was closed down and the instruments were moved to Andøya, where a new station was opened.

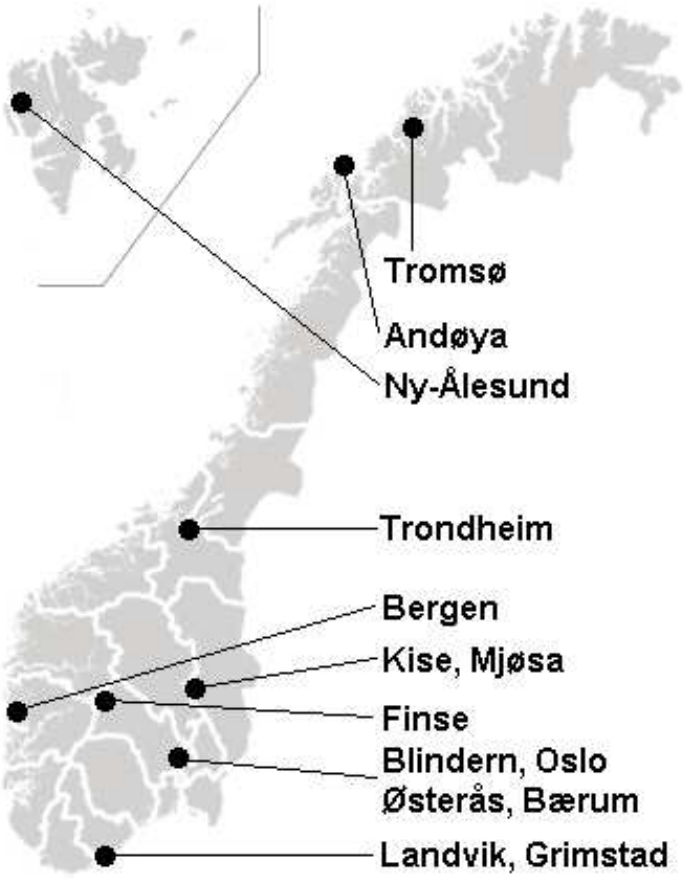

Figure 3.7: *Overview of the different UV-stations in Norway (Norwegian Radiation Protection Authority, 2007)*

The instruments used at all the stations are multi-channeled GUV (Ground-based UltraViolet radiometer) 541 from Biospherical Instruments (Norwegian Radiation Protection Authority, 2007). These sensors measure irradiance within 5 wavelength bands in the UV-region. The bandwidth is approximately 10 nm with the center at 305 nm, 313 nm, 320 nm, 340 nm and 380 nm. The GUV instruments are fully automatic and log the measured data every minute. To keep the instruments at an international standard, the instruments are calibrated every summer, and in addition, a spectral radiometer takes parallel measurements, which are compared to the GUV data at that site. The measured data allow calculation of different parameters, among these are biological effective irradiance, UV-doses and UV-index.

The instruments have shown to have an annual drift between each calibration, however, this is corrected for in the hourly values on the basis of the calibrations. The uncertainty in the measurements are within a range of $\pm$ 10 % (Bjørn Johnsen, NRPA, (personal comunication)).

Hourly CIE-weighted values are used for comparison with the modeled data in Chapter 4. Four of the stations in the measurement network were used;
Tromsø in the north for the period 1996-1999.
Landvik in the south for the period 1996-2004 (with some periods of missing data).
Oslo in the east for the period 1998-2002.
Bergen in the west for the period 2000-2004.

For leap years the 29. February was included in the provided dataset while 31. December was omitted, so that each year had the same number of days.

3.5 Cancer

The Cancer Registry of Norway is a population-based registry that has systematically collected notifications on cancer, and the registry is for practical purposes complete from 1953 (Cancer Registry of Norway, 2005).

Since 1960 all Norwegian inhabitants have received a 11-digit ID-number which is registered in the National Registry. The registry contains information on residence, occupation, education and whether or not the person has moved (Vassenden, 1987). In 1991 the National Registry was connected to the Cancer Registry for information on cancer disease. The ID-number makes it possible to register vital statistics on the entire population.

Data for cutaneous malignant melanoma (see Chapter 2.5) are used in this study. The received data set provides separate statistics for men and women for each county. The numbers are given as age-adjusted incidence rates per 100 000 inhabitants for both genders according to the world standard (Doll et al., 1966).

Chapter 4

Comparison and Trends

Using the method described in Chapter 3, UV data for 17 of the 19 counties in Norway were reconstructed for a 49 year period, 1957-2005.
Since the reconstructed data from STARneuro are instantaneous values (in W/m^2), they have to be integrated into hourly, daily, monthly and yearly values (in J/m^2) to be able to be compared to other data, and to look at specific trends. STARneuro will from now on only be referred to as STAR.
For some stations there were days of missing cloud observations, so reconstructions could not be made. To get a complete dataset of radiation, the monthly mean value of radiation for different periods were calculated and used for the missing days. To account for potential trends, means for the years 1957-1966, 1967-1976, 1977-1986, 1987-1996 and 1997-2005 have been used.

First, the reconstructed data will be compared to measured data (GUV) and other model runs (Lindfors-model). Then, the trends in the STAR-data and cancer-data will be discussed. In the last part, the correlation between UV and cancer will be investigated. The statistical equations used in this chapter are explained in Appendix D.

4.1 Observed and modeled UV

4.1.1 STAR vs GUV

GUV data for Tromsø, Landvik, Bergen and Oslo were used for the comparison between reconstructed and measured data. These four stations represents the country from north to south and west to east, respectively.

The reconstructions are not calculated for the exactly same coordinates as the GUV measurements, except for Bergen. The reason for this is that reconstructions have been made for the sites where the cloud observations were done, while the GUV instruments are not placed at the same sites. For Oslo, the GUV instrument is situated approximately 600 m south of the reconstruction site. For Kjevik, the measurements done at Landvik were used. This measuring station is situated in Aust-Agder, approximately 30 km northeast of Kjevik. In Tromsø, the nearest GUV is situated 1 km south of the reconstruction site.

When reconstructing UV data, the lowest solar elevations are always the hardest to get accurate, because just a small offset in value gives a large percentage deviation. Another reason is that the model does not take topography into account, so the question about obstacles in the horizon is a problem, especially at low solar elevations. The mountains surrounding Bergen can disturb the solar radiation up to an angle of approximately 10^o (Skartveit and Olseth, 1986). Landvik also has a similar elevation of the horizon (Planteforsk, 2007). To exclude these disturbances, solar elevations below 10^o will therefore be excluded when reconstructed and measured data are compared.

Reconstruction with cloud amount and cloud type

STAR with cloud input ii) described in Chapter 3.1, was applied when reconstructing the data used in this subsection.

Hourly values are difficult to compare since the measured data are minute values summed to hourly values, e.g. the value for 12 UTC consist of the data from 12.00-12.59, while the reconstructed data are instantaneous values from the time of the cloud observations, and then subsequently multiplied by 3600 s. Clouds can change very rapidly, and during one hour this might amount to a significant difference in accumulated UV. The solar elevation variation during the hour in question can also contribute to a difference between the reconstructed and measured data.

Figure 4.1 presents the comparison between the hourly erythemal UV from STAR and GUV for Bergen with solar elevations above 10^o for the period 2000-2004. The correlation is good, 0.90, however, the model gives an overestimation of 16 %. The overestimation is in agreement with findings of Sætre (2006) and Koepke et al. (2007). The root mean square deviation (RMSD) is 47 %. This RMSD is, however, expected since global radiation is not taken

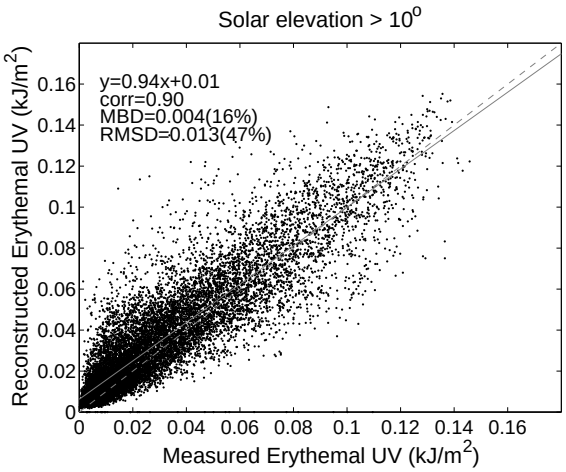

Figure 4.1: *Reconstructed (STAR) vs measured (GUV) hourly erythemal UV for Bergen with solar elevations above* 10^o *for the period 2000-2004. One-to-one line (broken line) and linear regression line (solid line) are also shown.*

into consideration when reconstructing the UV. Because of this, STAR calculates the same values for scattered cloudiness whether or not the solar disk is obscured.

Figure 4.2 shows similar results as Figure 4.1 but for different solar elevation intervals. For solar elevation below 10^o, the overestimation is quite high, 26 %. These values are small compared to the other solar elevation intervals. When comparing the mean bias deviation (MBD) of all solar elevation intervals, it is apparent that the $0 - 10^o$ interval had some disturbance in the horizon. Excluding the lower solar elevations was therefore a valid assumption. The MBD of the other solar elevation intervals have fairly similar value, so the disturbance in the horizon is probably eliminated.

Figures 4.1 and 4.2 are summed up in Table 4.1. The table shows RMSD, MBD, correlation coefficient (R) and the number of observations (n). Except for the lowest solar elevations, the statistical parameters are rather equal. The overestimation of the model is largest for intermediate solar elevations. For increasing solar elevations there is, however, a decrease in scatter (RMSD) and a slight increase in correlation.

Similar tables and figures were also made for Oslo, Kjevik and for Tromsø, however, the figures will not be shown.

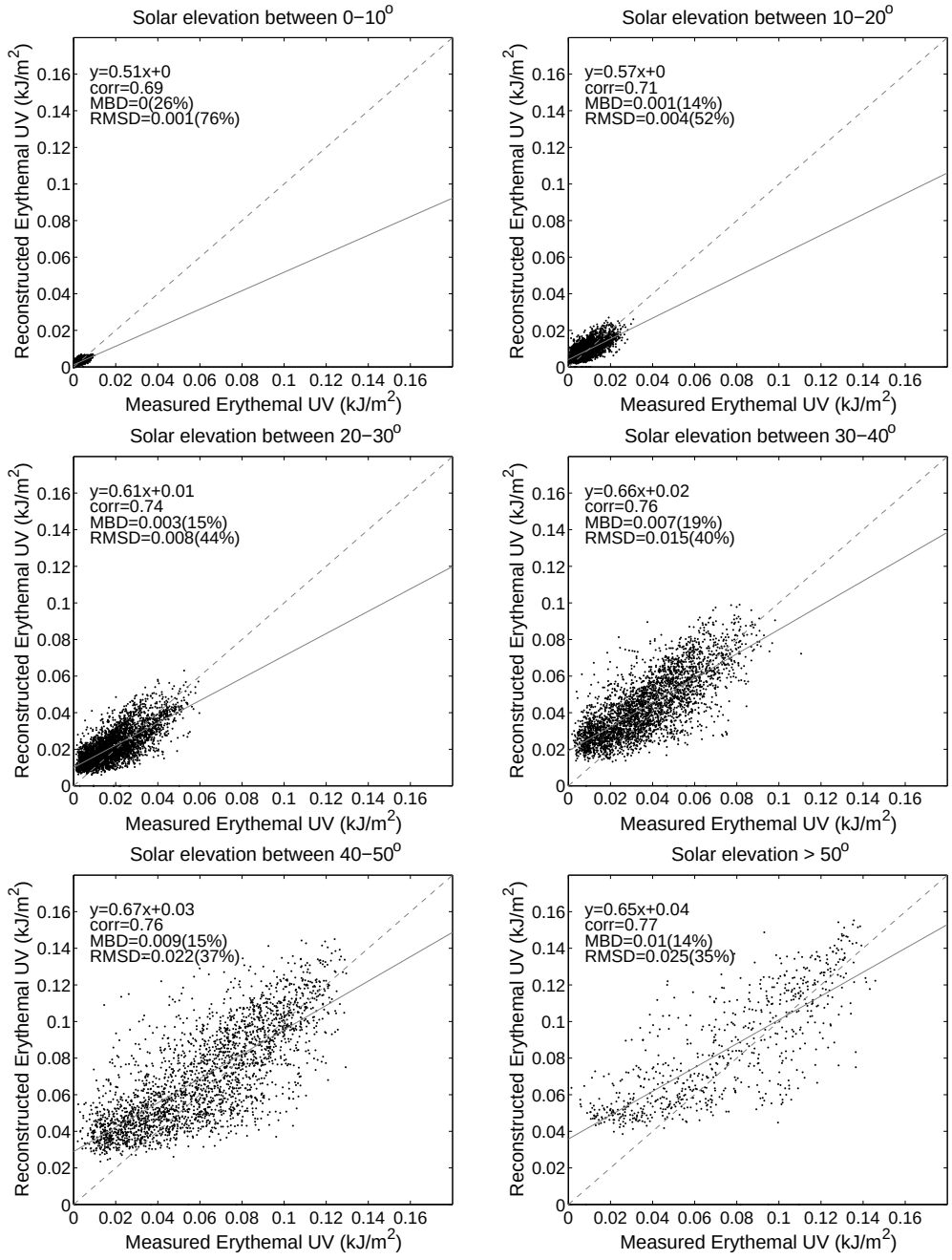

Figure 4.2: *Reconstructed vs measured hourly erythemal UV for Bergen in the period 2000-2004 for different solar elevation intervals. One-to-one line (broken) and linear regression line (solid) are also given.*

For Oslo (Table 4.2) the results were slightly better than for Bergen. The

Table 4.1: *Root Mean Square Deviation (RMSD) and Mean Bias Deviation (MBD; reconstructed - measured) for reconstructed vs measured hourly CIE-weighted UV for different solar elevation intervals in Bergen for the period 2000-2004. In addition, the correlation coefficient (R) and the number of hours (n) are given.*

Solar elev.	**RMSD** [kJ/m^2]	**MBD** [kJ/m^2]	**R**	**n**
$> 10^o$	0.013(47%)	0.004(16%)	0.90	15216
$0 - 10^o$	0.001(76%)	+0.000(26%)	0.69	6830
$10 - 20^o$	0.004(52%)	0.001(14%)	0.71	4863
$20 - 30^o$	0.008(44%)	0.003(15%)	0.74	3882
$30 - 40^o$	0.015(40%)	0.007(19%)	0.76	3236
$40 - 50^o$	0.022(37%)	0.009(15%)	0.76	2544
$> 50^o$	0.025(35%)	0.010(14%)	0.77	691

overestimation has decreased from 16 % to 11 %, and there is somewhat less

Table 4.2: *Same as for Table 4.1, but for Oslo 1998-2002.*

Solar elev.	**RMSD** [kJ/m^2]	**MBD** [kJ/m^2]	**R**	**n**
$> 10^o$	0.013(43%)	0.003(11%)	0.91	15306
$0 - 10^o$	0.001(74%)	+0.000(27%)	0.68	6748
$10 - 20^o$	0.004(50%)	0.001(11%)	0.69	4875
$20 - 30^o$	0.008(43%)	0.003(13%)	0.73	3897
$30 - 40^o$	0.015(37%)	0.004(10%)	0.74	3236
$40 - 50^o$	0.021(31%)	0.007(11%)	0.79	2529
$> 50^o$	0.027(33%)	0.008(9%)	0.74	780

scatter. Oslo has a more continental climate, and the air has got less water content than the maritime air in Bergen. This results in less dense clouds which might be more similar to the clouds at Garmisch-Partenkirchen. The total cloud amount might also be less than for the maritime areas. Another reason might be the choice of values for the other input parameters. The site of the measuring instrument is not at the same location (600 m apart) which can give a minor effect. Results from Kjevik/Landvik (Table 4.3) were quite similar to the results from Bergen and Oslo.

Table 4.3: *Same as for Table 4.1, but for Kjevik/Landvik 1996-2004.*

Solar elev.	**RMSD** [kJ/m^2]	**MBD** [kJ/m^2]	**R**	**n**
$> 10^o$	0.015(44%)	0.005(16%)	0.92	24864
$0 - 10^o$	0.002(84%)	+0.000(15%)	0.62	8880
$10 - 20^o$	0.004(55%)	0.001(15%)	0.68	7353
$20 - 30^o$	0.009(46%)	0.004(18%)	0.73	6106
$30 - 40^o$	0.016(40%)	0.008(19%)	0.77	5573
$40 - 50^o$	0.023(34%)	0.011(17%)	0.79	3866
$> 50^o$	0.027(31%)	0.010(12%)	0.76	1966

Data for Tromsø (Table 4.4) show some results deviating from the three southern stations, and show a very good agreement with the measured data. Both for all solar elevations above 10^o collectively, and for all solar elevation intervals above 10^o, the MBD is only negligible (below 1 %). Both the RMSD and the correlation coefficients are rather similar to those at the southern stations. Statistics for all four stations for solar elevation above 10^o are summed in Table 4.5.

The reasons for the good average agreement between the reconstructed and measured UV data in Tromsø can be as follows:

- more reliable ozone data because of the long term measured ozone series from Tromsø (no interpolation needed)

Table 4.4: *Same as for Table 4.1, but for Tromsø 1996-1999.*

Solar elev.	**RMSD** [kJ/m^2]	**MBD** [kJ/m^2]	**R**	**n**
$> 10^o$	0.011(42%)	+0.000(0%)	0.88	11278
$0 - 10^o$	0.001(62%)	+0.000(13%)	0.77	6444
$10 - 20^o$	0.004(44%)	-0.000(−1%)	0.72	4241
$20 - 30^o$	0.008(38%)	+0.000(0%)	0.70	3379
$30 - 40^o$	0.015(35%)	+0.000(1%)	0.70	2787
$> 40^o$	0.020(33%)	-0.000(−0%)	0.68	871

Table 4.5: *Same as for Table 4.1, but for solar elevations above* 10^o *for each station.*

Stations	**RMSD** [kJ/m^2]	**MBD** [kJ/m^2]	**R**	**n**
Bergen	0.013(47%)	0.004(16%)	0.90	15216
Oslo	0.013(43%)	0.003(11%)	0.91	15306
Kjevik	0.015(44%)	0.005(16%)	0.92	24864
Tromsø	0.011(42%)	0.000(0%)	0.88	11278

- the cloud climate is more similar to that of Garmisch-Partenkirchen
- different errors can by chance be canceled out

For a further study of the better average agreement at Tromsø, cloud free and completely overcast data for Tromsø, Bergen, Oslo and Kjevik were selected. For cloud free conditions, ozone has the dominant effect on the radiation transfer, while for overcast, the cloud effect is the dominant. Cloud free and overcast conditions were selected on the basis of total cloud amount equal to 0 and minimum 7 octas, respectively.

Table 4.6: *Same as for Table 4.1, but for cloud free measurements for solar elevation above* 20^o *for each station.*

Stations	**RMSD** [kJ/m^2]	**MBD** [kJ/m^2]	**R**	**n**
Bergen	0.012(22%)	0.001(1%)	0.93	152
Oslo	0.008(15%)	0.001(2%)	0.97	86
Kjevik	0.011(21%)	0.004(7%)	0.95	332
Tromsø	0.008(20%)	0.001(4%)	0.96	140

To be sure to exclude the effect of mountains, only solar elevation above 20^o were used for this investigation. For cloud free cases, shown in Table 4.6, it is evident that the ozone effect is not the contributing factor for giving the low MBD in Tromsø compared to the other stations. Since all four stations show the same low MBD values, the ozone effect seems to have minor influence. Either the ozone interpolation has been a success for the other stations, or the ozone effect is not the contributing factor.

Tromsø is situated at high latitudes, which give cloud optical depths that might be similar to those at Garmisch-Partenkirchen. Since the temperature at high latitudes are lower than in the south, the air can hold less water vapor. This result in a reduced optical depth of the clouds. When comparing the reconstructed and measured data for overcast conditions, the MBD for Tromsø is still quite low (Table 4.7). The southern stations have considerably higher MBD, where it is largest for Bergen and Kjevik. This can imply that, in the south the clouds are more optically thick on the coast than away from the coast. When it comes to errors canceling each other, this is more difficult to verify.

For all four stations, the overcast data amounts to more than 50 % of all the observations when all solar elevations are taken into account. Cloud free observations are sparce. However, these observations have the highest UV values so this can influence the total statistics more than would be expected when looking at the number of observations. When comparing these results

Table 4.7: *Same as for Table 4.1, but for overcast conditions (7 or 8 octas) for solar elevation above* 20^o.

Stations	**RMSD** [kJ/m^2]	**MBD** [kJ/m^2]	**R**	**n**
Bergen	0.015(53%)	0.005(20%)	0.72	5401
Oslo	0.016(56%)	0.003(11%)	0.74	5277
Kjevik	0.018(63%)	0.005(18%)	0.75	7590
Tromsø	0.014(53%)	-0.001(−5%)	0.63	3797

to the results of the COST 726 report (Koepke et al., 2007) it is evident that the model reconstructs best for places like Davos and Tromsø, which have similar to the conditions at Garmisch-Partenkirchen, and overestimates for places with clouds of other optical depths.

Reconstruction with only total cloud amount

For the years 1981-1997, total cloud amount was the only available cloud information for Oslo. It is therefore of interest to investigate the difference between having only total cloud amount as input to STAR and having detailed cloud information (see Chapter 3.2.5) as input. STAR was therefore run for both cases. In this section, STAR with cloud input i) was used (see Chapter 3.1). The results from these sensitivity tests can in the future also be applicable to reconstructions for other stations, where only total cloud amount is available as cloud information.

Figure 4.3 shows the two model runs for Oslo with all available cloud information and only total cloud cover for the highest solar elevation intervals. When reducing the cloud information the reconstructed values start forming in discrete bands, which have not been investigated in earlier research. The main reason for the bands forming is that only cloud amount as input gives only 9 discrete possibilities (0 to 8), while additional cloud information gives more possibilities. Different cloud types can be more frequent for certain solar elevations, e.g. fog or stratus clouds in the morning, and convective clouds in the afternoon. Besides, certain cloud types are also more frequent

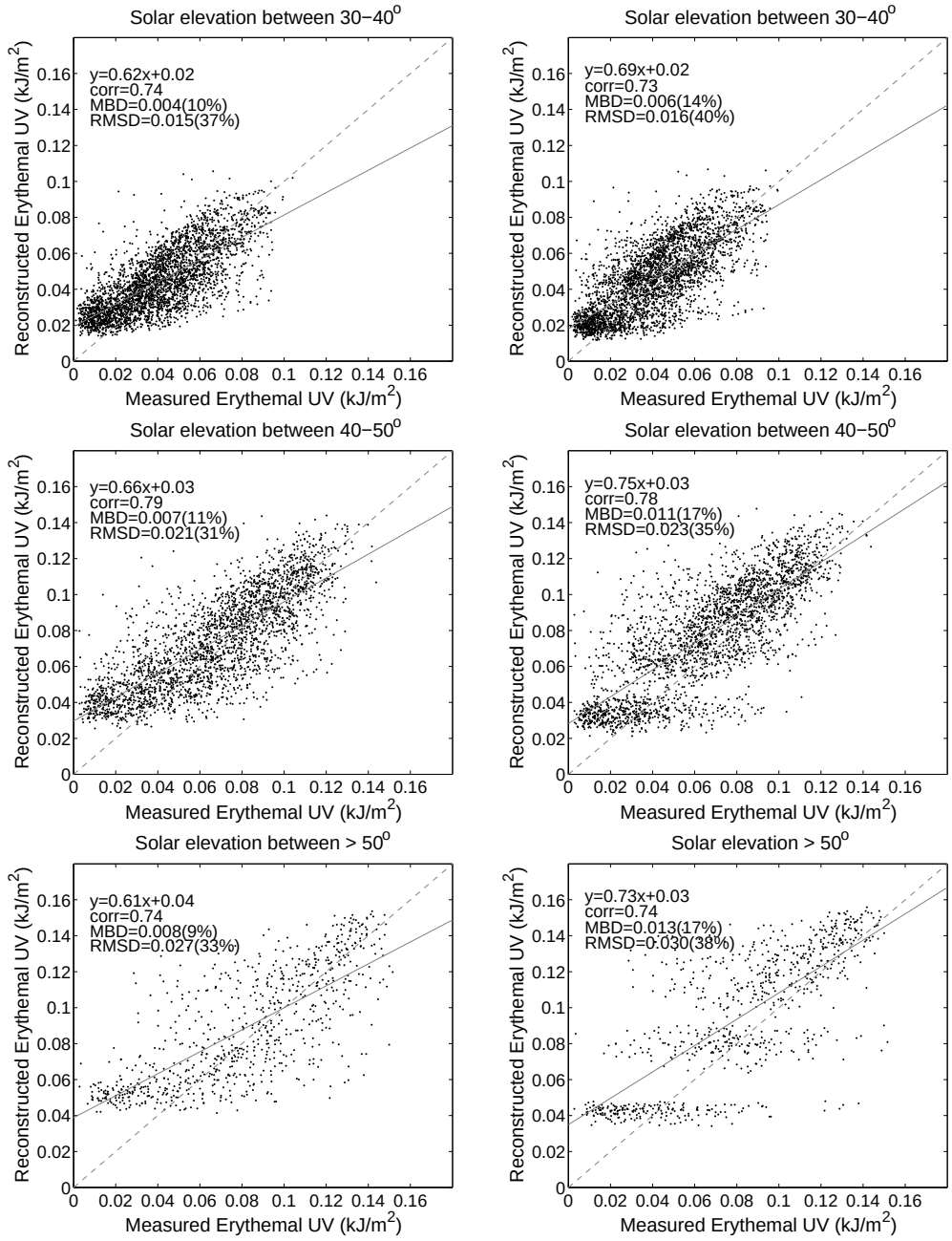

Figure 4.3: *Hourly reconstructed (STAR) vs measured (GUV) erythemal UV values with all available cloud information (left), and only total cloud amount (right) as input, for Oslo in the period 1998-2002 with varying solar elevation. One-to-one line (broken) and regression line(solid).*

for certain cloud amounts, however, this can vary from place to place.

These bands starts appearing for the interval between 30-40^o and get more pronounced as the solar elevation increase. In the interval above 50^o, the data are split into three clear bands. For high UV values, i.e. low cloud amounts, there are probably smaller difference in UV radiation for the different cloud amounts, because the probability of obscuring the sun is low. The lowest band (reconstructed values around 0.04 kJ/m^2) is related to overcast conditions, i.e. cloud amount 7 or 8 octa. Since there are high measured values (UV up to 0.14 kJ/m^2), there seems to have been either thin, high clouds or the sun has not been obscured. Since the cloud observations are only taken every three hours, the cloud input might not be representative for that hour. The middle band (reconstructed values around 0.08 kJ/m^2) includes the highest measured values. Scattered cloudiness seems to be the reason for this, since for scattered cloudiness, the measured value might exceed the clear sky value (as explained in Chapter 2.4.5).

Table 4.8: *Root Mean Square Deviation (RMSD) and Mean Bias Deviation (MBD; reconstructed - measured) for reconstructed with only total cloud amount vs measured hourly CIE-weighted UV for different solar elevation intervals in Oslo for the period 1998-2002. In addition, the correlation coefficient (R) and the number of hours (n) are given.*

Solar elev.	**RMSD** [kJ/m^2]	**MBD** [kJ/m^2]	**R**	**n**
$> 10^o$	0.015(47%)	0.005(16%)	0.91	15306
$10 - 20^o$	0.004(52%)	0.001(14%)	0.69	4875
$20 - 30^o$	0.009(45%)	0.003(16%)	0.73	3897
$30 - 40^o$	0.016(40%)	0.006(14%)	0.73	3236
$40 - 50^o$	0.023(35%)	0.011(17%)	0.78	2529
$> 50^o$	0.030(38%)	0.013(17%)	0.74	780

Table 4.8 shows the statistics for the reconstruction only using total cloud amount as input vs measured hourly CIE-weighted UV for different solar elevation intervals in Oslo for the period 1998-2002. The change from cloud

Table 4.9: *Relative deviation for Root Mean Square Deviation (RMSD) and Mean Bias Deviation (MBD; reconstructed with only NN - detailed reconstruction) for reconstructed with only total cloud amount vs reconstructed with detailed cloud input for hourly CIE-weighted UV for solar elevation above* 10^o *for all stations. In addition, the correlation coefficient (R) and the number of hours (n) are given. The variables are calculated in % compared to the measured values.*

Stations	**ΔRMSD** [kJ/m^2]	**ΔMBD** [kJ/m^2]	**ΔR**	**n**
Bergen	0.002(7%)	0.002(8%)	-0.00	15216
Oslo	0.001(5%)	0.002(5%)	-0.00	15306
Kjevik	0.002(5%)	0.002(5%)	-0.00	24864
Tromsø	0.001(3%)	0.001(4%)	-0.01	11278

amount and cloud type as cloud input (Table 4.2) to only total cloud amount as cloud input gives increases both RMSD and MBD. The increase is nearly independent on the solar elevation interval.

Table 4.9 summarizes the relative deviation for RMSD, MBD and the correlation coefficients for the two model runs for all investigated stations. The percentage increase of RMSD and MBD compared to the mean measured values are also shown.

Even when reconstructing with detailed cloud information, there is a general overestimation (positive MBD). This overestimation is increased when reducing the amount of cloud input both for RMSD and MBD, while the correlation coefficients stay the same. The RMSD increased by additional 3-7 %, while MBD increased by 4-8 % compared to the measured values for the various stations. For Tromsø the reconstruction is still highly satisfactory with MBD of only 5 % for all solar elevations over 10^o, even if the amount of input is reduced.

When this reconstruction is used on the Oslo data for the period 1981-1997, it will result in an additional increase of 5 % compared to the measured values.

4.1.2 STAR vs Lindfors

Daily values

In the following, daily values from the STAR model and the Lindfors model (see Chapter 3.3) will be compared. For hourly values there can be a time lag between reconstructed and measured values, as explained in Chapter 4.1.1. For daily values this problem is removed.

Based on the Lindfors model, a reconstruction of UV data was made for Bergen for the period 1982-2005 (Lindfors et al., 2007). The period for reconstruction was limited by the availability of global radiation measurements.

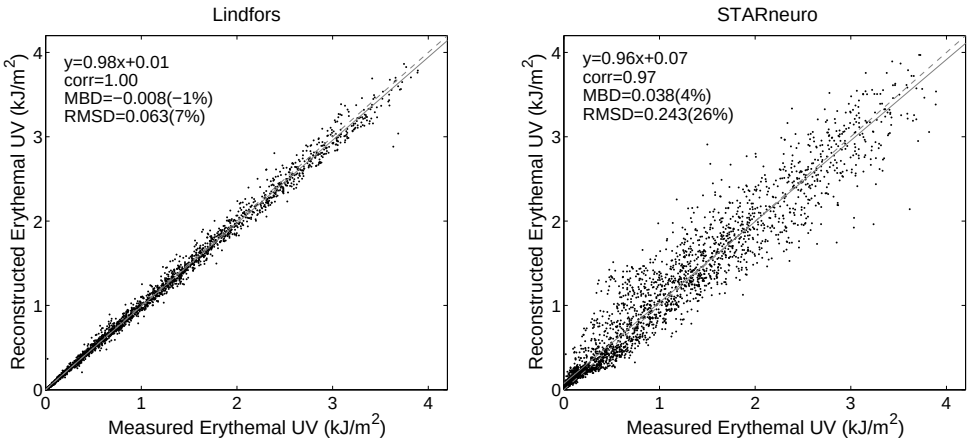

Figure 4.4: *Reconstructed daily erythemal UV by the Lindfors model (left) and the STAR model (right) vs measured (GUV) for Bergen for the period 2000-2004. One-to-one line(broken) and regression line(solid) are also given.*

Figure 4.4 illustrates the daily reconstructed values for the Lindfors model and STAR compared to measured data. The Lindfors model shows a better performance, with an underestimation of only 1 %, and with a low RMSD (7 %). The main reason for the low RMSD is that in the Lindfors model global radiation is used as input for the reconstruction. Measured global radiation contains additional information whether the sun is obscured or not. STAR can also use global radiation as input, but because of the lack of global radiation data for large parts of Norway, only the cloud information is used. For STAR there is a moderate overestimation of 4 %, and a RMSD of 26 %. For both models, the results are satisfactory with regards to daily values. The data from Figure 4.4 are summed up in Table 4.10.

Table 4.10: *Root Mean Square Deviation (RMSD) and Mean Bias Deviation (MBD; reconstructed - measured) for reconstructed values for STAR and the Lindfors model vs measured daily CIE-weighted UV for Bergen for the period 2000-2004. In addition, the correlation coefficient (R) and the number of hours (n) are given.*

Model	**RMSD** [kJ/m^2]	**MBD** [kJ/m^2]	**R**	**n**
STAR	0.243(26%)	0.038(4%)	0.97	3010
Lindfors	0.063(7%)	-0.008(−1%)	1.00	2979

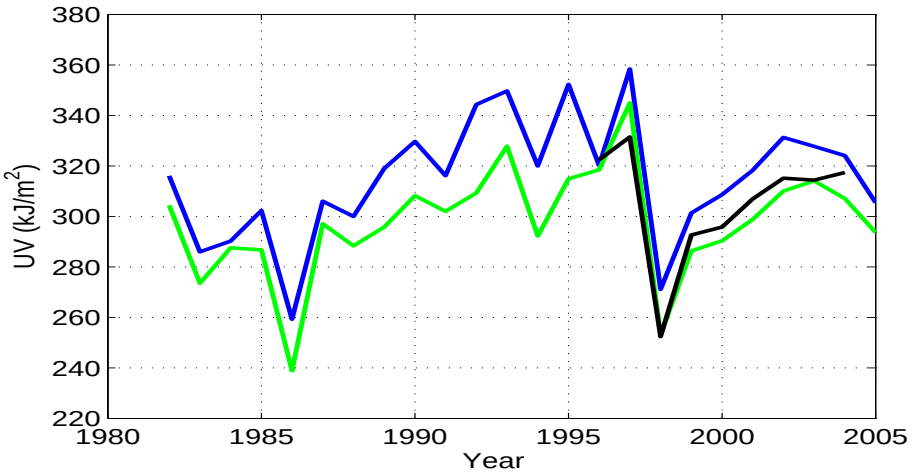

Figure 4.5: *Yearly sum of CIE-weighted UV modeled by the STARneuro model (blue), and the Lindfors model(green) and measured by GUV (black).*

In Figure 4.5 the yearly sum of reconstructed and measured values are illustrated. Days where either the reconstructed Lindfors values or GUV values are missing are excluded in all three datasets so that they are comparable. This figure is therefore not representative when looking for absolute values or trends.

The two models and the measurements agree quite well in the representation

of the year-to-year variability but differ slightly in the absolute level. STAR overestimates the UV-radiation, while the Lindfors model alternates between a slight over- and underestimation.

4.2 Temporal and spatial variations

In the following, annual variations in both erythemal UV and the cases of cancer will be studied, together with trends for the period 1957-2005. Possible connections between erythemal UV and cancer will be investigated.

4.2.1 Variations in UV radiation

Annual sums of erythemal UV are reconstructed for each station. According to Figures 4.6 and 4.7, there are gradients in both north-south and east-west directions, with the largest gradient between north and south. This is expected due to the latitudinal solar elevation decrease towards north. Besides, for the northernmost stations the sun is below the horizon for the entire day in winter time (Figure 4.8). This is partly compensated for by the long summer days with midnight sun. In addition, differences in cloud amount and optical properties between northern and southern stations (see discussion in Chapter 4.1.1) will also affect the results. For the east-west gradient (Figure 4.7) mainly the different cloud properties account for the difference in radiation. As discussed in Chapter 4.1.1, the western part of the country has a more maritime climate than the eastern part. As a consequence of prevailing westerlies in the area, moist air that comes in from the sea, will undergo orographic lifting when it meets the mountains, and produce dense clouds. The clouds produced by the air that arrives the eastern side of the mountains, will be less dense (Wallace and Hobbs, 1977) or even disappear. This results in less radiation in the western compared to the eastern part. For the stations in this work, there are no overall trends that apply to all stations, some have positive and some have negative trends for the period 1957-2005.

Monthly decadal trends

The total ozone amount has a negligible effect on UVA, but a considerable effect on UVB. UVA is predominantly influenced by the cloud amount and cloud type, which also has a comparable effect on UVB. By comparing UVA and UVB trends and taking total ozone into consideration, the effects of clouds and ozone on erythemally weighted UV radiation can be separated. By studying absolute values of radiation it will not be possible to compare differences between the different stations. Therefore, the focus will be on the relative changes expressed as trends in % per decade.

Figure 4.9 shows the variations of the monthly sum of erythemal UV for

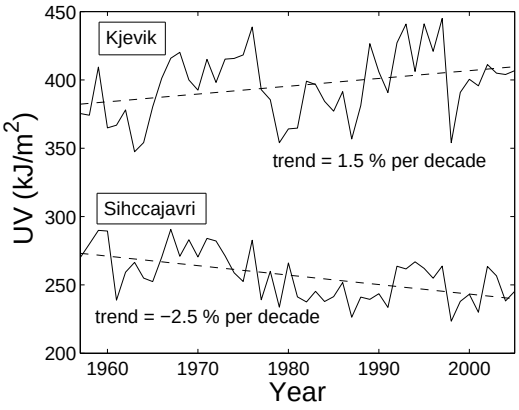

Figure 4.6: *Yearly sum of erythemal UV for Kjevik in the south and Sihccajavri in the north. For each station, the linear regression and the decadal trend is given.*

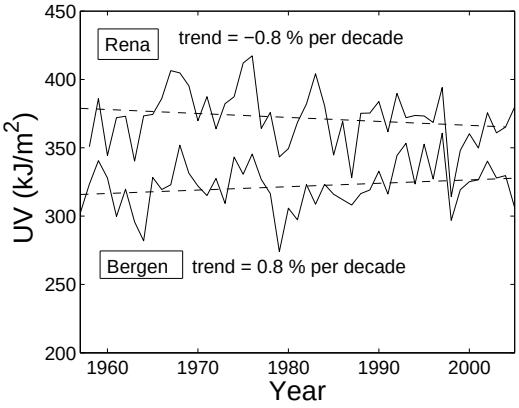

Figure 4.7: *Yearly sum of erythemal UV for Rena in the east and Bergen in the west. For each station, the linear regression and the decadal trend is given.*

2005 for Tromsø and Kjevik, representing the northernmost and the southernmost stations. The maximum summer irradiance for Kjevik is 1.5 times that of Tromsø. In addition to the seasonal variation, there are also changes from year to year. Tables C.1-C.3 show the decadal trends of UVA, UVB and erythemally weighted irradiance, for each month and for each station.

Three stations are left out of the discussion, because the time periods for these stations are shorter than for the rest of the stations, so they can not be directly compared to the others. These stations are Oslo, Rena and Færder Fyr. For the rest of the stations the trends are calculated on the basis of the period 1957-2005.

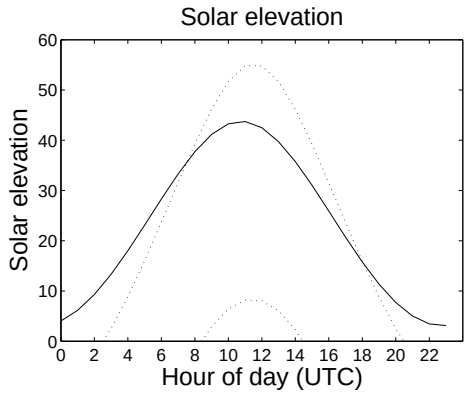

Figure 4.8: *Solar elevation for Kjevik (dashed line) and Tromsø (solid line) for summer solstice, 22.June (upper), and winter solstice, 21.December (lower).*

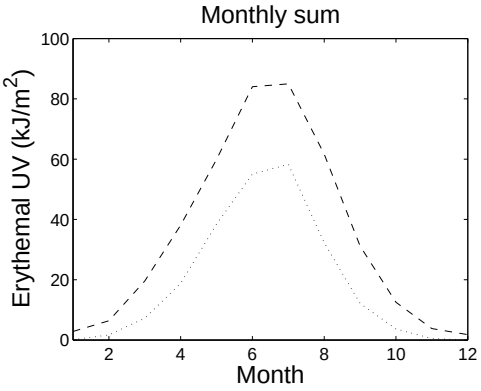

Figure 4.9: *Monthly sum of erythemal UV for Kjevik (dashed line) and Tromsø (dotted line) for 2005.*

There are no stations that have significantly higher positive trends than the others, however the strongest trends are found at Sola, Kjevik, Lyngdal and Værnes. Sihccajavri has a markedly larger negative trend than the other stations.

As an example for mainly negative and mainly positive trend in erythemally weighted radiation, Sihccajavri and Lyngdal have been selected for a detailed discussion. In this work, the erythemal UV is of main interest. As shown in Table 4.11 the trends for Sihccajavri are negative for all months except January, which only has a marginal positive trend. There are, however, few days with sun above the horizon for this month, and then only a few hours every day. For January to March there is a decrease in ozone of about 2 %.

As sensitivity studies with the STAR model at clear sky showed (Chapter 2.4.2), 1 % decrease in ozone results in 0.7-1.2 % increase in erythemally weighted UV, an increase of 1.5-2.3 % in UV is therefore expected. From Table 4.11, this is not the case. The erythemally weighted UV show a slight reduction, which must be explained by cloud effects.

Table 4.11: *Monthly decadal trends (%) of UVA and UVB radiation, erythemally weighted radiation (ERY), ozone amount (O_3) and total cloud amount (NN) for Sihccajavri (1957-2005).*

Month	**UVA**	**UVB**	**ERY**	**O_3**	**NN**
January	-1.7	3.6	0.1	-1.3	4.4
February	-2.8	3.4	-0.9	-2.5	4.9
March	-4.0	3.7	-0.1	-2.5	5.5
April	-3.6	-0.3	-1.9	-1.7	7.2
May	-3.5	-2.3	-2.9	-1.0	6.3
June	-3.0	-2.5	-2.7	-0.4	5.8
July	-2.9	-2.4	-2.7	-0.6	5.3
August	-2.5	-2.3	-2.5	-0.1	3.8
September	-2.3	-1.9	-2.1	-0.2	2.6
October	-2.2	-2.6	-1.7	0.3	2.5
November	-1.9	-1.4	-1.7	-0.3	2.3
December	-	-	-	-0.1	2.6

The negative trend in UVA for Sihccajavri can have different reasons, like a possible increase in cloud amount, a change in optical thickness of the clouds or a shift in cloud types. When studying this further, there seems to have been a slight increase in both yearly (Figure 4.10) and monthly mean total cloud amount for all the months in this period. This coincide very well with the trends in UVA, however, this is not the only explanation. In cloud amount, there is a positive annual trend of 4.3 % per decade, while there are monthly variations between 2.3-7.2 % per decade. The months of maximum decrease in UVA does not coincide excactly with the maximum increase of total cloud cover. The other two possible explanations mentioned above is hard to investigate, however, the rest of the explanation probably lies within

Figure 4.10: *Mean annual cloud amount for Sihccajavri for the period 1957-2005. The linear regression and the decadal trend is also given.*

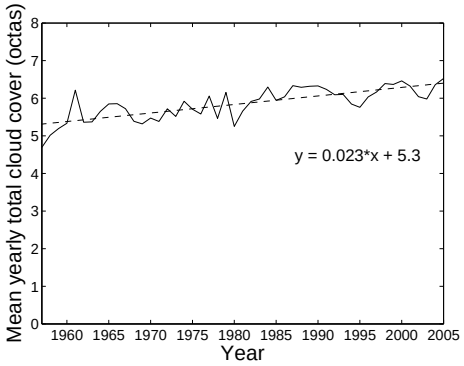

these parameters.

Table 4.12: *Monthly decadal trends (%) of UVA and UVB radiation, erythemally weighted radiation (ERY), ozone amount (O_3) and total cloud amount (NN) for Lyngdal-Nummedalen (1957-2005).*

Month	**UVA**	**UVB**	**ERY**	**O_3**	**NN**
January	1.8	5.7	3.3	-1.5	-2.2
February	1.4	8.9	3.3	-2.5	-2.3
March	-0.1	7.7	3.9	-2.5	+0.0
April	0.0	3.5	2.6	-1.6	-0.5
May	2.5	4.2	4.2	-1.0	-4.1
June	-0.8	-0.3	-0.3	-0.5	1.0
July	2.0	2.8	3.0	-0.6	-3.6
August	1.4	1.8	1.9	-0.3	-2.1
September	1.3	1.8	1.8	-0.3	-2.2
October	0.7	0.5	0.5	0.2	-1.1
November	1.0	1.4	1.0	-0.3	-1.5
December	0.9	0.9	1.0	-0.3	-2.2

When studying the results for Lyngdal-Nummedalen (Table 4.12) it is seen

that for April there is no trend in UVA, i.e. no trend in cloud amount/optical properties. The only effect applying here is thus the ozone effect. For October, on the other hand, the ozone trend is close to 0 and this give only a cloud effect. It can thus be concluded that for negative trends in total ozone content there will be an increase in UVB and erythemally weighted radiation, if the cloud conditions remain constant. The cloud effect, seen in the trends in UVA will cancel or increase these trends depending on whether the trend in UVA is decreasing or increasing, respectively. As shown for Sihccajavri, when there is a negative trend in UVA most of this can be assigned to the change in total cloud amount. This is true for all stations (not shown here).

4.2.2 Variations in cancer incidences

Graphs of temporal variation in cutaneous malignant melanoma(CMM) incidence rates for all counties in Norway are shown in Figures E.1-E.19.

Figure 4.11 shows the temporal variation for Vest-Agder and Finnmark. There is a marked north-south gradient both for women and men (see Robsahm and Tretli (2001) and Magnus (1973)). Since the solar radiation is assumed to be such an important risk factor for CMM (Magnus, 1973), there are reasons to believe that the low incidence rate in Finnmark is connected to the low solar radiation level in northern areas. When averaging over the whole period, 1957-2005, the incidence rates in Southern Norway is almost 3 times that of Northern Norway. The maximum gradient show that the southern county (Aust-Agder) has almost 4 times higher number of incidences than the northern one (Finnmark).

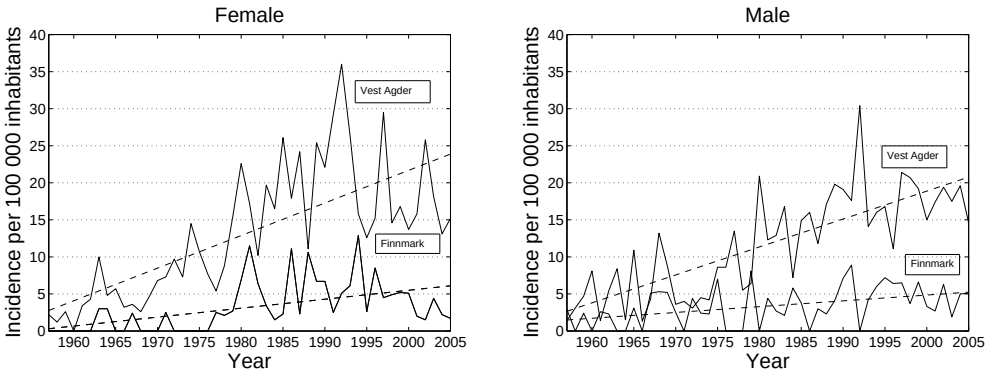

Figure 4.11: *Annual cancer incidences for Vest-Agder and Finnmark for female (left) and male (right) for the period 1957-2005. Linear regression lines are shown as dashed lines.*

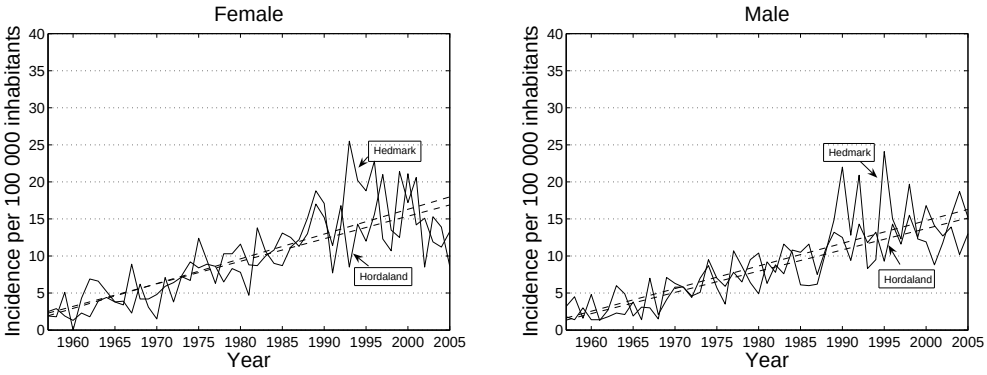

Figure 4.12: *Annual cancer incidences for Hedmark and Hordaland for female (left) and male (right) for the period 1957-2005. Linear regression lines are shown as dashed lines.*

The east-west gradient (Figure 4.12) is not as pronounced as the north-south, however, the values for Hedmark are slightly higher than for Hordaland.

Looking at the temporal change there have been quite a dramatic development in CMM incidence rates over the period. There are large variations from year to year, however, overall there is marked increase. For the entire Norwegian population, the CMM incidence has increased by approximately a factor of 6 for women, and a factor of 10 for men since 1957. For most stations there is an increase until the middle of the 1990's and then the incidences levels off, and for some stations it even starts to decrease (e.g. Aust-Agder). Table 4.13 shows the coefficient for the linear regression line for the different counties. The result of multiplying the slope of the line, a, with 10, is the decadal increase in incidences per 100 000 inhabitants, which varies between 1.2 and 5.3 for women and between 0.8 and 4.5 for men for the various counties.

Several hypothesis are presented about the increasing trends in CMM. Some argue that changes in diagnosis or classifications might be the reason, or maybe over-reporting of incidences. These statements are by Magnus (1991), however, found unlikely. Others put the blame on the new clothing fashions and increased vacations to sunny areas. Nevertheless, the 5 year survival rate has increased from 70 to 89 % for females and 47 to 80 % for males, for diagnosis given in the period 1958-1962 to 1993-1997 (Kreftregisteret, 2007). This is probably due to an earlier detection of the melanomas because of increased focus on skin cancer.

The incidences are higher for women than for men. This might have something to do with the anatomic site of occurrence for men and women, which are different. A higher percentage of incidences for men occur on the upper body, while for women the lower legs have highest incidences (Thune et al., 1993).

Table 4.13: *Coefficients for linear regression (y=ax+b) of CMM incidences per 100 000 inhabitants for female (left) and male (right) for all counties in the period 1957-2005, where x=year-1957.*

County	**Female:**		**Male:**	
	a	**b**	**a**	**b**
Finnmark	0.12	0.30	0.08	1.48
Troms	0.18	1.29	0.13	2.08
Nordland	0.17	1.43	0.19	0.52
Nord-Trøndelag	0.35	0.68	0.33	-0.01
Sør-Trøndelag	0.35	0.98	0.35	0.60
Møre og Romsdal	0.33	0.46	0.29	-0.13
Sogn og Fjordane	0.25	0.77	0.25	0.24
Hordaland	0.30	2.28	0.29	1.36
Rogaland	0.50	2.23	0.41	1.14
Vest-Agder	0.44	2.76	0.38	2.67
Aust-Agder	0.46	2.75	0.45	2.42
Telemark	0.32	5.00	0.33	2.27
Vestfold	0.53	1.14	0.41	2.84
Østfold	0.43	2.81	0.40	2.10
Akershus	0.35	3.14	0.37	2.39
Oslo	0.28	4.94	0.28	4.65
Buskerud	0.36	3.05	0.35	1.77
Oppland	0.29	1.51	0.31	0.28
Hedmark	0.33	1.93	0.31	1.63

4.3 Correlation between UV and cancer

According to Armstrong and Kricker (1993) there is assumed to be a connection between UV exposure and development of cutaneous malignant melanoma (CMM). Figure 4.13 gives the mean incidence rate of malignant melanoma as a function of mean yearly sum of erythemal UV for the period 1957-2005 for female and male. The numbers indicate the region as shown in

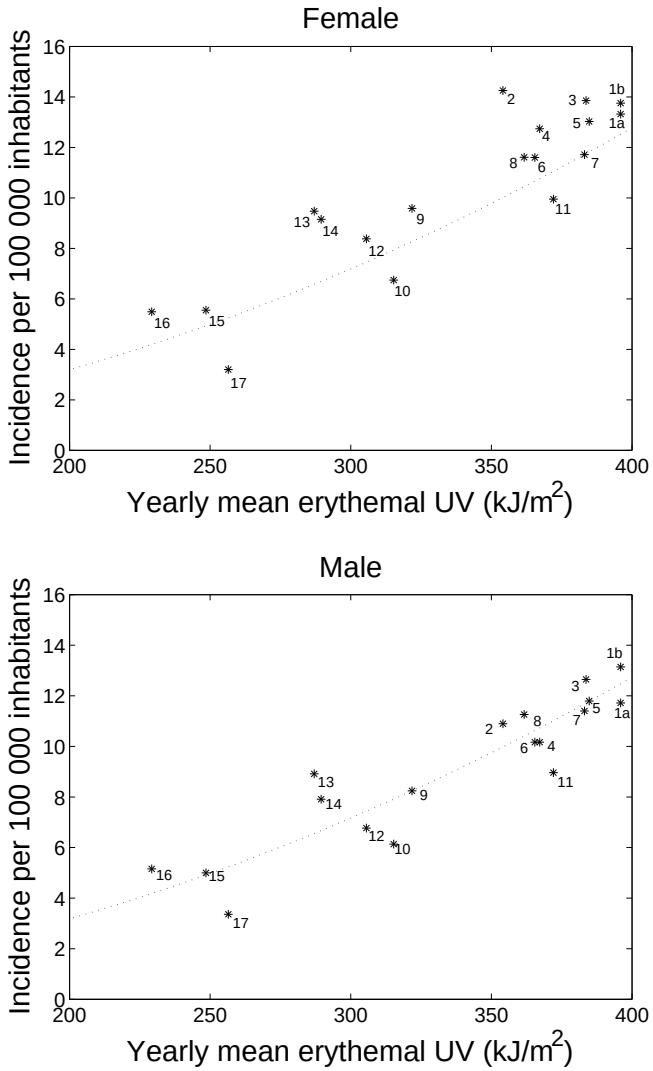

Figure 4.13: *Mean incidence rate of malignant melanoma vs mean erythemal UV for the period 1957-2005 for female (upper) and male (lower) for 18 counties. (Station numbers are the same as in Figure 3.6). Dotted line shows the quadratic fit.*

Figure 3.6, where the highest numbers are to the north. The numbers 1a and 1b in the figure mean that the radiation data are taken from station 1 (Kjevik), but are compared to cancer incidences both for Vest-Agder(a) and Aust-Agder(b). The UV reconstruction site, Kjevik, is located almost at the border between these two counties. Nevertheless, in Chapter 4.1.1 these data are compared to measurements for Landvik, which is situated in Aust-Agder. As this comparison shows similar values, the reconstructed UV data for Kjevik are assumed to be representative for both counties. The dotted curve shows the quadratic curve fit. This was used because the agreement between the quadratic fit and the values were better than for a linear regression. This is in accordance with findings published by Henriksen and Svendby (1997). For Oslo (7), reconstructed UV was based on detailed cloud information for the periods 1957-1980 and 1998-2005. For the period 1981-1997, the reconstruction is based on total cloud amount only (see also page 50) was used.

According to Figure 4.13, there is an obvious connection between average UV and incidence of CMM. However, this figure is a mean of almost 50 years, and thus the year to year variability is not seen. All stations follow, more or less the quadratic fit both for male and female. The incidence rate as a function of erythemal UV are divided into three different clusters of counties. The northern stations are found in the lower left part of the figure, as they have the lowest amount of both UV radiation and cancer incidences. According to Figure 3.6 on page 33, there is a long north-south distance between the northern reconstruction sites and the southern ones. The second cluster consists of the middle and western part of Norway (except Rogaland), having both intermediate level of UV and intermediate number of cancer. The southern and eastern part are in the last cluster, with both the highest radiation level and the highest occurrence of cancer. This coincide well with the less dense clouds occurring in the east (as discussed in Chapter 4.2.1).

The UV radiation that might inflict skin damage occurs usually between April and August (Robsahm and Tretli, 2001), while the sun and level of outdoor activity is highest. During the other months, it is cold, and people wear many layers of clothes, protecting against harmful UV radiation.

For better to analyze variations in both UV and cancer, the data was smoothed out, and a 5 year running average is used. With different time lag (in years), the 5 year running averages of the sum of erythemal UV for April to August is cross-correlated with the 5 year running averages of cancer incidences. The results are shown for all counties in Table 4.14. Both the maximum correlation coefficient and the time lag vary considerably. Very often the maximum

County	M/F	**UVA**	**Lag**	**UVB**	**Lag**	**ERY**	**Lag**
Finnmark	M	0.46	27	0.49	27	0.50	27
	F	0.48	23	0.46	22	0.47	22
Troms	M	0.52	22	0.70	0	0.57	0
	F	0.33	22	0.45	1	0.38	2
Nordland	M	0.33	21	0.75	0	0.71	0
	F	0.24	0	0.44	0	0.41	0
Nord-Trøndelag	M	0.23	31	0.32	0	0.27	0
	F	0.18	25	0.39	0	0.34	0
Sør-Trøndelag	M	0.33	22	0.35	0	0.27	0
	F	0.30	20	0.17	0	0.08	0
Møre og Romsdal	M	0.49	28	0.35	28	0.39	28
	F	0.42	28	0.34	28	0.37	28
Sogn og Fjordane	M	0.46	21	0.51	5	0.46	6
	F	0.49	12	0.38	0	0.34	10
Hordaland	M	0.30	23	0.50	0	0.46	0
	F	0.27	23	0.48	0	0.44	0
Rogaland	M	0.47	0	0.60	0	0.58	0
	F	0.45	0	0.58	0	0.55	0
Vest-Agder	M	0.33	8	0.37	0	0.34	0
	F	0.36	15	0.39	0	0.37	0
Aust-Agder	M	0.34	18	0.52	0	0.49	0
	F	0.45	3	0.53	2	0.51	2
Telemark	M	0.28	23	0.14	24	0.16	24
	F	0.26	16	0.10	17	0.13	16
Vestfold	M	0.41	0	0.50	0	0.50	0
	F	0.48	3	0.58	0	0.57	0
Østfold	M	0.42	20	0.26	1	0.27	24
	F	0.37	23	0.23	4	0.22	25
Akershus	M	0.47	19	0.24	5	0.26	19
	F	0.38	17	0.24	7	0.24	8
Oslo	M	0.63	0	0.75	0	0.88	0
	F	0.65	1	0.70	0	0.86	0
Buskerud	M	0.56	0	0.62	0	0.61	0
	F	0.66	0	0.66	0	0.65	0
Hedmark	M	0.48	21	0.47	24	0.48	24
	F	0.49	20	0.43	24	0.44	24

Table 4.14: *Maximum correlation coefficients between 5 year running average for the sum of UV (UVA, UVB and erythemally weighted UV (ERY)) and 5 year running average for cancer incidences, separately for male (M) and female (F), with the corresponding time lag (in years), for all counties for the summer months (April-August).*

correlation coefficient appears at lag zero. It is very unlikely that the cancer develops in the few months from the summer to the end of the year. Otherwise, the correlation show a time lag of more than 20 years. Somewhere between these two extremes are more likely. People have been diagnosed with CMM down to the age-group 5-9 years (Cancer Registry of Norway, 2005), however, this is very rare. A defective gene is the reason for the cancer to develop in a large birthmark. This type of malignant melanoma is called a Juvenile melanoma. For people in the age-group 10-20 years old, most CMM cases are the Juvenile type, however, regular CMM types are found, but then mainly in the eyes (Cancer Registry of Norway, (personal communication)). Cancer incidence increases with age. It is assumed that cancer occur when the cells has been exposed to damaging radiation a number of times, and then the cells start to mutate.

For counties where the cancer incidence does not start to decrease or level off from the mid 1990's, the 5 year running mean will just continue to increase linearly. The variation in UV shows more oscillations. When correlating these two lines, a lagged correlation will not appear, because there is no maximum in cancer incidences that can be correlated to the maximum in radiation (shown in Figure 4.14). If a small rise in cancer incidence occur at the same place as an increase in UV, this can be enough to create a larger correlation between the two time series.

To hopefully see valid results, the counties with low numbers of inhabitants or low cancer incidences, have to be excluded. For a closer study of the correlation between radiation and cancer for each of the "summer" months, the counties Rogaland, Hordaland, Oslo, Akershus and Vest-Agder were chosen. Except for Vest-Agder, these are the counties with most inhabitants (SSB, 2005), however, Vest-Agder is the region with most cancer cases per 100 000 inhabitants. For Rogaland and Oslo no significant results were found. Therefore, only results for Hordaland , Akershus and Vest-Agder are shown (Tables 4.15 - 4.17).

For Hordaland, UVB and erythemaly weighted UV have correlations with time lag of 5 and 25 years, for both June and August, respectively (Table 4.15), however, only statistically significant for June. For all months except August, UVA has a significant and positive correlation with cancer. For April, June and July, the correlation coefficients are also statistically significant within 1 %.

For Vest-Agder (Table 4.16), the same pattern is shown for April and June

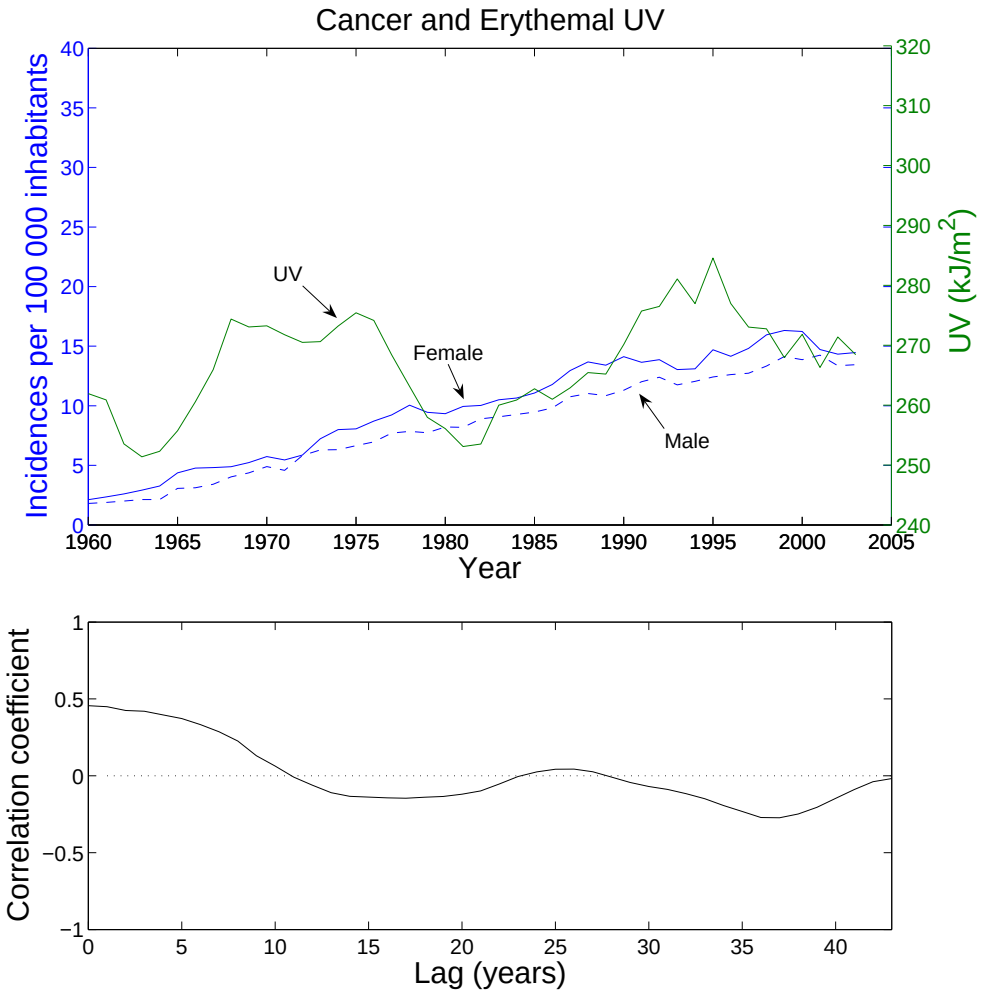

Figure 4.14: *Upper: 5 year running mean for the sum of reconstructed erythemally weighted UV for April to August for Bergen (green) and cancer incidences; males (dashed blue), females (fully drawn blue) for Hordaland. Lower: Correlation coefficients with the corresponding time lag for the upper figure (male).*

as for Hordaland. The range in time lag for females is drastically reduced compared to Hordaland, with a time lag of 15-16 years for female, however, 4-22 for males.

For Akershus, UVB and erythemally weighted UV seems to have the maximum correlation for a time lag that coincide better with cancer to what would be expected, than the other stations. When UVB and ERY has a positive lag, the years seem to coincide well the time lag that is found for UVA. For April, it is only UVA that has a maximum correlation for a lag

Table 4.15: *Maximum correlation coefficients for cross-correlation between UV-radiation (UVA, UVB and ERY for Bergen) and cancer for Hordaland, with corresponding time lag (in years), for female (F) and male (M).*

Month	**F/M**	**UVA**	**Lag**	**UVB**	**Lag**	**ERY**	**Lag**
April	F	**0.40**	**23**	0.58	0	0.51	0
	M	**0.40**	**26**	0.60	0	0.54	0
May	F	**0.41**	**2**	0.60	0	0.57	0
	M	**0.44**	**1**	0.63	0	0.59	0
June	F	**0.31**	**7**	**0.38**	**5**	**0.38**	**5**
	M	**0.30**	**7**	**0.37**	**5**	**0.36**	**5**
July	F	**0.42**	**10**	0.45	0	0.44	0
	M	**0.39**	**11**	0.43	0	0.42	0
August	F	0.26	24	0.23	25	0.22	25
	M	0.29	24	0.25	25	0.25	25

Bold text; statistically significant within 5 %, with time lag > 0 years.

not equal to zero.

As only the maximum correlation and the corresponding time lag was given in Tables 4.14 - 4.17 considerable amounts of information are lost. In Table 4.14 it appears to be a large variation in time lag for both female and male in Østfold from UVB to erythemally weighted UV despite that erythemally weighted UV has highest weight for UVB. Figure 4.15 shows the 5 year running mean for reconstructed UVB corresponding to the values given in Table 4.14. Here, a second maximum has a correlation coefficient that is almost the same as the first maximum. Thus, the maximum correlation coefficients might give a wrong impression. Regions of maximum correlation coefficients illustrate the true picture better than only the maximum correlation coefficient.

The 5 year running mean for reconstructed UVA in April for Kjevik and cancer incidences for males and females for Vest-Agder are shown in Figure 4.16. The correlation coefficients are given here as a function of time lag. According to the figure a time lag from exposure of UV radiation to diagnosis

Table 4.16: *Maximum correlation coefficients for cross-correlation between UV-radiation (UVA, UVB and ERY for Kjevik) and cancer for Vest-Agder, with corresponding time lag (in years), for female (F) and male (M).*

Month	**F/M**	**UVA**	**Lag**	**UVB**	**Lag**	**ERY**	**Lag**
April	F	**0.43**	**15**	0.53	0	0.46	0
	M	**0.40**	**19**	0.58	0	0.47	0
May	F	0.71	0	0.75	0	0.75	0
	M	0.69	0	0.75	0	0.74	0
June	F	**0.42**	**16**	**0.31**	**17**	**0.32**	**17**
	M	**0.35**	**22**	0.29	24	0.30	24
July	F	0.49	0	0.50	0	0.50	0
	M	**0.48**	**4**	0.48	0	0.48	0
August	F	**0.35**	**16**	0.29	17	0.29	17
	M	0.28	19	0.22	22	0.23	22

Bold text; statistically significant within 5 %, with time lag > 0 years.

of CMM there might be about 10-20 years. However, one should be careful when interpreting correlation estimates made for large time lags, usually they should not exceed 10-20 % of the data series. Then, the correlation is based on too few samples (Emery and Thomson, 2001). In this omparison, that amounts to a lag of less than 10 years.

Most researchers believe that CMM is caused by sunburn in early summer when the "white winterly bodies" are exposed either to strong spring or early summer sun, or when people travel to southern countries and is getting "roasted" at the beach to get a quick tan in a short time. However, there is a large discussion amongst the researchers whether it is UVA or erythemal UV (mainly UVB) that causes CMM to develop (Moan et al., 1999; Koh et al., 1990).

From Tables 4.15 - 4.17, there is no way of telling either what is the time lag from exposure to developing skin cancer, which month has most to say with regard to cancer inducing UV, or what type of UV is most important. However, when comparing these tables to Figure 4.16, it might seem like it

Table 4.17: *Maximum correlation coefficients for cross-correlation between UV-radiation (UVA, UVB and ERY for Gardermoen) and cancer for Akershus, with corresponding time lag (in years), for female (F) and male (M).*

Month	**F/M**	**UVA**	**Lag**	**UVB**	**Lag**	**ERY**	**Lag**
April	F	**0.32**	**22**	0.43	0	0.26	0
	M	**0.38**	**20**	0.55	0	0.37	0
May	F	0.45	0	0.65	0	0.63	0
	M	**0.49**	**1**	0.70	0	0.67	0
June	F	**0.36**	**23**	**0.35**	**25**	**0.35**	**25**
	M	**0.37**	**22**	**0.36**	**26**	**0.36**	**26**
July	F	**0.38**	**17**	**0.38**	**8**	**0.38**	**8**
	M	**0.44**	**14**	**0.34**	**14**	**0.34**	**14**
August	F	**0.34**	**17**	0.26	17	0.27	17
	M	**0.41**	**19**	**0.32**	**20**	**0.33**	**20**

Bold text; statistically significant within 5 %, with time lag > 0 years.

is the UVA that shows most correspondence with the cancer incidences.

Setlow et al. (1993) presents a study on CMM development in fish that is exposed to UV radiation for different wavelengths, to see if specific wavelengths produced more CMM. Their result was that the UVA has more effect than the CIE action spectrum would imply. The CIE and Setlow cancer action spectra are shown in Figure 4.17. Maybe the results would be more conclusive if this spectrum was used. Moan et al. (1999) also found that UVA might be the main reason for CMM development.

From the discussion above there are indications that UVA is the most important parameter for developing CMM. The time lag from UV exposure to diagnosis of CMM, is mostly found in the range of 15-25 years.

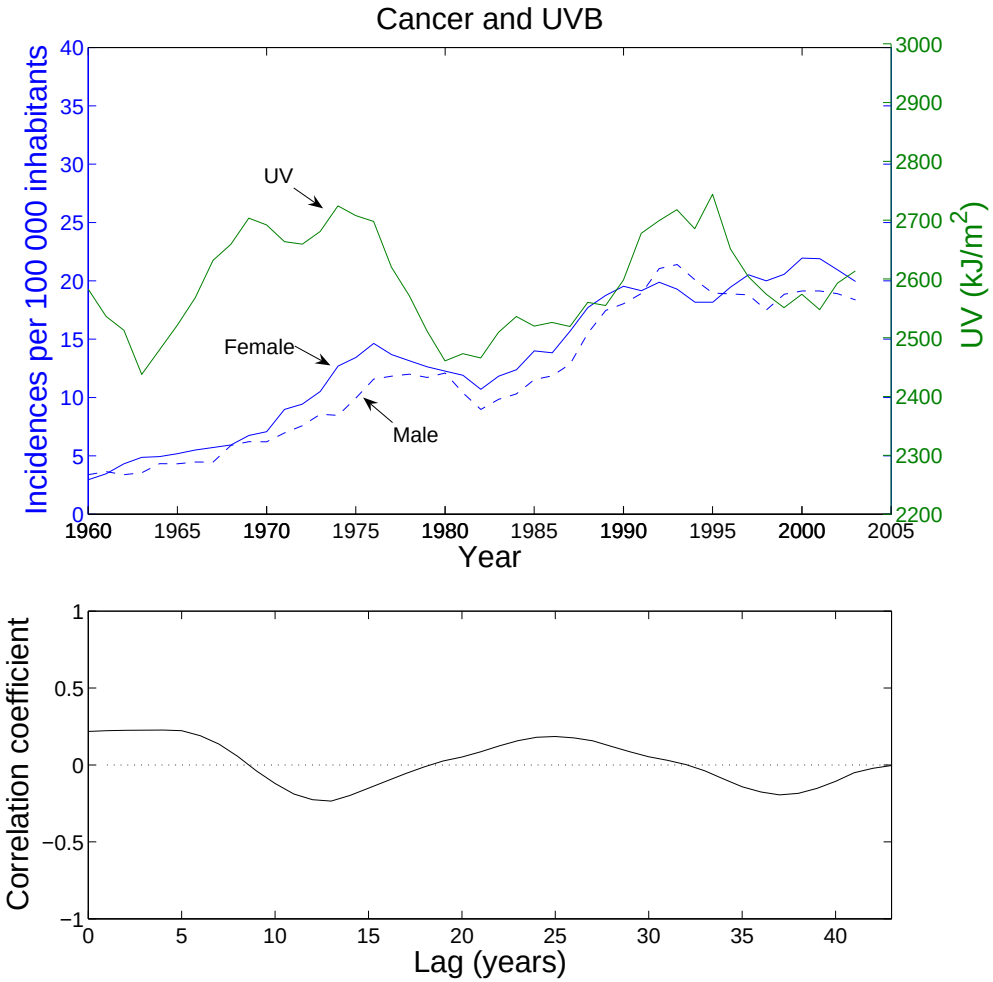

Figure 4.15: *Upper: 5 year running mean for the sum of reconstructed UVB for April to August for Rygge (green) and cancer incidences; males (dashed blue), females (fully drawn blue) for Østfold. Lower: Correlation coefficients with the corresponding time lag for the upper figure (female).*

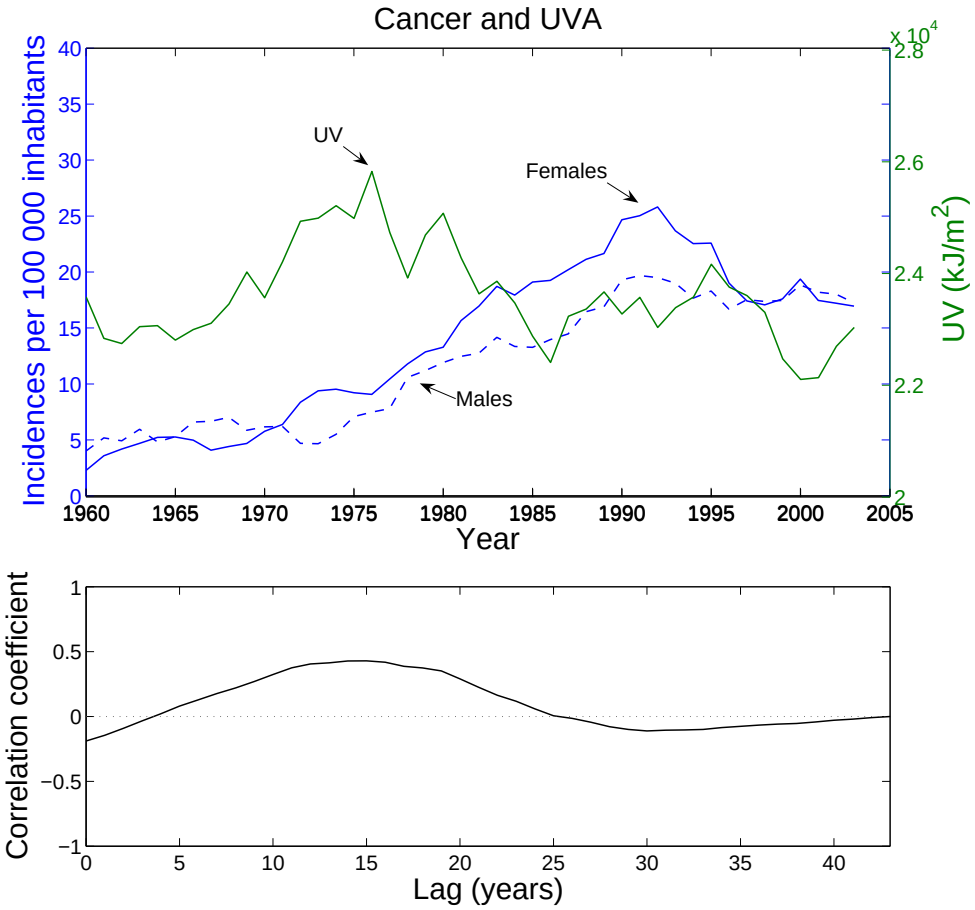

Figure 4.16: *Upper: 5 year running mean for reconstructed UVA in April for Kjevik (green) and cancer incidences; males (dashed blue), females (fully drawn blue) for Vest-Agder. Lower: Correlation coefficients with the corresponding time lag for the upper figure (female).*

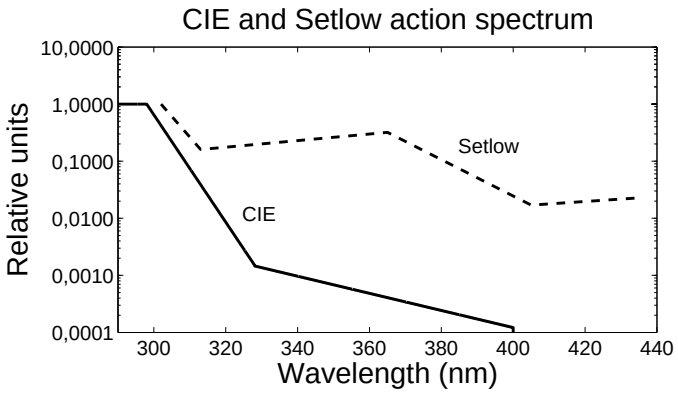

Figure 4.17: *Action spectrum for UV induced erythema in human skin (CIE) and action spectrum for melanoma induction in fish (Setlow) (values taken from Setlow et al. (1993)).*

Chapter 5

Summary and Conclusion

The UV radiation for 17 of the 19 counties in Norway has been reconstructed with the model STARneuro for the time period 1957-2005. One goal of this thesis was to investigate if this model was suitable to reconstruct reliable UV data for the entire country. The reconstructed data were then used to study trends in UV radiation during the period. The data were also used to find possible connections between the UV level and incidences of the skin cancer type cutaneous malignant melanoma (CMM).

STAR was run for two different cloud information input, one with detailed cloud information (cloud type and cloud amount for low, middle-high and high clouds) and one with only total cloud amount as input. This was done because for Oslo in the period 1981-1997 the only available cloud information was the total cloud amount.

The model was run for all 17 stations with detailed cloud information as cloud input. The reconstructed values were compared to measured values for four places in Norway, representing different regions in the country. For hourly values, the comparison showed varying degrees of agreement, from deviations close to zero for Tromsø to an average overestimation of 16 % for Bergen, and with deviations somewhere in between but closer to Bergen, for the other stations. A selection of data divided into clear sky and overcast cases, showed a reasonable agreement between reconstructed and measured data for all stations at clear sky. At overcast, the agreement was significantly worse for all stations but Tromsø. As the cloud algorithm for STARneuro is developed on data from Garmisch-Partenkirchen, a probable reason for the good agreement in Tromsø was a more similar cloud optical thickness at these two locations.

A comparison between model runs with only total cloud amount as input and the measured radiation showed that the overestimation increased when the cloud information was reduced. The overestimation compared to the measured values increased by another 4-8 % compared to the measured values for the various stations. For Tromsø, even the reduced amount of cloud information gave satisfying results, with an overall overestimation of only 5 %.

For daily values, the STARneuro reconstruction for Bergen was compared to both measured values and to results from another model, the Lindfors model which uses global radiation as input. This fact gives the Lindfors model an advantage compared to STAR, because additional information about the placement of the clouds compared to the sun is then implicitly given. Both models show satisfactory results with regards to average deviations. STAR gives an overestimation of 4 % while the Lindfors model gives an underestimation of 1 %. The difference in these models is evident in the scatter of the data, where the Lindfors model has very limited scatter because global radiation is used as input.

When comparing the reconstructed time series for the different stations, both north-south and east-west gradients were found, with the largest gradient between north and south. This was due to the latitudinal solar elevation decrease towards north in addition to the cloud optical thickness comparison to Garmisch-Partenkirchen, while the east-west variation was due to differences in both the cloud optical thickness and the total cloud amount. Clouds in the west could be optically thicker because of the moist air coming in from the sea. This results in higher levels of radiation in the east.

There were no apparent trends in the UV that applied to all reconstruction sites, some had rising annual trends and some decreasing. The differences between the sites were because of mainly two reasons. One, the variations in total ozone amount affects the amount of UVB reaching the ground, and the second reason was the change in cloud amount which affects both the amount of UVA and UVB. Decreasing ozone results in increased amount of UVB, while UVA is only negligibly affected by the changes in ozone. The cloud amount, which affects both UVA and UVB, cause a decrease in the amount of UV radiation reaching the surface for an increasing cloud amount.

The average cancer incidences in the Southern Norway is almost 3 times that of Northern Norway. The east-west difference is not that pronounced, however, the eastern part has slightly higher incidence rates. Since 1957

there has been a quite dramatic increase in incidence rates, 6-fold for women and 9-10 fold for men. For most regions there is an increasing trend up to the mid 90s, where the increase levels off, or at some stations even starts to decrease. The incidences are higher for women than for men.

There seems to be a connection between UV exposure and the development of CMM. The regions with high levels of UV radiation also have high levels of cancer incidences. There is, however, no conclusive answers, but there are strong indications that UVA contributes significantly to the increasing incidences of CMM.

Even if the amount of UV radiation is known at a given place at a given time, the individual exposure dose is not known. The potential of cancer incidences might be high because of fair weather, however, people does not necessary spend their time out in the sun. If there has been a rainy summer with low UV radiation, people might have taken vacations in southern countries.

There are a lot of different factors that have to be mapped before anything conclusive can be said about the implications the UV radiation have on the incidence rate of CMM. These factors include both clothing fashions, e.g. long skirts and pants vs short skirts and shorts, sunbathing habits, local traditions of time spent outdoors, patterns of vacations. If time is spent outdoors, the use of tanning lotion and how effective the tanning lotions been with regards to the different UV regions is an important factor. Moving from one county to another might change the UV exposure rate. Without taking the mobility of people and the vacations into consideration, there will be a misrepresenting of the incidence rate compared to the UV dose during life.

This work has compiled a comprehensive UV data set for Norway. Its duration of nearly 50 years and its temporal and spatial resolution make it an unique tool for a wide range of photo-biological research in the future.

Appendix A

Station Information

A.1 Ozone

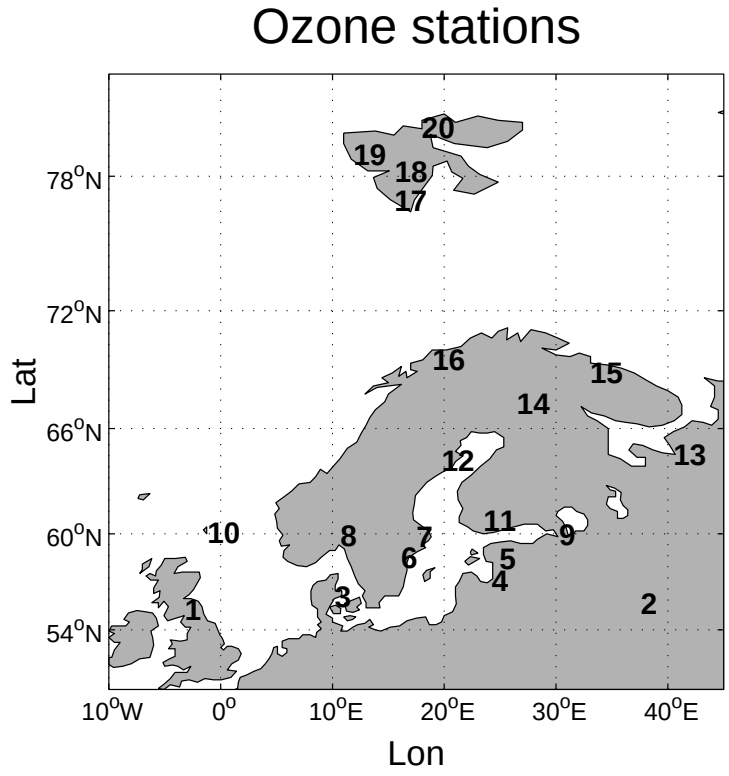

Figure A.1: *Map of the ozone stations (numbering as first column of table A.1).*

	Station(WOUDCnr)	Country	Lat	Lon	Height	Year	Type
1	Eskdalemuir (39)	GBR	3.20^{o}W	55.32^{o}N	242 m	1957-1963	D
2	Moscow (116)	RUS	37.57^{o}E	55.75^{o}N	187 m	1974-2004	D,B
3	Århus (34)	DNK	10.20^{o}E	56.17^{o}N	53 m	1957-1988	D
4	Riga (121)	LVA	24.25^{o}E	57.19^{o}N	7 m	1973-1999	F
5	Tahkuse (350)	EST	24.94^{o}E	58.52^{o}N	23 m	1995-1998	F
6	Norrkøping (279)	SWE	16.15^{o}E	58.58^{o}N	43 m	1988-2005	B
7	Uppsala (54)	SWE	17.52^{o}E	59.85^{o}N	15 m	1957-1966	D
8	Oslo (165)	NOR	10.72^{o}E	59.91^{o}N	90 m	1969-1998, 2004-2005	B
9	St. Petersburg (42)	RUS	30.30^{o}E	59.97^{o}N	74 m	1973-2003	F
10	Lerwick (43)	GBR	1.18^{o}W	60.10^{o}N	80 m	1977-2005	D
11	Joikoinen (404)	FIN	23.50^{o}E	60.81^{o}N	103 m	1999-2001	B
12	Vindeln (284)	SWE	19.77^{o}E	64.24^{o}N	225 m	1991-2005	D,B
13	Arhangelsk (271)	RUS	40.50^{o}E	64.58^{o}N	0 m	1974-2003	F
14	Sodankylä (262)	FIN	26.50^{o}E	67.33^{o}N	179 m	1988-2005	B
15	Murmansk (117)	RUS	33.05^{o}E	68.97^{o}N	46 m	1973-2003	F
16	Tromsø* (52)	NOR	18.95^{o}E	69.65^{o}N	100 m	1957-2005	D,B,T
17	Svalbard Hornsund (189)	NOR	15.55^{o}E	77.00^{o}N	11 m	1970-1983	F
18	Longyear (44)	NOR	15.58^{o}E	78.22^{o}N	1 m	1950-1966, 1984-1993	D
19	Ny Ålesund (89)	NOR	11.88^{o}E	78.93^{o}N	242.5 m	1966-1997	D
20	Murchinson Bay (46)	NOR	18.00^{o}E	80.00^{o}N	0 m	1958	D

Table A.1: *Ozone stations.*
*Where Andøya is used from 2002-2005 (69.30^{o}N, 16.15^{o}E).
The time series are not complete during the periods.
F=Filter, D=Dobson, B=Brewer, T=TOMS.

A.2 Synoptic stations

Finnmark - Sihccajavri

The only available station for Finnmark were Sihccajavri. The station has been operative since January 1912 and is located 382 m above sea level at 68.75^oN, 23.53^oE. The station lacks pressure observation throughout the entire period, so the reduced standard pressure were used, i.e. 965.5 hPa according to equation 3.2. The synoptic information is missing in the period; 10/3 - 30/4-1995.

Troms - Tromsø

The station has been operative since July 1920 and is located 100 m above sea level at 69.65^oN, 18.95^oE. Before 1968 the snow observations were only sporadic, so the input of ground albedo in that period have been affected by this. Otherwise the data are quite good.

Nordland - Bodø VI

The station has been operative since January 1953 and is located 11 m above sea level at 67.27^oN, 14.43^oE. The station has no snow depth after November 1988 but it still has snow cover observations. The pressure observations are missing from 1. November 2005 so the standard pressure, 1013.25hPa, is used. The totality of 18 days are missing throughout the period; 2/8 - 6/8-2005, and 1/11 - 13/11-2005.

Nord Trøndelag - Værnes

The station has been operative since 1946 and is located 12 m above sea level at 63.46^oN, 10.94^oE. The station lacks pressure observations in the period 1/6 - 31/12-2005, so the standard pressure, 1013.25 hPa, were used. There are also 3 days of synoptic observations missing; 8/5-2004, 16/10-2005 and 15/12-2005.

Sør Trøndelag - Ørland III

The station has been operative since July 1954 and is located 10 m above sea level at 63.70^oN, 9.60^oE. The station has generally good data, but certain observations from April 2005 and onwards are missing for some days. If there is only one observation per day, this is copied throughout this day. There are also 5 days missing throughout the period; 2/8 - 6/8-2005.

Møre og Romsdal - Tafjord

The station has been operative since 1925 and is located 15 m above sea level at 62.23^oN, 7.42^oE. The station has missing synoptic observations for 63 days; 26/11-1970, 1/6 - 31/7-1984 and 3/5-2005.

Sogn og Fjordane - Takle

The station has been operative since 1950 and is located 38 m above sea level at 61.02^oN, 5.50^oE. The station have missing pressure observations for the entire period, so the standard pressure, 1013.25 hPa, were used. 48 days of synoptic observations are also missing; 20/7 - 25/7-2001, 1/9 - 30/9-2004, 15/3 - 23/3-2005 and 14/7 - 16/7-2005.

Hordaland - Bergen (Florida)

The station has been operative since 1949 and is located 12 m above sea level at 60.38^oN, 5.33^oE. Generally good data. For missing data in the database, the data has been manually collected from Norwegian Meteorological Institute and put into the dataset.

Rogaland - Sola

The station has been operative since July 1935 and is located 7 m above sea level at 58.88^oN, 5.64^oE. No missing data.

Vest-Agder - Kjevik

The station has been operative since 1946 and is located 12 m above sea level at 58.20^oN, 8.07^oE. One day is missing in the synoptic observations; 3/12-2005.

Aust-Agder

Since there were no suitable synoptic stations in Aust-Agder and Kjevik is almost on the border between Aust-Agder and Vest-Agder, Kjevik is used as representative for both Vest- and Aust-Agder.

Telemark - Tveitsund

The station has been operative since June 1944 and is located 252 m above sea level at 59.03^oN, 8.52^oE. Pressure observations are lacking prior to 1982 and in the period 2/11 - 17/11-2003. The pressure used for these periods were

the reduces standard pressure, 981.75 hPa. 35 days of synoptic observations are missing; 23/10 - 3/11-2000, 2/3 - 16/3-2002, 17/6 - 21/6-2005 and 18/11 - 20/11-2005.

Vestfold - Færder Fyr

The station has been operative since January 1885 and is located 6 m above sea level at 59.03^oN, 10.53^oE. The synoptic observations after 2003 are so sparse that they are excluded from the reconstruction. There are no snow observations at this station, so the ground albedo is set to snow free conditions. In the period 24/10 - 31/10-2000 there are no pressure observations, so the pressure is set to the standard pressure, 1013.25 hPa. During 1957 and 1958 there are 41 days of observations missing and these are concentrated in January-March and October-December both years.

Østfold - Rygge

The station has been operative since March 1955 and is located 40 m above sea level at 59.38^oN, 10.79^oE. There are no pressure observations from June 2005, so the standard pressure, 1013.25 hPa, were used. There are sparse snow observations at the end of 2005. The only day of missing synoptic observations for this station is 21/5-2005.

Akershus - Gardermoen

The station has been operative since April 1940 and is located 202 m above sea level at 60.21^oN, 11.08^oE. 9 days of synoptic observations are missing; 30/4-2004, 12/6-2005, 26/7-2005, 2/8 - 4/8-2005, 6/8-2005, 31/10-2005 and 23/12-2005.

Oslo - Blindern

The station has been operative since February 1937 and is located 94 m above sea level at 59.94^oN, 10.72^oE. Prior to November 1957 no snow observations were made. For missing pressure observations, from 1/6-2005, the reduced standard pressure, 1001.5 hPa, were used. In the period 1981-1997 the specified cloud information is missing because only the total cloud amount is were observed. The reconstruction was then made for 1957-1980, and then with only total cloud amount in the period 1981-1997, and then again with all the cloud information for the period 1998-2005. For the last period 48 days of observations were missing; 28/7 - 1/8-2005.

Buskerud - Lygdal i Nummedalen

The station has been operative since June 1954 and is located 288 m above sea level at 59.91^oN, 9.52^oE. No missing data.

Oppland

No suitable observation stations in this region.

Hedmark - Rena-Haugedalen

The station has been operative since January 1958 and is located 240 m above sea level at 61.16^oN, 11.44^oE. Since the station was not operative until 1958, the reconstruction for this station was done for the period 1958-2005. Until April 2004, there were no pressure observations, so standard pressure was reduced to the height of the station, i.e 983.25 hPa. Beside missing entire 1957, additionally 14 days were missing; 31/12 - 2/11-2001, 7/1-2005, 3/5-2005, 30/7 - 31/7-2005 and 13/9 - 15/9-2005.

A.3 UV-stations

Station	Lat	Lon	Elevation	Start	End
Ny-Ålesund	78.92^{o}N	11.92^{o}E	400 m	1995	-
Tromsø	69.68^{o}N	18.97^{o}E	60 m	1995	2000
Andøya	69.28^{o}N	16.02^{o}E	380 m	2000	-
Trondheim	63.42^{o}N	10.40^{o}E	65 m	1996	-
Kise*	60.77^{o}N	10.80^{o}E	130 m	1996	-
Finse	60.60^{o}N	7.52^{o}E	1210 m	2003	-
Bergen	60.38^{o}N	5.33^{o}E	40 m	1996	-
Østerås	59.95^{o}N	10.60^{o}E	135 m	1999	-
Blindern	59.93^{o}N	10.72^{o}E	95 m	1994	-
Landvik	58.33^{o}N	8.52^{o}E	10 m	1996	-

Table A.2: *UV measurement stations from north to south*
*In the autumn of 2004 had a change of horizon.

Appendix B

Cloud information

Low cloud types:
CL1: Cumulus humilis or fractus (Cu). Cumulus with small vertical extent (fair weather clouds).
CL2: Cumulus mediocris or congestus (Cu). Cumulus with medium to large vertical extent. The cloud base is dark and almost horizontal.
CL3: Cumulonimbus calvus (Cb) without an anvil (precipitable cloud).
CL4: Stratocumulus cumologenitus (Sc) formed by spreading of cumulus clouds.
CL5: Stratocumulus (Sc) not formed by spreading of cumulus clouds.
CL6: Stratus nebulosus or fractus (St). Uniform fog clouds.
CL7: Stratus fractus or cumulus fractus (St). Fog clouds with precipitation (mix of fog clouds and cumulus clouds).
CL8: Cumulus and stratocumulus (Cu) with cloud base at different levels.
CL9: Cumulonimbus capilatus(Cb) with the top formed as an anvil. Thunder cloud.
X: When the sky can not be observed.
Medium-high cloud types:
CM1: Altostratus translusidus (As). Thin altostratus.
CM2: Altostratus opacus or nimbostratus (Ns) Thick altostratus with precipitation.
CM3: Altocumulus translucidus (Ac).
CM4: Altocumulus translucidus or lenticularis (Ac), often appear in several layers in lenticular form.
CM5: Altocumulus translucidus or opacus (Ac), formed by updraft of an incoming front.
CM6: Altocumulus cumulogenitus or cumulonimbogenitus (Ac) clouds formed by the spreading of cumulus cloud tops.
CM7: Altocumulus translucidus or opacus and altostratus or nimbostratus

(Ac) in two or more levels, at times dense layers.
CM8: Altocumulus castellanus or floccus (Ac). Small dots.
CM9: Altocumulus (Ac) in a chaotic sky.
High cloud types:
CH1: Cirrus fibratus and uncinus (Ci). Thin layer.
CH2: Cirrus spissatus, castellanus or floccus (Ci). Dense layer of cirrus.
CH3: Cirrus spissatus cumulonimbogenitus (Ci). Dense layer of cirrus at the top of a Cb-anvil.
CH4: Cirrus uncinus or fibratus (Ci) formed by an updraft.
CH5: Cirrostratus (Cs) from an updraft that has not yet reached 45deg above the horizon.
CH6: Cirrostratus (Cs) from an updraft that has reached more than 45 deg above the horizon.
CH7: Cirrostratus (Cs) fully covering the sky.
CH8: Cirrostratus (Cs) that only partially covers the sky.
CH9: Cirrocumulus (Cc).

Appendix C

Decadal trends in UVA, UVB and ERY

Table C.1: *Trends in UVA in % per decade for the period 1957-2005 from north to south*

Station	**Jan**	**Feb**	**March**	**April**	**May**	**June**	**July**	**Aug**	**Sept**	**Oct**	**Nov**	**Dec**
Tromsø	0.6	-0.7	-0.6	-0.5	-0.5	0.9	-0.4	-0.7	-0.5	-0.4	-0.2	-
Sihccajavri	-1.7	-2.8	-4.0	-3.6	-3.5	-3.0	-2.9	-2.5	-2.3	-2.2	-1.9	-
Bodø	-1.0	-1.0	-0.3	1.2	-0.3	0.7	1.2	-0.5	0.9	1.8	-0.2	-0.0
Ørland	-1.4	-0.3	-0.9	0.8	0.3	-0.2	0.8	-0.4	1.6	2.4	-0.1	-0.6
Værnes	-0.5	-0.3	-0.7	1.3	0.6	-0.2	1.8	0.1	2.0	3.1	0.4	0.3
Tafjord	-0.5	-0.9	-2.7	-0.7	-0.9	-1.6	0.3	-1.0	-0.2	0.4	-0.1	0.7
Rena - Haugedal*	-0.9	-0.5	-1.1	-2.5	-0.8	-2.8	-0.4	-1.4	-2.3	-0.9	-1.5	-0.6
Takle	-0.5	-0.4	-2.0	-0.1	0.5	-0.0	-0.0	0.5	1.2	0.7	0.8	0.9
Bergen - Florida	-2.3	-1.2	-2.7	-0.9	0.2	-0.7	0.4	0.1	-0.2	-0.4	-0.6	-1.4
Gardermoen	0.2	0.5	-0.9	-1.3	0.6	-2.2	-0.1	0.2	-0.4	0.1	0.2	0.1
Oslo*	-4.0	-0.2	-5.0	1.1	0.6	0.1	1.7	2.0	-1.3	0.8	7.0	3.7
Lyngdal-Nummedalen	1.8	1.4	-0.1	0.0	2.5	-0.8	2.0	1.4	1.3	0.7	1.0	0.9
Rygge	0.4	0.7	-0.8	-1.2	0.5	-2.3	-0.2	-0.1	0.1	-0.2	-0.4	0.1
Tveitsund	0.1	0.8	-1.4	-1.7	0.9	-2.6	0.2	-0.2	-1.5	-0.3	0.6	-0.3
Færder Fyr*	3.5	4.1	-0.6	-1.0	1.6	-1.4	1.1	1.6	0.7	0.7	0.4	0.5
Sola	0.5	-0.2	-0.8	0.2	1.7	-0.2	1.0	2.1	0.8	1.9	1.2	1.1
Kjevik	1.4	1.3	0.2	-0.3	1.7	-0.8	1.5	1.2	-0.3	0.4	1.0	0.6

(*)Shorter periods: Rena; 1958-2005, Oslo;1957-1980, Færder Fyr;1957-2003

Table C.2: *Trends in UVB in % per decade for the period 1957-2005 from north to south*

Station	**Jan**	**Feb**	**March**	**April**	**May**	**June**	**July**	**Aug**	**Sept**	**Oct**	**Nov**	**Dec**
Tromsø	5.8	5.5	8.7	4.3	1.5	1.7	0.5	-0.5	-0.1	-0.8	-0.1	-
Sihccajavri	3.6	3.4	3.7	-0.3	-2.3	-2.5	-2.4	-2.3	-1.9	-2.6	-1.4	-
Bodø	3.0	5.9	8.5	6.2	1.3	1.5	2.1	-0.1	1.6	1.8	0.3	1.0
Ørland	1.9	7.3	6.9	5.1	2.0	0.4	1.7	0.0	2.4	2.2	0.4	-0.3
Værnes	3.0	7.3	7.8	5.8	2.3	0.4	2.8	0.5	2.7	3.1	0.7	0.6
Tafjord	3.7	6.9	4.2	2.8	0.2	-1.3	0.7	-0.7	0.2	0.2	0.6	1.2
Rena - Haugedal*	3.3	5.7	6.7	0.8	0.5	-2.4	0.3	-1.0	-2.0	-1.0	-0.7	0.2
Takle	3.6	7.0	4.2	3.3	1.7	0.5	0.3	0.9	2.1	0.4	0.9	1.3
Bergen - Florida	2.0	6.9	3.9	2.8	1.6	-0.0	1.3	0.6	0.5	-0.4	0.1	-0.7
Gardermoen	4.1	8.0	6.5	1.8	2.0	-1.7	0.6	0.6	-0.0	0.1	0.5	0.3
Oslo*	-3.1	8.0	-5.3	-3.5	-0.2	-0.1	1.2	1.3	-4.9	-3.8	-1.5	-4.9
Lyngdal - Nummedalen	5.7	8.9	7.7	3.5	4.2	-0.3	2.8	1.8	1.8	0.5	1.4	0.9
Rygge	4.3	8.2	6.5	2.0	1.9	-1.8	0.5	0.3	0.5	-0.5	0.9	0.4
Tveitsund	4.6	7.7	6.0	1.3	2.4	-2.3	0.8	0.1	-1.2	-0.3	1.4	-0.2
Færder Fyr*	7.3	0.1	6.4	2.2	3.2	-1.0	1.7	1.8	0.9	-0.2	-1.3	-0.9
Sola	4.7	7.3	6.1	3.9	3.2	0.4	1.8	2.7	1.5	1.9	1.6	0.9
Kjevik	6.0	8.5	7.9	3.0	3.1	-0.4	2.2	1.5	-0.0	0.1	1.1	0.1

(*)Shorter periods: Rena; 1958-2005, Oslo;1957-1980, Færder Fyr;1957-2003

Table C.3: *Trends in Erythemal UV in % per decade for the period 1957-2005 from north to south*

Station	**Jan**	**Feb**	**March**	**April**	**May**	**June**	**July**	**Aug**	**Sept**	**Oct**	**Nov**	**Dec**
Tromsø	2.3	1.3	2.1	2.3	0.8	1.7	0.3	-0.7	-0.3	-0.5	-0.1	-
Sihccajavri	0.1	-0.9	-0.1	-1.9	-2.9	-2.7	-2.7	-2.5	-2.1	-1.7	-1.7	-
Bodø	0.4	1.3	2.4	4.5	0.9	1.4	2.1	-0.1	1.5	1.3	-0.1	0.3
Ørland	-0.1	2.0	1.9	3.8	1.7	0.4	1.8	-0.2	2.3	1.6	0.1	-0.6
Værnes	0.9	2.0	2.3	4.5	2.1	0.4	2.9	0.5	2.7	2.2	0.6	0.3
Tafjord	1.2	1.8	0.4	1.7	-0.1	-1.4	0.7	-0.9	0.2	0.0	0.2	0.9
Rena - Haugedal*	0.6	1.5	2.7	-0.3	0.2	-2.6	0.3	-1.1	-2.2	-0.7	-1.2	-0.2
Takle	1.2	2.0	0.8	2.3	1.5	0.5	0.3	0.9	2.1	0.2	1.0	1.1
Bergen - Florida	-0.6	1.2	0.5	1.8	1.4	-0.1	1.3	0.7	0.5	-0.6	-0.3	-1.1
Gardermoen	1.7	2.6	2.8	0.9	1.8	-1.8	0.6	0.6	-0.1	0.1	0.4	0.2
Oslo*	-3.7	3.0	-5.1	-2.4	-0.1	-0.0	1.3	1.5	-4.8	-1.1	3.2	-0.3
Lyngdal - Nummedalen	3.3	3.3	3.9	2.6	4.2	-0.3	3.0	1.9	1.8	0.5	0.9	1.0
Rygge	2.0	2.7	2.9	1.1	1.7	-2.0	0.5	0.3	0.4	-0.5	0.6	0.3
Tveitsund	1.7	2.7	2.5	0.3	2.2	-2.4	0.9	0.0	-1.5	0	0.7	-0.3
Færder Fyr*	5.0	5.7	3.1	1.4	3.3	-1.0	1.9	1.9	0.9	0.1	-0.1	0.5
Sola	2.1	2.2	2.7	3.0	3.1	0.4	1.9	2.8	1.6	1.8	1.4	1.2
Kjevik	2.9	3.2	4.4	2.1	3.0	-0.5	2.3	1.5	-0.1	0.2	1.1	0.7

(*)Shorter periods: Rena; 1958-2005, Oslo;1957-1980, Færder Fyr;1957-2003

Appendix D

Statistics

When comparing the modeled and measured data the equations below were used to see how well the data coincided.

$$MBD = \frac{\sum(R_i - M)}{n} \tag{D.1}$$

MBD = mean bias deviation M=Measured R=Reconstructed n=number of observations

Mean bias deviation (MBD) implies how large the mean of the deviation is between the modeled and the measured data.

$$RMSD = \sqrt{\frac{\sum(R_i - M)^2}{n}} \tag{D.2}$$

The root mean square deviation (RMSD) implies how large the scatter of the data is around the one-to-one line.

Appendix E

Cancer incidences

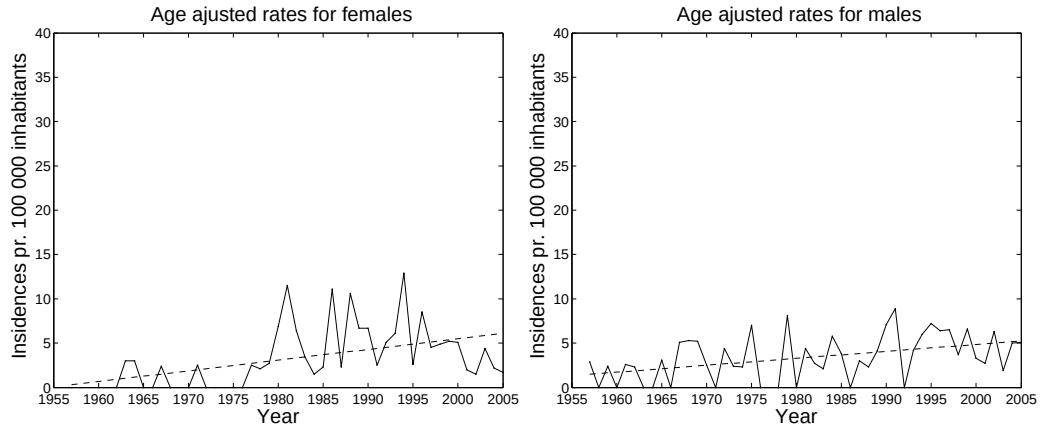

Figure E.1: *Age-adjusted incidence rates for females (left) and males (right) pr. 100 000 inhabitants in Finnmark. Linear trend (dotted line).*

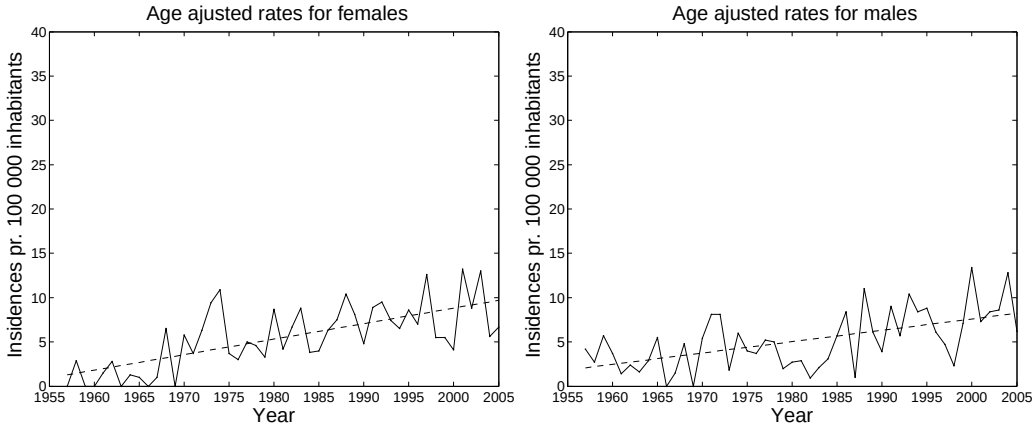

Figure E.2: *Age-adjusted incidence rates for females (left) and males (right) pr. 100 000 inhabitants in Troms. Linear trend (dotted line).*

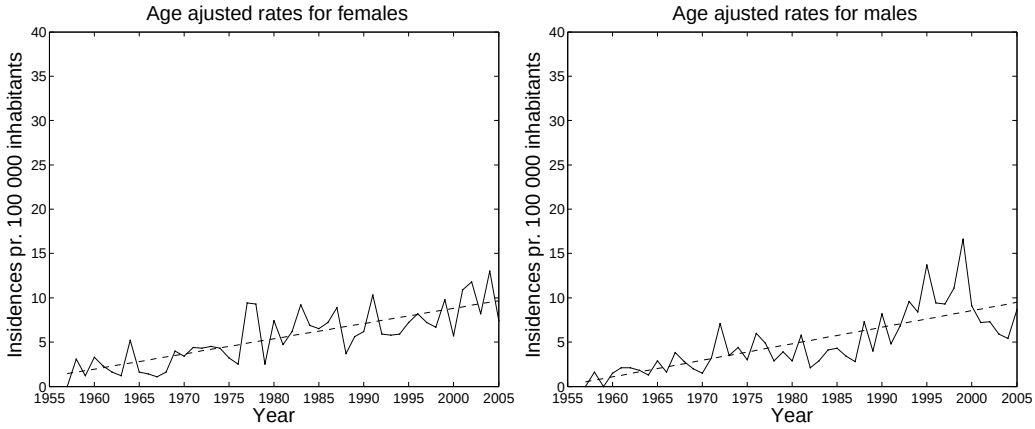

Figure E.3: *Age-adjusted incidence rates for females (left) and males (right) pr. 100 000 inhabitants in Nordland. Linear trend (dotted line).*

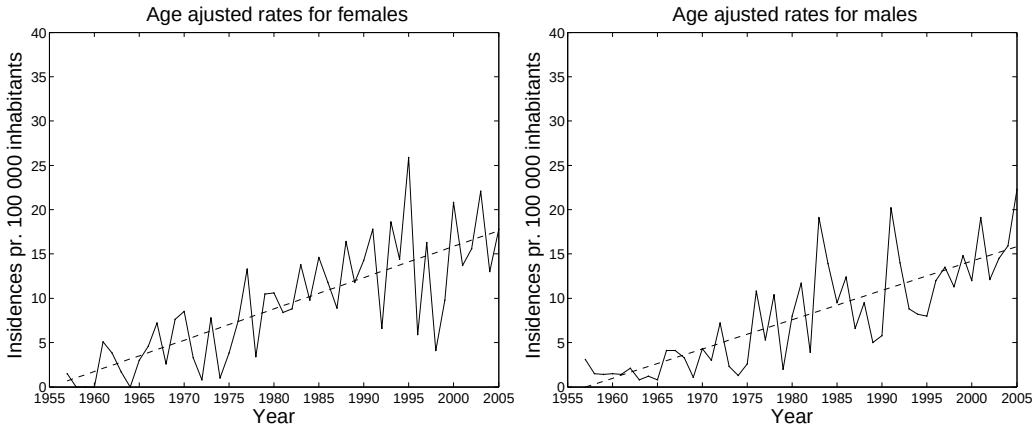

Figure E.4: *Age-adjusted incidence rates for females (left) and males (right) pr. 100 000 inhabitants in Nord-Trøndelag. Linear trend (dotted line).*

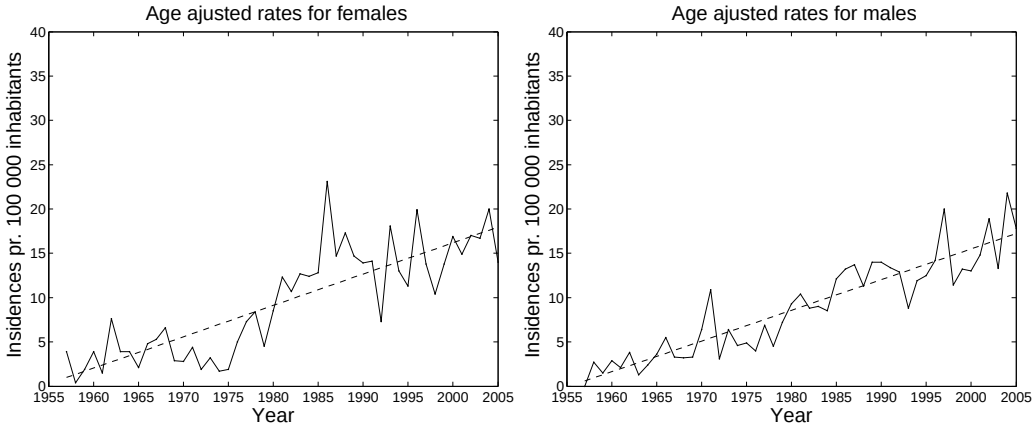

Figure E.5: *Age-adjusted incidence rates for females (left) and males (right) pr. 100 000 inhabitants in Sør-Trøndelag. Linear trend (dotted line).*

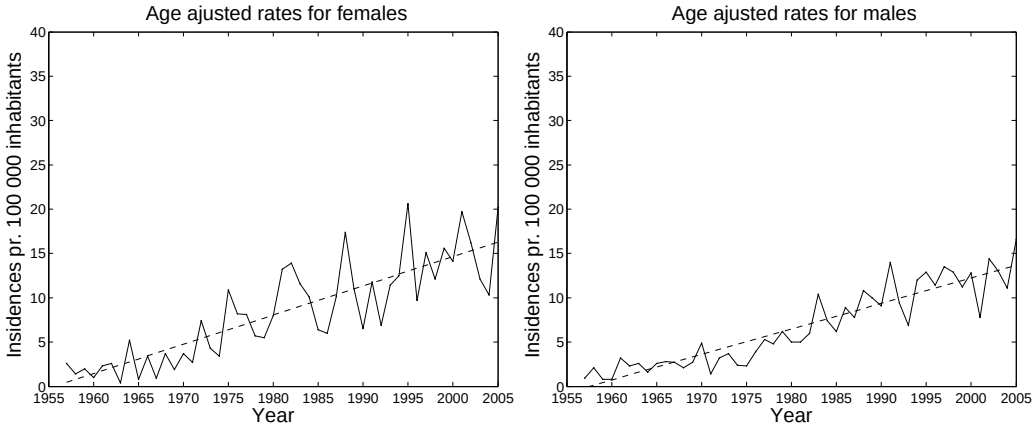

Figure E.6: *Age-adjusted incidence rates for females (left) and males (right) pr. 100 000 inhabitants in Møre og Romsdal. Linear trend (dotted line).*

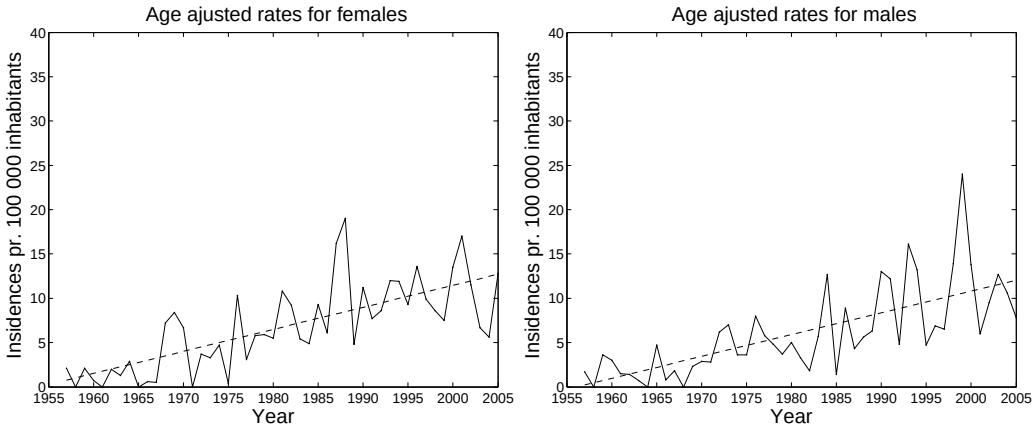

Figure E.7: *Age-adjusted incidence rates for females (left) and males (right) pr. 100 000 inhabitants in Sogn og Fjordane. Linear trend (dotted line).*

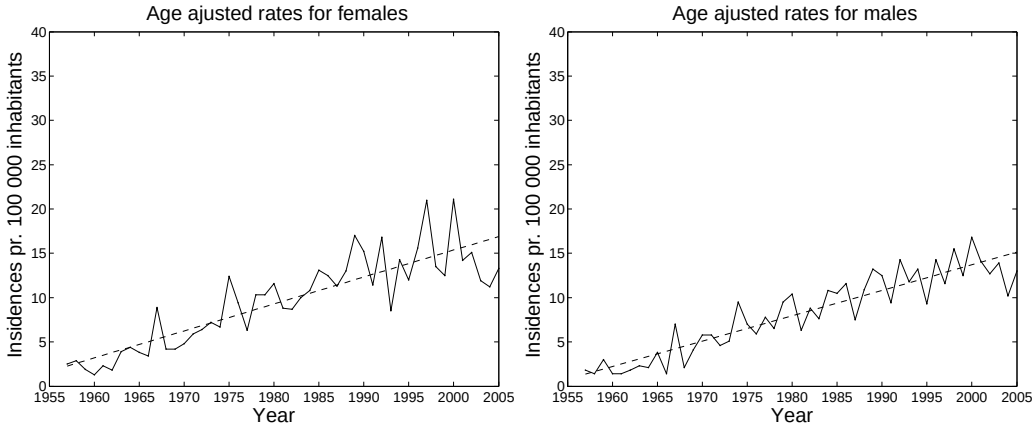

Figure E.8: *Age-adjusted incidence rates for females (left) and males (right) pr. 100 000 inhabitants in Hordaland. Linear trend (dotted line).*

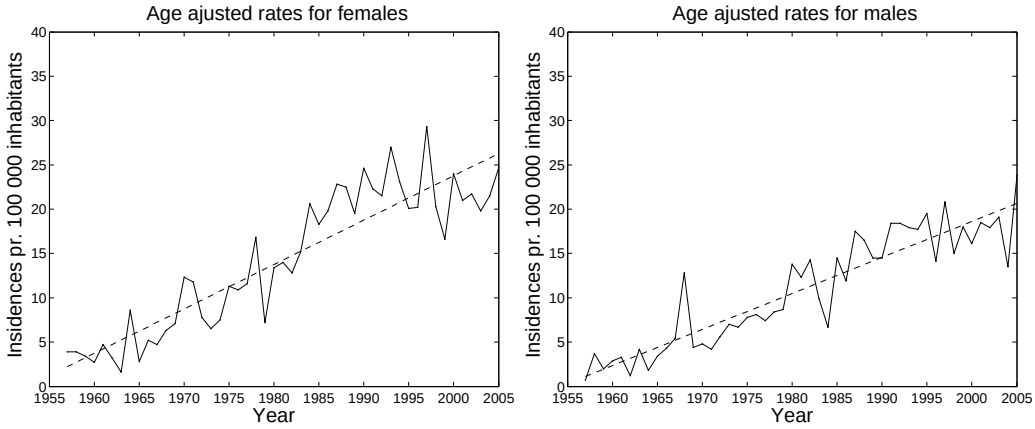

Figure E.9: *Age-adjusted incidence rates for females (left) and males (right) pr. 100 000 inhabitants in Rogaland. Linear trend (dotted line).*

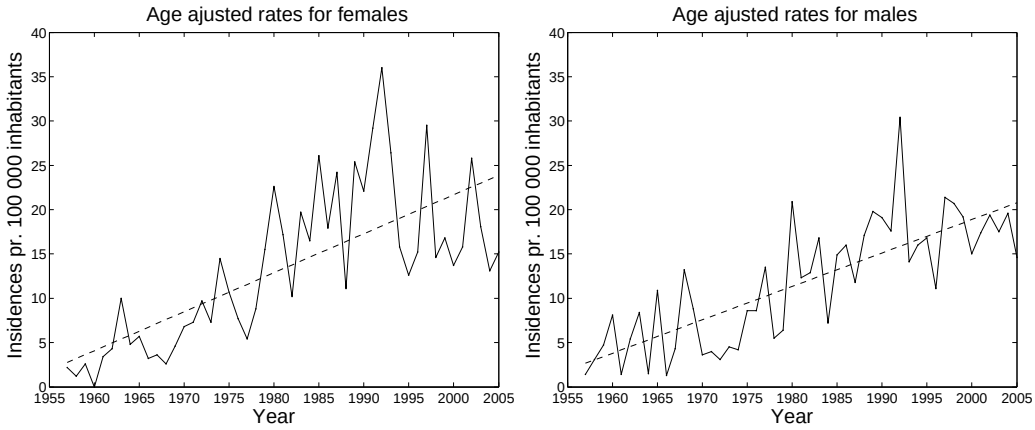

Figure E.10: *Age-adjusted incidence rates for females (left) and males (right) pr. 100 000 inhabitants in Vest-Agder. Linear trend (dotted line).*

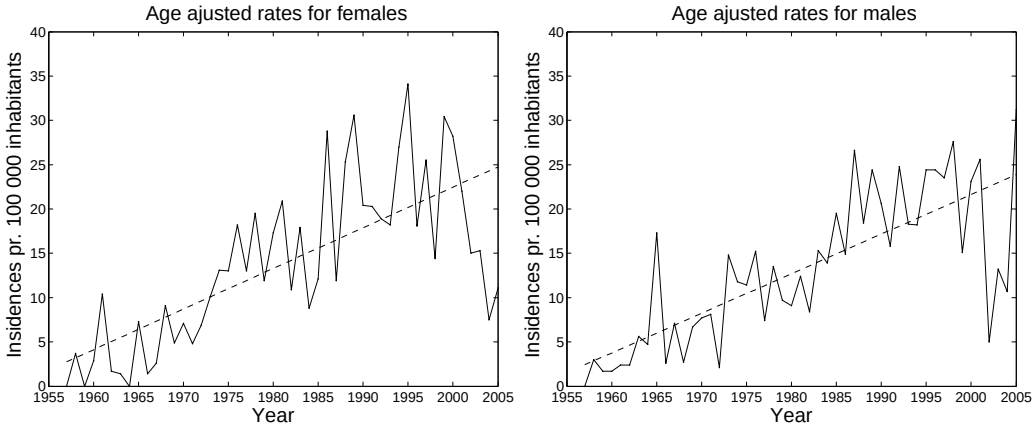

Figure E.11: *Age-adjusted incidence rates for females (left) and males (right) pr. 100 000 inhabitants in Aust-Agder. Linear trend (dotted line).*

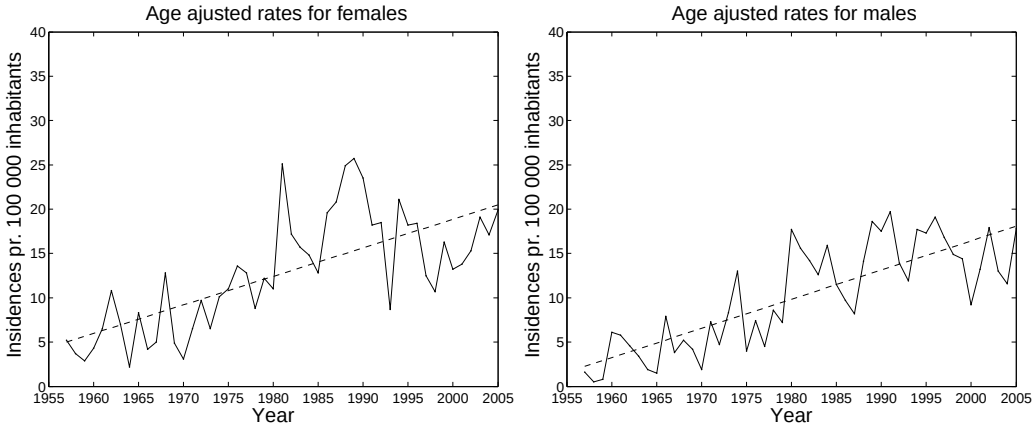

Figure E.12: *Age-adjusted incidence rates for females (left) and males (right) pr. 100 000 inhabitants in Telemark. Linear trend (dotted line).*

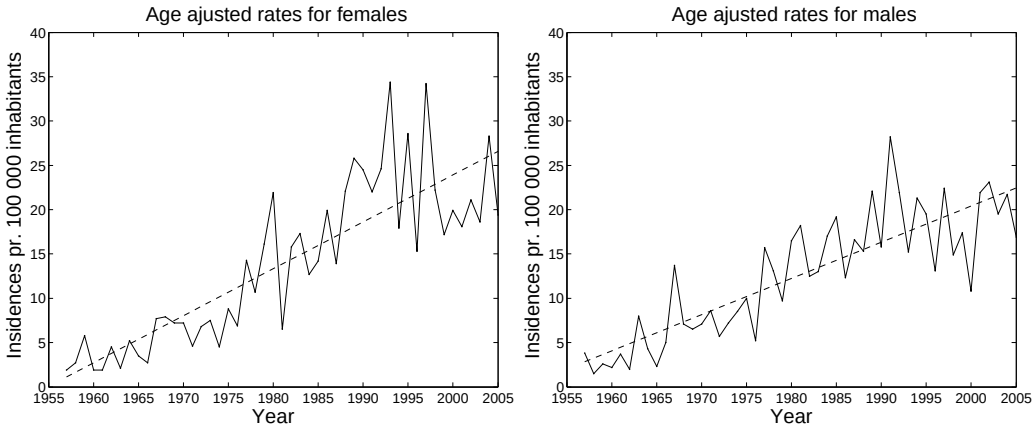

Figure E.13: *Age-adjusted incidence rates for females (left) and males (right) pr. 100 000 inhabitants in Vestfold. Linear trend (dotted line).*

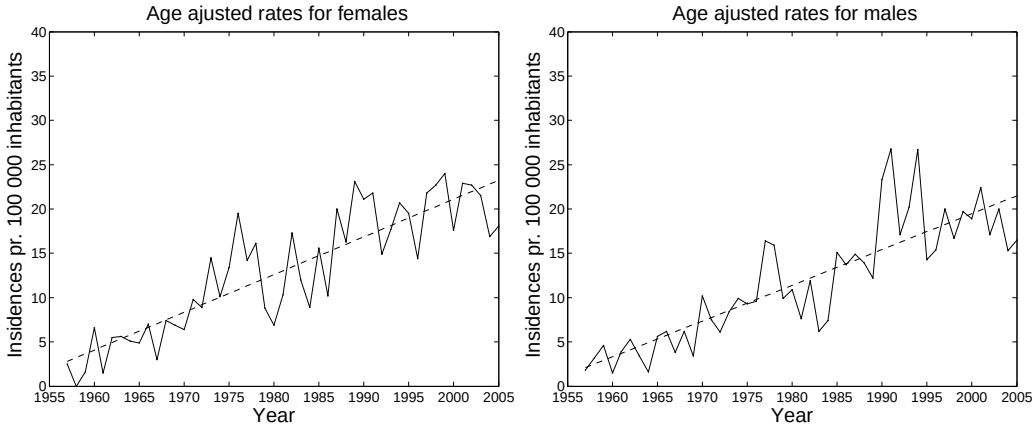

Figure E.14: *Age-adjusted incidence rates for females (left) and males (right) pr. 100 000 inhabitants in Østfold. Linear trend (dotted line).*

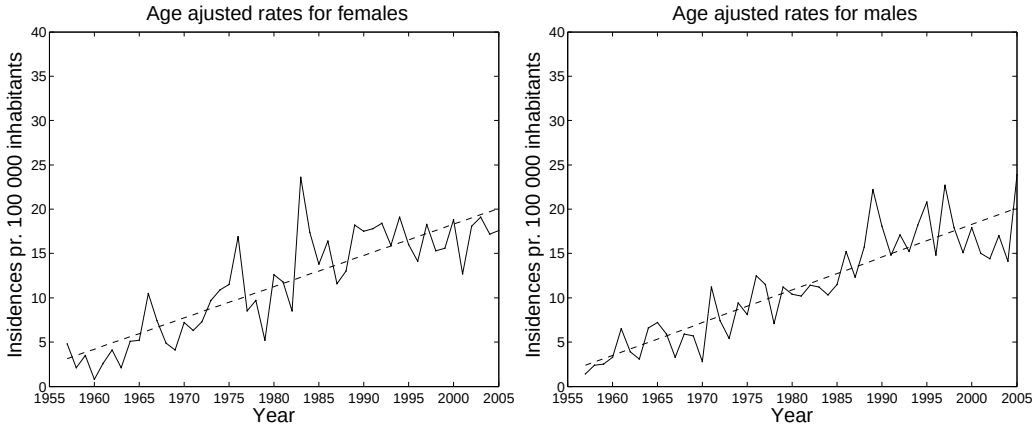

Figure E.15: *Age-adjusted incidence rates for females (left) and males (right) pr. 100 000 inhabitants in Akershus. Linear trend (dotted line).*

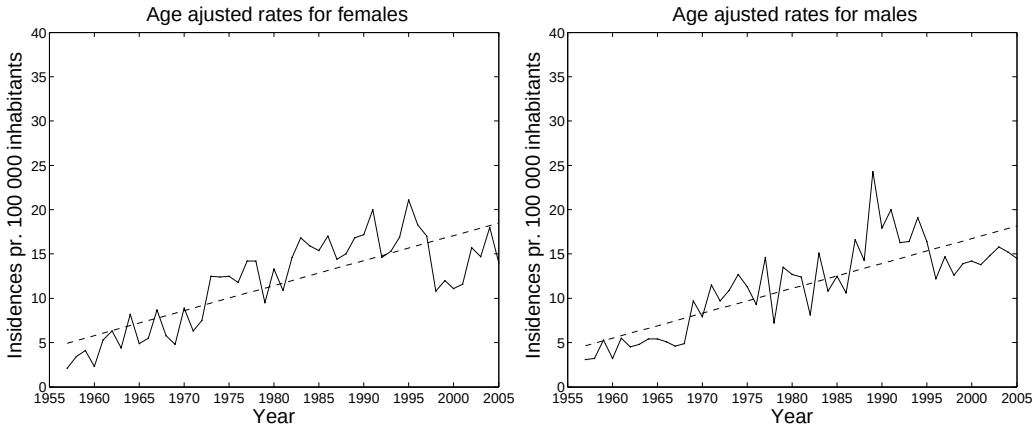

Figure E.16: *Age-adjusted incidence rates for females (left) and males (right) pr. 100 000 inhabitants in Oslo. Linear trend (dotted line).*

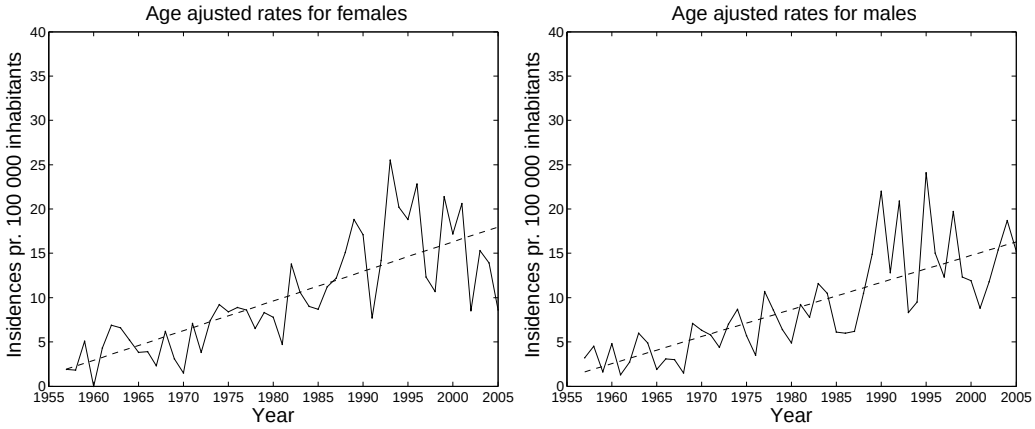

Figure E.17: *Age-adjusted incidence rates for females (left) and males (right) pr. 100 000 inhabitants in Hedmark. Linear trend (dotted line).*

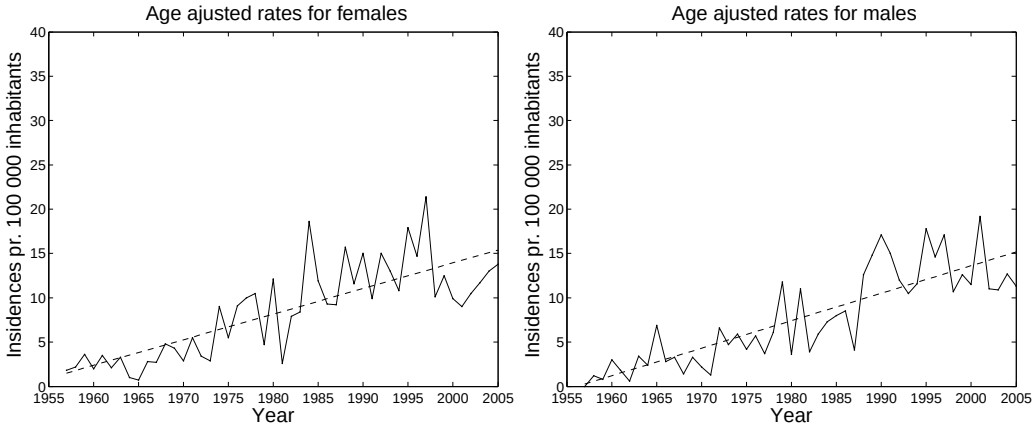

Figure E.18: *Age-adjusted incidence rates for females (left) and males (right) pr. 100 000 inhabitants in Oppland. Linear trend (dotted line).*

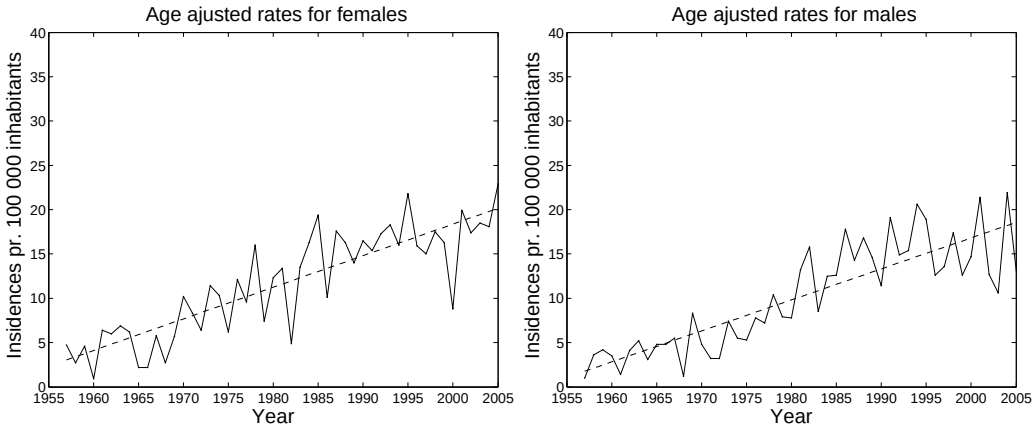

Figure E.19: *Age-adjusted incidence rates for females (left) and males (right) pr. 100 000 inhabitants in Buskerud. Linear trend (dotted line).*

Bibliography

Armstrong, B. K. and A. Kricker (1993). How much melanoma is caused by sun exposure? *Melanoma Res. 3*, 395–401.

Autier, P., J. Dore, and F. Lejeune *et al.* (1994). Risk factors of the cutaneous melanoma: results from an EORTC case-control study. *Melanoma Res. 4*, 79–85.

Autier, P. and J. F. Dore (1998). Influence of sun exposures during childhood and during adulthood on melanoma risk. *Int J Cancer 77*, 533–537.

Berwick, M., B. Armstrong, L. Ben-Porat, J. Fine, A. Kricker, C. Eberle, and R. Barnhill (2005). Sun exposure and mortality from melanoma. *J Natl Cancer Inst 97*, 195–199.

Caldwell, M. M. and S. D. Flint (1994). Stratospheric ozone reduction, solar UV-B radiation and terrestrial ecosystems. *Climatic Change 28*(4), 375–394.

Cancer Registry of Norway (2005). Cancer in Norway 2002. Technical report, Cancer Registry of Norway.

Carlson, T. (2005). UV-stråling i Norge. Satellittestimater, modellestimater og bakkemålinger. Master's thesis, Geofysisk institutt, Universitetet i Bergen.

Chen, Y. T., R. Dubrow, T. R. Holford, T. Zheng, R. L. Barnhill, J. Fine, and B. M. (1996). Malignant melanoma risk factors by anatomic site: a case-control study and polychotomous logistic regression analysis. *Int J Cancer 67*(5), 636–643.

COST 726 (2007). Long term changes and climatology of UV radiation over Europe; (Last update sept. 2006). http://cost726.org/.

Diffey, B. L. (2004). Climate change, ozone depletion and the impact on ultraviolet exposure of human skin. *Phys Med Biol 49*, R1–R11.

Doll, R., P. Payne, and J. Waterhouse (1966). *Cancer incidence in five continents*, Volume I. Springer, Berlin.

Egan, K. M., J. A. Sosman, and W. Blot (2005). Sunlight and reduced risk of cancer: is the real story vitamin D? *J Natl Cancer Inst 97*, 161–163.

Emery, W. J. and R. E. Thomson (2001). *Data Analysis Methods in Physical Oceanography* (Second and Revised ed.). Elsevier B.V.

Feister, U. and R. Grewe (1995). Spectral albedo measurements in the UV and visible region over different types of surfaces. *Photochem. Photobiol. 62*(4), 736–744.

Hartmann, D. L. (1994). *Global Physical Climatology*. Academic Press.

Henriksen, T. and T. Svendby (1997). *Ozonlag, UV-stråling og helse*. Fysisk institutt, Universitetet i Oslo.

Herman, J., P. Bhartia, J. Ziemke, Z. Ahmad, and D. Larko (1996). UV-B increases (1979-1992) from decrease in total ozone. *J. Geophys. Res. Lett. 23(16)*, 2117–2120.

Hughes, A. M., B. K. Armstrong, C. M. Vajdic, J. Turner, A. E. Grulich, L. Fritschi, S. Milliken, J. Kaldor, G. Benke, and A. Kricker (2004). Sun exposure may protect against non-hodgkin lymphoma: a case-control study. *Int J Cancer 112*, 865–871.

Iqbal, M. (1983). *An Introduction to Solar Radiation*. Academic Press.

IRI (2006). Interpolation techniques. http://ingrid.ldeo.columbia.edu/dochelp/StatTutorial/Interpolation/.

Iscovich, J. and G. R. Howe (1998). Cancer incidence patterns (1972-91) among migrants from the Soviet Union to israel. *Cancer Causes and Control 9*(1), 29–36.

Khlat, M., A. Vail, M. Parkin, and A. Green (1992). Mortality from melanoma in migrants to Australia: Variation by age at arrival and duration of stay. *Am J Epidemiol 135*(10), 1103–1113.

Koepke, P., H. De Backer, A. Bais, A. Curylo, K. Eerme, U. Feister, B. Johnsen, J. Junk, A. Kazantzidis, J. Krzyscin, A. Lindfors, J. A. Olseth, P. den Outer, A. Pribullova, A. Schmalwieser, H. Slaper, H. Staiger, J. Verdebout, L. Vuilleumier, and P. Weihs (2007). Modelling solar UV radiation in the past: Comparison of algorithms and effects of the selected input data. Technical report, Cost 726.

Koepke, P., J. Reuder, and H. Schwander (2002). Solar UV radiation and its variability due to the atmospheric components. *Recent Res. Devel. in Photochem. and Photobiol. 6*, 11–34.

Koh, H. K., B. E. Kligler, and R. A. Lew (1990). Sunlight and cutaneous malignant melanoma: evidence for and against causation. *Photochem. Photobiol. 51*, 765–779.

Komhyr, W. D., R. D. Grass, R. D. Evans, R. K. Leonard, D. M. Quincy, D. J. Hofmann, and G. L. Koenig (1994). Unprecedented 1993 ozone decrease over the United States from Dobson spectrophotometer observations. *Geoph. Res. Letters 21*(3), 201–204.

Kreftforeningen (2007, April). Spørsmål og svar om føflekkreft. http://www.kreftforeningen.no/forebygg/http://www.kreftforeningen.no /om_kreft/kreftformer.

Kreftregisteret (2007, April). Fakta om kreft, (last updated; 8 sep. 2005). http://kreftregisteret.no/ramme.htm?start.htm .

Lim, H. and K. Cooper (1999). The health impact of solar radiation and prevention strategies. *J Am Acad Dermatol 41*, 81–84.

Lindfors, A., J. Kaurola, T. Koskela, K. Lakkala, W. Josefsson, and J. A. Olseth (2007). A method or reconstruction of past UV radiation based on radiative transfer modeling: applied to four stations in northern Europe. In *J. Geophys. Res.*, pp. 1–17.

Liou, K. N. (1992). *Radiation and Cloud Processes in the Atmosphere*. Oxford university press.

Long, C. S. (2003, June). SPARC newsletter 21: UV Index Forecasting Practices around the World. http://www.aero.jussieu.fr/∼sparc/News21/index.html.

Longstreth, J., F. R. de Gruijl, M. L. Kripke, S. Abseck, F. Arnold, H. I. Slaper, G. Velders, Y. Takizawa, and J. C. van der Leun (1998). Health risks. *J Photochem Photobiol B. 46*(1-3), 20–39.

Madronich, S. and F. R. De Gruijl (1994). Stratospheric ozone depletion between 1979 and 1992: Implications for biological active ultraviolet-B radiation and non-melanoma skin cancer incidence. *Photochem. and Photobiol. 59*(5), 541–546.

Magnus, K. (1973). Incidence of malignant melanoma of the skin in Norway, 1955-1970. Variations in time and space and solar radiation. *Cancer 32*(5), 1275–1286.

Magnus, K. (1991). The nordic profile of skin cancer incidence. a comparative epidemiological study of the three main types of skin cancer. *Int. J. Cancer 47*, 12–19.

Mayer, B. and A. Kylling (2005). Technical note: The libRadtran software package for radiative transfer calculation - description and examples of use. *Atm. Chem. and Phys. 5*, 1855–1877, doi:1680–7324/acp/2005–5–1855.

McKinlay, A. F. and B. L. Diffey (1987). A reference action spectrum for ultraviolet induced erythema in human skin. *CIE J 6*, 17–22.

McPeters, R. D., P. K. Bhartia, A. J. Krueger, J. R. Herman, B. M. Schlesinger, C. G. Wellemeyer, C. J. Seftor, G. Jaross, S. L. Taylor, T. Swissler, O. Torres, G. Labow, W. Byerly, and R. P. Cebula (1996). *Nimbus 7 Total Ozone Mapping Spectrometer (TOMS) Data Products User's Guide*.

met.no (2006). Norwegian Meteorological Institute. http://www.eklima.no.

Moan, J., A. Dahlback, and R. Setlow (1999). Epidemiological support for a hypothesis for melanoma induction indicating a role for UVA radiation. *Photochem. Photobiol. 70*, 243–247.

Moan, J. and A. Dalback (1992). The relationship between skin cancers, solar radiation and ozone depletion. *Br J Cancer 65*(6), 916–921.

Nakajima, T. and M. Tanaka (1988). Algorithms for radiative intensity calculations in moderately thick atmospheres using a truncation approximation. *J. Quant. Spectrosc. Radiat. Transfer 40*, 51–69.

NASA (2005, April 14). Studying earth's enviroment from space. (last updated; june 2000). http://www.ccpo.odu.edu/SEES/index.html.

Norge.no (2007). http://kart.norge.no.

Norwegian Radiation Protection Authority (2007). UV, sol og solarium. http://www.nrpa.no.

Olseth, J. A. and A. Skartveit (1989). Observed and modelled hourly luminous efficacies under arbitrary cloudiness. *Sloar Energy 42*(3), 221–233.

Parkin, D. M. and M. Klath (1996). Studies of cancer in migrants: rationale and methodology. *Eur J Cancer 32A*, 761–771.

Planteforsk (2007). Landvik stationinformation and horizon. http://fou02.planteforsk.no/lmt/stasjon.php?siteid=29.

Reuder, J. and P. Koepke (April 2005). Reconstruction of UV radiation over Southern Germany for the past decades. *Meteorologische Zeitschrift 14*, 237–246(10).

Robsahm, T. and S. Tretli (2001). Cutaneous malignant melanoma in Norway: variation by residence before and after the age of 17. *Cancer Causes Control 12*, 569–576.

Robsahm, T. and S. Tretli (2004). Ultraviolet radiation and health. *Nor J Epidemiol 14*(2), 187–191.

Ruggaber, A., R. Dlugi, and T. Nakajima (1994). Modelling radiation quantities and photolysis frequencies in the troposphere. *J. Atmmos. Chem. 18*, 172–210.

Schwander, H. (1999). *Simulation des Einflusses von Bewölkung auf die UV-Strahlung mittels Neuronaler Netze*. Ph. D. thesis, Ludwig Maximilians Universität, München.

Schwander, H., A. Kaifel, A. Ruggaber, and P. Koepke (2001). Spectral radiative-transfer modeling with minimized computation time by use of neural-network technique. *Applied Optics 40*(3).

Schwander, H., P. Koepke, A. Kaifel, and G. Seckmeyer (2002). Modification of spectral UV irradiance by clouds. *J. Geophys. Res. 107(D16)*, AAC7–1 to AAC7–12.

Schwander, H., B. Mayer, A. Ruggaber, A. Albold, G. Seckmeyer, and P. koepke (1999). Method to determine snow albedo values in the UV for radiative transfer modelling. *Appl. Opt. 38*(18), 3869–3875.

Seinfeld, J. H. and S. N. Pandis (1998). *Atmospheric Chemistry and Physics*. John Wiley & Sons, Inc. New York.

Setlow, R. B., E. Grist, K. Thompson, and A. D. Woodhead (1993). Wavelength effective in induction of malignant melanoma. *Proc Natl Acad Sci USA 90*, 6666–6670.

Skartveit, A. and J. A. Olseth (1986). Modelling slope irradiance at high latitudes. *Solar Energy 36*(4), 333–344.

Smedby, K. E., H. Hjalgrim, M. Melbye, A. Torrång, K. Rostgaard, L. Munksgaard, J. Adami, M. Hansen, A. Porwit-MacDonald, B. A. Jensen, G. Roos, B. B. Pedersen, C. Sundstöm, B. Glimelius, and H. O. Adami (2005). Ultraviolet radiation exposure and risk of malignant lymphomas. *J Natl Cancer Inst 97*, 199–209.

SSB (2005). Statistisk Sentralbyrå; Folkemengde etter fylke, 1951-2005. http://www.ssb.no/emner/02/02/folkendrhistlf/tab-2005-06-09-03.html.

Sætre, O. (2006). Målt og modellert UV-stråling i Bergen. Master's thesis, Geofysisk institutt , Univ. i Bergen, http://web.gfi.uib.no/publikasjoner/pdf/Saetre.pdf.

Svenøe, T. (2000). *Re-evaluation, statistical analysis and prediction based on the Tromsø total ozone record*. Ph. D. thesis, University of Tromsø.

Thune, I., A. Olsen, G. Albrektsen, and S. Tretli (1993). Cutaneous malignant melanoma: Assosiation with height, weight and body-surface area. a prospective study in Norway. *Int. J. Cancer 55*, 555–561.

United Nations Enviromental Programme (1998). *Environmental Effects of Ozone Depletion: 1998 Assessment*. UNEP, Nairobi, Kenya.

Vassenden, K. (1987). Population and housing census 1960, 1970 and 1980, documentation of the comparable files. Statistisk Sentralbyrå, Oslo.

Wallace, J. M. and P. V. Hobbs (1977). *Atmospheric Science an introductory survey*. Academic press.

WMO (1987). *International Cloud Atlas*. World Meteorological Organization.

WMO (2003). *Scientific Assessment of Ozone Depletion: 2002, Global Ozone Research and Monitoring Project - Report No. 47*. Geneva.

WMO (2006). *Scientific Assessment of Ozone Depletion: 2006, Global Ozone Research and Monitoring Project - Report No. 50*. Geneva.